LOST IN SPACE

WHERE THE OUTER BOUND OF LOCALIZATION SPACE SETS THE LOWER BOUND ON LOCALIZATION PERFORMANCE

Bram Jeroen Dil

Graduation committee:

Chairman:	Prof.dr. A.J. Mouthaan
Promoter:	Prof.dr. P.J.M. Havinga, University of Twente
Prof.dr.	G.J.M. Smit, University of Twente
Prof.dr.	C.H. Slump, University of Twente
Prof.dr.	F. Gustafsson, Linköping University
Prof.dr.	K. Römer, University of Lübeck
Prof.dr.	Á. Lédeczi, Vanderbilt University

CTIT Ph.D.-thesis Series No. 13-248
Centre for Telematics and Information Technology
University of Twente
P.O. Box 217, NL – 7500 AE Enschede

ISSN 1381-3617
ISBN 978-90-365-1691-4

This thesis was edited with TeXnicCenter, typeset with LaTeX2e, and printed by Wöhrmann Printing Service, Zuthpen, The Netherlands.

Cover Copyright © NASA

Thesis Copyright © Bram Jeroen Dil
All rights reserved. No part of this book may be reproduced or transmitted, in any form or by any means, electronic or mechanical, including photocopying, microfilming, and recording, or by any information storage or retrieval system, without the prior written permission of the author.

LOST IN SPACE

WHERE THE OUTER BOUND OF LOCALIZATION SPACE SETS THE LOWER BOUND ON LOCALIZATION PERFORMANCE

PROEFSCHRIFT

ter verkrijging van
de graad van doctor aan de Universiteit Twente,
op gezag van de rector magnificus,
Prof. dr. H. Brinksma,
volgens besluit van het College voor Promoties,
in het openbaar te verdedigen
op donderdag 25 april 2013 om 16.45 uur

door

Bram Jeroen Dil

geboren op 2 januari 1983
te Eindhoven

Dit proefschrift is goedgekeurd door:
Prof.dr. (promotor): P.J.M. Havinga

Abstract

This research reflects my theoretical and experimental journey into the lost space of wireless radio localization in the far field of 2.4GHz Commercial-Off-The-Shelf (COTS) radios. At the end of this journey, we arrive at the conclusion that existing phase- and time-based localization systems such as Radio Interferometric Positioning Systems (RIPS) and Time-Of-Flight (TOF) are not reliable in dynamic indoor environments. Our new localization system uses space-based rather than phase- or time-based measurements and shows adequate robustness for such environments.

In the far field, the measured signals are a function of the four wave parameters time, position, temporal frequency and spatial frequency. These wave parameters are variables in propagation models that represent solutions to the Maxwell equations that govern the propagation of radio waves. Localization reduces to fitting the measured signals to the appropriate propagation model at the unknown locations. We identify three types of localization systems based on how the measurements deal with wave parameters: RSS-, phase- and TOF-based systems. The first part of this research explores these individual systems.

This journey starts by introducing a novel distributed connectivity-based localization system using a commonly employed flooding protocol. It exploits a certain part of the information in the protocol that other algorithms consider as redundant or false. This increases the localization performance in comparison with similar RSS-based systems, especially in harsh but static environments.

In static environments, it is assumed that the optimal propagation model settings are known beforehand and are constant over space, time and hardware. In real indoor environments, these optimal propagation model settings depend on the locally and time varying permittivity and permeability of localization space. The challenge then becomes to determine the conditions under which RSS-based localization systems can calculate the optimal propagation model settings on-the-fly allowing for dynamic environments. These conditions turn out to be constraints on the localization surface acting as a spatial

filter. Experiments verify that this approach can cope with dynamic environmental influences, like unknown and varying antenna orientations. However, the localization performance of such systems is of the order of meters, inadequate for many applications. The located objects remain lost in space.

The research then turns to exploit the temporal coherence of our radio transmitters. Their narrow bandwidths allow two different transmitters to interfere and produce beat signals. Phase measurements of beat signals inherently provide better localization performance, both in theory and in practice. Although the approach taken is unique and successful, earlier successful measurements in a different frequency regime had proven the feasibility of this rather complex but accurate localization technique. Our experiments in outdoor environments show accuracies of the order of decimeters. However, theory and experiments show that this approach cannot provide reliable indoor localization.

The final challenge then becomes to achieve robust outdoor as well as indoor localization. As space and time are interconnected through the constant speed of light, performing measurements in the space domain rather than in the time domain enable one to account for the high degree of spatial dispersion in dynamic indoor environments. We call this approach space-based RSS. It is a simple and inexpensive localization technique that turns out to yield localization performances approaching the theoretical limits as given by diffraction theory of electromagnetic radiation. Space-based RSS provides a similar localization performance as phase- and TOF-based localization systems in outdoor environments. In Non-Line-Of-Sight (NLOS) indoor environments, space-based RSS outperforms existing phase- and TOF-based localization systems and provides our required robust localization performance.

In theory, resolving power in the far-field is determined by the ratio of wavelength and the outer dimension of localization space. This outer dimension in turn is limited by the spatial filter used as a constraint on our calibration-free localization system. In the end, it is not surprising that the outer bound of localization space sets the lower bound on localization performance in an inversely proportional relationship. Such relationships are commonly expressed by the well-known uncertainty principles for Fourier conjugates of wave parameters as well as by the equivalent Cramer-Rao-Lower-Bound principle. For the first time, this research compares these limits achieved by the relevant existing localization techniques, both in theory and in practice, and both in outdoor and indoor environments. As all measurements of comparable localization techniques such as RSS-, TOF- and phase-based localization were performed by us, this should leave little or no doubt about the validation of this theoretical and experimental comparison.

Samenvatting

Dit onderzoek beschrijft mijn theoretische en experimentele reis in het verloren verre veld van draadloze netwerken van 2.4GHz radio's. Aan het einde van de reis komen we tot de conclusie dat bestaande fase- en tijd-gebaseerde lokalisatiesystemen, zoals Radio Interferometrische PositioneringsSystemen (RIPS) en systemen gebaseerd op Time-Of-Flight (TOF), binnenshuis onbetrouwbaar zijn. Ons nieuwe lokalisatiesystem is wel betrouwbaar in dat soort omgevingen en is gebaseerd op ruimte- in plaats van op fase- of tijd-gebaseerde metingen.

In het verre veld zijn de gemeten radiosignalen een functie van de vier golfparameters tijd, positie, tijdfrequentie en ruimtefrequentie. Deze golfparameters zijn variabelen in propagatiemodellen. Propagatiemodellen zijn oplossingen van de Maxwell vergelijkingen die de voortplanting van radiogolven beschrijven of in parametervorm empirisch benaderen. Lokalisatie is dan terug te voeren tot het fitten van de gemeten radiosignalen met het gekozen propagatiemodel op de onbekende locaties. Wij identificeren drie lokalisatiesysteemtypes gebaseerd op hoe de metingen invloed hebben op de golfparameters: Signaal Sterkte- (RSS), Fase- en Time-Of-Flight-gebaseerde systemen. Het eerste deel van dit onderzoek beschrijft en vergelijkt deze drie systeemtypes.

Onze reis begint met het introduceren van een nieuw gedistribueerd op connectiviteit gebaseerd lokalisatiesysteem. Daarbij wordt gebruik gemaakt van een veel gebruikt "flooding" protocol. Ons nieuwe lokalisatiesysteem maakt gebruik van een bepaald deel van de informatie in dat protocol dat andere lokalisatiesystemen als overbodig of vals beschouwen. Dit verhoogt de lokalisatienauwkeurigheid in vergelijking tot dezelfde soort RSS-gebaseerde systemen, vooral in complexe maar statische omgevingen.

In statische omgevingen wordt aangenomen dat de optimale propagatiemodelparameters vooraf bekend zijn en dat deze niet variëren over de ruimte, tijd en met de hardware. Binnenshuis, bijvoorbeeld in kantooromgevingen zijn deze parameters afhankelijk van de lokale en tijdsafhankelijke permittiviteit en permeabiliteit van de ruimte. De uitdaging is dan om de voorwaarden te vin-

den, waaronder RSS-gebaseerde lokalisatiesystemen deze parameters "on-the-fly" kunnen bepalen. In dat geval kunnen lokalisatiesystemen in dynamische omgevingen werken, zelfs binnenshuis. De gevonden voorwaarden vormen beperkingen op het lokalisatieoppervlak. Ze werken als een ruimtelijk filter. Experimenten met onbekende en variërende antenneoriëntaties laten zien dat deze aanpak de lokalisatienauwkeurigheid verhoogt. Echter, de lokalisatienauwkeurigheid van dergelijke systemen blijft in de orde van enkele meters wat voor veel toepassingen onvoldoende is. De objecten blijven verdwaald in de ruimte.

Het onderzoek richt zich daarna op de tijdscoherentie van radiozenders. De smalle bandbreedtes maken het mogelijk dat twee verschillende radiozenders interfereren en een verschilsignaal produceren. Lokalisatie gebaseerd op fasemetingen van verschilsignalen geven in theorie en praktijk een betere lokalisatienauwkeurigheid. Hoewel de aanpak effectief en uniek is, hadden eerdere metingen in een andere frequentieband de effectiviteit van deze complexe en nauwkeurige lokalisatietechniek al bewezen. Onze experimenten in een vrije buiten-omgeving laten nauwkeurigheden zien in de orde van decimeters. Theorie en praktijk laten echter zien dat deze aanpak geen betrouwbare lokalisatie binnenshuis kan opleveren.

Onze laatste uitdaging werd om een nauwkeurige lokalisatie zowel binnen als buiten te verkrijgen. Daar in het verre veld van elektromagnetische straling ruimte en tijd verbonden zijn met de constante lichtsnelheid, wordt door het uitvoeren van metingen over het ruimtedomein de grote ruimtelijke spreiding in dynamische binnen-omgevingen bepaald. We noemen deze aanpak "space-based RSS". Het is een eenvoudige en relatief goedkope techniek, waarbij de theoretische ondergrens van de meetnauwkeurigheid wordt bepaald door de diffractie aan de buitengrens van het lokalisatieoppervlak. Deze lokalisatietechniek levert in vrije buitenomgevingen dezelfde nauwkeurigheid op als op fase- en TOF-gebaseerde technieken. Binnenshuis blijkt space-based RSS echter deze beide andere technieken ver achter zich te laten in nauwkeurigheid.

In theorie wordt het oplossende vermogen van het verre veld bepaald door het quotiënt van golflengte en de buitengrens van het lokalisatieoppervlak. Deze buitengrens wordt bepaald door het ruimtelijk filter dat toegepast wordt op ons kalibratievrije lokalisatiesysteem. Uiteindelijk is het daarom niet verrassend, dat die buitengrens de ondergrens van de lokalisatienauwkeurigheid bepaalt in een omgekeerd evenredigheidsverband. Dergelijke verbanden worden uitgedrukt als onzekerheidsrelaties voor Fourier-geconjugeerde golfparameters of door het gelijkwaardige Cramer-Rao-Lower-Bound principe. Voor het eerst vergelijkt dit onderzoek deze ondergrenzen die behaald worden door

de verschillende lokalisatietechnieken, zowel in theorie als praktijk, en zowel in binnen- als buitenomgevingen. Daar alle metingen met de verschillende lokalisatiesysteemtypes binnen ons laboratorium zelf verricht zijn, laat dit weinig twijfel over de validering van deze theoretische vergelijking met de praktijk.

Acknowledgments

Nine years ago, I met my advisor Paul Havinga during a course called "Bachelor Referaat". In this course, you get the opportunity to do research. Paul gave me the opportunity to extend this research, which resulted in my first scientific contribution. During my Bachelor's and Master's period, Paul gave me the opportunity to deepen and broaden my insight in the field of localization, and I really enjoyed doing it. So when Paul offered me to do a PhD with him, I was happy to meet that new challenge. During my PhD he helped me to start my own company, apply for patents, perform research and write papers. I am very grateful to Paul for his continuing support.

One of the other major influences throughout my research is my dad. I want to thank him for his endless patience to help and challenge me to do better. What I enjoyed the most, is the fun we had together in the process. I also want to thank the rest of my family for being there for me, especially my mother, Jessica, Nico and Radhika. For example, it is always a delight to go to my parents' place, especially when my mother made her delicious fresh tomato soup with spicy meat balls.

I would like to thank all my helpful colleagues at Ambient Systems and the Pervasive Systems group, especially Wouter van Kleunen for helping me with programming the radio modules and a lot of other stuff; Wim Korevaar, Berend Jan van der Zwaag and Arta Dilo for the useful discussions and for structuring my thoughts. I would like to thank Bhaskar Krishnamachari for my relatively short but inspiring visit to USC LA; Ákos Lédeczi and Cindy Kleinfeld for their contributions to my SENSYS paper.

I would like to thank my best friends Rob, Niels, Andries, and Wouter for their friendship and support through the years. In addition, I would like to thank Ada and her friends for our travels. Finally, I would like to thank my judo teachers and friends for making sure there was nothing wrong with my physical condition, especially Niels, Andries, and Ward which were my training buddies for years, and not to forget Wouter, Sietse, Stefan, Wilco, Andre, Hamed, Bram, Sil and Ferdinand.

Contents

CHAPTER 1

Introduction

My journey into the field of radio localization started with studying the original work and patents of Loran ([2]) and Decca ([3]). These early contributions from the 1940s already revealed that radio waves can be used as a measure of distance to locate unidentified objects in the lost space of naval and air defense systems. Combining ideas from these early contributions resulted in the Global Positioning System (GPS), which is probably the most well-known localization system nowadays. GPS receivers at unknown positions measure Time-Of-Flight (TOF) in Line-Of-Sight (LOS) from an array of transmitting satellites at known positions. One can calculate the traveling distance of the waves, as the constant speed of light connects traveling time with traveling distance when transmitter en receiver are in LOS. The localization performance of the radiation equals the inverse of the natural bandwidth of the radiation times the speed of light. The natural bandwidth of the radiation is a function of the Q-factor of the resonators. The localization performance of GPS is of the order of several meters when there are four or more Satellites in LOS.

Our research theoretically and experimentally investigates the resolving power and robustness of RSS-, TOF- and phase-based localization systems operating in the far field of 2.4GHz Commercial-Off-The-Shelf (COTS) radios. We only compare localization systems operating at 2.4 GHz and exclude frequency-specific advantages that may be present in other frequency bands. The 2.4 GHz band is a globally free band, which enjoys the interest of many industrial applications such as Wi-Fi, Bluetooth and 802.15.4.

Localization performance of localization systems is fundamentally determined by the resolving power of the radiation. Resolving power is defined as the lower bound (smallest measurable quantity) divided by the upper bound (measuring range). This ratio equals to the inverse of the effective number of measurements. In the far field, the resolving power in time, frequency and space domains are interchangeable as long as the effective number of measure-

ments is equal and as long as the receivers are in LOS of the transmitters.

Chapter 2 presents a novel connectivity-based localization system that increases the resolving power by measuring connectivity to neighboring radios ([17], and [37]). In this case, the resolving power depends on the spatial density of radios, which is an unwanted property when this density increases.

The robustness for the spatial dispersion of the environment depends on how well propagation models can account for hardware variations of antennas and spatial and temporal variations of the environments. Chapter 3 introduces a novel technique for the automatic and optimal calibration of RSS-based localization systems ([34], [35] and [40]). This novel technique performs the calibration of the propagation model so fast that temporal changes in the environment can be neglected as spatial variations are practically instantaneously accounted for.

In Chapter 4, we design and implement a novel phase-based localization system that does not require calibration and is implementable on most COTS radios ([32] and [38]). We call this localization system SRIPS. To our knowledge, this is the only phase-based localization system that operates on 2.4 GHz COTS radios. The resolving power of these types of phase-based localization systems depend on the coherence between two autonomous transmitters.

In Chapter 5, we design and implement a novel space-based RSS localization system that increases the resolving power by using a mobile node with unknown positions while it meanders over localization space. We theoretically show that RSS-, phase- and TOF-based localization systems can be designed to provide similar resolving powers. Our measurements with our space-based RSS localization system, SRIPS ([38]) and TOF-based localization system ([46]) in a 20×20 m^2 LOS outdoor environment verify this design opportunity. Such localization systems all show a localization performance in the order of several decimeters, as long as the nodes remain in LOS.

In Non-Line-Of-Sight (NLOS) indoor environments, the localization performance depends on whether the spatial variation of the far fields in NLOS from the nodes still has sufficient resolving power to provide adequate localization performance. From a theoretical point of view, one would expect that to be the case, as the resolving power of incoherent radiation should be determined by Rayleigh's diffraction limit ([17]). The resolving power of coherent radiation is roughly a factor of two better and is determined by the Shannon-Nyquist sample theorem. Chapter 5 shows that performing measurements in the space domain rather than in the time domain indeed enable standard gradient search algorithms to localize the nodes in NLOS dynamic indoor environments with a high degree of spatial dispersion. Our far-field measurements in a 40x15 m2

NLOS indoor office environment verify and show that our space-based RSS localization system provides a robust localization performance of 1 meter and outperforms existing SRIPS ([38]) and TOF-based ([46]) localization systems. This one-meter localization performance is not yet the theoretical lower bound of Rayleigh's diffraction limit, as the effective number of measurements has not yet been reached in our setup. This result is close enough to provide justification for the theoretical model used.

In summary, RSS-, phase- and TOF-based localization can be designed to provide similar resolving powers in outdoor LOS environments as we show in theory and practice. These localization techniques differ in robustness for spatial and temporal environmental influences. Only our space-based RSS does not leave the user lost in space in environments with a high degree of spatial dispersion such as NLOS indoor office environments.

1.1 Challenges and Goals

This research aims to strike a balance between theory, experiments and applicability. This means that we try to achieve the theoretical limits, verify these theories with experiments, and use these theories in a practical implementation. Practical means that our findings are competitive and applicable in industrial applications.

Our main goal and challenge is to theoretically and experimentally analyze the various localization systems operating in the far field. We aim to use these theories to design, develop and implement localization systems. We consider the most important performance metrics as:

- **Localization Performance**
  We define localization performance as the measured positioning error in an ideal environment, in which the propagation model matches the environment. We measure performance in outdoor LOS environments.

- **Robustness to Environmental Influences**
  We measure the robustness to static and dynamic environmental influences by measuring the positioning error in (NLOS) indoor environments. A relatively high performance in outdoor environments does not necessarily imply a relatively high performance in indoor environments (Chapter 5). Robustness to environmental influences is an important criterion in indoor localization.

- **Low Deployment and Maintenance Costs**
  Most localization systems require an extensive calibration phase to account for environmental influences and individual hardware differences before and during localization. The calibration costs increase with increasing localization area and increasing amount of radios. These costs determine the scalability and thus applicability of a localization system, especially in dynamic environments with a large amount of radios.

- **Implementable on readily available radio platforms**
  Our system should be implementable on most COTS radio platforms. This significantly lowers certification and production costs and may facilitate a relatively short time-to-market.

In addition to this list, energy consumption and scalability are important design requirements for localization systems. First, our nodes with unknown positions are battery-powered. This means that lower energy consumption implies longer life times. Secondly, we strive for high scalability of our localization systems, which usually determines the maximum number of nodes that can be localized per unit time. Energy consumption and scalability requirements both depend on the envisioned application, communication protocol and radio platform. These latter criteria are not on our list and are only addressed in some detail.

1.2 Hypothesizes

On the basis of our challenges and goals, we make the following four hypothesizes regarding RSS-based localization:

1. Localization performance in the far field of incoherent multiplexed signals is bounded by the wavelength of the radiation. Sampling beyond this lower bound does not improve localization performance.

2. Calibration-free localization systems can provide similar performance as optimally calibrated localization systems.

3. RSS-based localization systems using narrowband signals can be designed to provide similar performance in LOS environments as phase- and TOF-based systems.

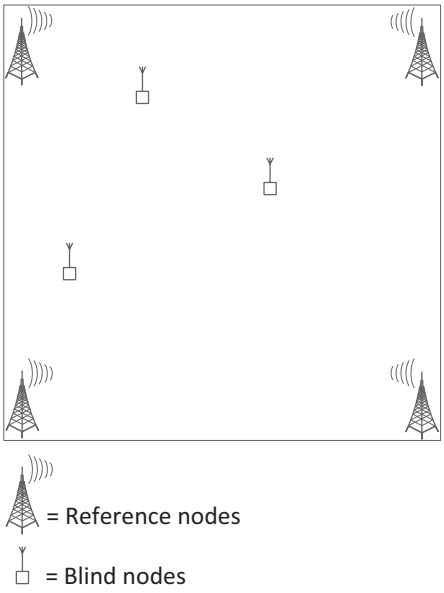

Figure 1.1: Typical localization set-up

4. Space-based RSS localization systems provide better robustness to environmental influences than other localization systems operating in the far field.

1.3 Related Work

Figure 1.1 shows a typical localization set-up. This set-up consists of four fixed radio beacons called reference nodes that transmit the required signals for localization. In this setup, the four reference nodes are located at the four corners of the localization area. Blind nodes do not know their locations and position themselves using the received signals from the reference nodes. In the far field, the measured signals are a function of the wave parameters time, position, temporal frequency and spatial frequency. Localization systems estimate blind node positions by measuring these wave parameters from sampling radio signals over space, time, or phase domains. We identify three localization systems based on how the measurements deal with these wave parameters:

- Received Signal Strength-based (RSS-based) localization
- Time-Of-Flight-based (TOF-based) localization
- Phase-based localization

We identify four types of RSS-based localization approaches: range-, sequence-, connectivity- and fingerprinting-based localization. Range-based localization assumes that RSS is a function of distance ([4]). This function converts the RSS measurements to distance estimates, which are used to estimate the position ([13]). Sequence-based localization assumes that RSS decays over distance without assuming that the RSS decay is described by a certain function. Sequence-based localization systems only use the ordered sequence of RSS measurements ([12] and [18]). Connectivity-based localization assumes that the packet delivery rate is a function of distance. This type of system only uses connectivity information depending on whether a packet is received or not. Connectivity-based localization suffers from the same fading effects as the other types of RSS-based localization systems, because connectivity measurements are a binary quantization of RSS measurements ([14]). Therefore, connectivity-based localization systems are less accurate than the other types of RSS based localization systems. Fingerprinting-based localization systems assume that RSS is a function of position (e.g. [5] and [26]) instead of being a function of distance.

These RSS-based localization systems are implementable on most COTS 2.4 GHz platforms. They differ in performance/robustness and deployment/ maintenance costs. Range- and connectivity-based localization both assume that the RSS decay is described by a function. We use the Log-Normal Shadowing Model to describe the RSS over distance decay ([4]). This model has two wave parameters as independent variables that account for environmental influences and hardware differences. Conventional range- and connectivity-based localization systems calibrate this model by performing calibration measurements before deployment ([6] and [14]). Such an approach cannot cope with spatial dispersion that influences the RSS measurements like passing human beings. Fingerprinting-based localization systems can calibrate for such effects when these effects are static. In other words, fingerprinting-based localization systems are more robust for static environmental influences than conventional range- and connectivity-based localization systems. In case of dynamic environmental influences, range-based localization systems perform better than fingerprinting-based localization systems ([34]). Fingerprinting-based localization systems require significantly more calibration measurements

than conventional range- and connectivity-based localization systems ([35]). Conventional range-based localization systems provide the same performance as fingerprinting-based localization systems in LOS environments ([35]). Sequence-based localization systems do not require calibration. Their performance is less than the other calibrated localization systems ([34]). Table 1.1 shows the performances of the four RSS-based localization systems.

We identify two COTS TOF localization systems in the 2.4 GHz band: hardware-supported TOF and not-hardware-supported TOF systems. On most radio platforms, radios are available that have a TOF engine, like the 802.15.4 platform ([44]), the Wi-Fi platform ([45]), and the 802.15.4a platform ([46]). We compare our localization systems to radios that implement the 802.15.4a platform ([46]). The signal modulation in the 802.15.4a standard is specifically designed for high-performance and robust ranging. It uses the entire 80 MHz bandwidth at 2.4 GHz, and the ranging performance increases linearly with the bandwidth (Chapter 5). The signal modulation in the 802.15.4 and the Wi-Fi standards is not specifically designed for ranging and uses less bandwidth than the 802.15.4a standard. 802.15.4a radios provide adequate ranging and localization performance in outdoor LOS environments. However, NLOS ranging decreases the performance significantly ([39]). We verify this with our own experiments in Chapter 5. In case of not-hardware-supported TOF, two radios transmit an extensive amount of messages hence and forth and measure TOF ([36] and [41]). The advantage of this approach is that it can be implemented on most COTS radios without a TOF engine. However, it requires an extensive amount of time and messages in comparison with the hardware-supported TOF radios, and it performs less. We do not consider this TOF system in our research. Table 1.1 shows the performance of the 802.15.4a radios.

There is one COTS phase-based localization system available at 2.4 GHz, which we present in Chapter 4 called SRIPS ([38]). This system is based on work presented in [19]. SRIPS relies on two independent senders, transmitting unmodulated carrier waves at slightly different frequencies. The frequency difference generates a frequency beat signal at the receiving antennas, which is measured by two independent receivers. The measured phase difference between the receiver pairs is a function of the distances between the senders and receivers involved. Our study shows that SRIPS provides similar performances as TOF in outdoor environments, but it cannot provide reliable localization in NLOS indoor environments.

Table 1.1: Performance Localization Systems

Localization System	Performance LOS outdoor	Robust NLOS indoor	Calibration Costs
Fingerprinting	+	-	- - -
Range	+	-	-
Sequence	-	-	+
Connectivity	-	-	-
TOF	++	-	+
COM-LOC++	+	+	-
Self-Adaptive	+	+	+
SRIPS	++	-	+
Space-Based	++	++	-

1.4 Contributions

We consider our five main contributions in the order of appearance:

Connectivity-Based Localization
We introduce a new distributed connectivity-based localization system that provides similar or better results than RSS-based shortest distance localization systems, especially in harsh environments. Table 1.1 shows the performance of COM-LOC++. We assume that COMLOC++ is calibrated before deployment. COM-LOC++ provides similar results as shortest distance RSS- and range-based localization systems in an ideal outdoor environment. In harsh environments, COM-LOC++ outperforms these RSS-based localization systems.

RSS-Based and Calibration-Free Localization
We present the constraints under which calibration-free localization systems provide similar or better results than calibration-extensive localization systems. Table 1.1 shows the performance of these calibration-free localization systems, which we call Self Adaptive Localization (SAL) systems. SAL estimates the parameters of the Log-Normal Shadowing model on-the-fly and does not require any calibration before deployment. In a static environment, it provides similar results as the RSS- and range-based localization systems. In a dynamic environment with unknown antenna orientations, it outperforms its conventional

range-based counterpart.

Phase-Based Localization operating on COTS 2.4 GHz Radios
We present a Radio Interferometric Positioning System that is implementable on any radio platform, which we call SRIPS. Table 1.1 shows the performance of SRIPS. SRIPS does not require any calibration. In an outdoor LOS environment, it provides the same performance as the 802.15.4a TOF localization system. In an indoor environment, it cannot provide reliable localization results.

A New High-Performing Robust RSS-based Localization System
An RSS-based localization system that provides similar performance and better robustness than other 2.4 GHz RSS-, TOF- and phase-based localization systems. We call this localization system space-based RSS. Table 1.1 shows the performance of space-based RSS. We assume that the optimal calibration settings are known before deployment. In an outdoor LOS environment, it provides similar results as SRIPS and the 802.15.4a TOF localization system. In an NLOS indoor environment, it outperforms the other localization systems.

Analyze and Compare Localization Systems operating in the Far Field
We theoretically and experimentally show that TOF-, phase- and RSS-based localization systems can be designed to provide the same localization performance in LOS outdoor environments.

In the first three chapters of this research, we focus on individual localization systems. These localization systems are in order of appearance: Connectivity-, RSS- and Phase-based localization. In the last chapter, we theoretically and experimentally connect the localization systems and describe our space-based RSS localization system.

Bibliography

[1] M.Sargent, E.Willis Lamb, R.L.Fork: Theory of a Zeeman Laser I. Physical Review, vol. 164, Issue 2, December 1967.

[2] C.Powell: Hyperbolic Origins. Journal of Navigation (1981), 34: pp 424-436.

[3] W.F.Blanchard: Hyperbolic Airborne Radio Navigation Aids A Navigators View of their History and Development. Journal of Navigation, 1991.

[4] Hashemi H.: The indoor radio propagation channel, Proc. IEEE, July 1993, pp. 943- 996.

[5] P.Bahl and V.N. Padmanabhan: RADAR: An In-Building RF-Based User Location and Tracking System, in Proceedings of the 19th IEEE International Conference on Computer Communications (INFOCOM), March 2000.

[6] N.Patwari, R.J.O'Dea, Y.Wang: Relative Location in Wireless Networks. Presented at IEEE Vehicular Technology Conference, Spring, Rhodes, Greece, May 2001.

[7] D.Niculescu, B.Nath: Ad hoc positioning systems. In: IEEE Globecom 2001, San Antonio. 2001.

[8] J.Hightower, C.Vakili, G.Borriello, R.Want: Design and calibration of the spoton ad-hoc location sensing system. August 2001.

[9] K.Whitehouse, D.Culler: Calibration as Parameter Estimation in Sensor Networks. In ACM International Workshop on Wireless Sensor Networks and Applications, Atlanta, GA, USA, September 2002.

[10] D.Li and Y.H.Hu: Energy based collaborative source localization using acoustic micro-sensor array. J.EUROSIP Applied Signal Process., vol. 4, 2003.

[11] IEEE Standard 802.15.4-2003. http://standards.ieee.org/getieee802/download/802.15.4-2003.pdf, 2012.

[12] T.He, C.Huang, B.M.Blum, J.Stankovic, T.Abdelzaher: Range-free localization schemes for large scale sensor networks. MobiCom, San Diego, California, September 2003, pp. 81-95.

[13] N.Patwari, A.O.H. III, M. Perkins, N. S. Correal, and R.J.O'Dea: Relative location estimation in wireless sensor networks. IEEE Transactions on Signal Processing, vol. 51, no. 8, August 2003.

[14] N.Patwari and A.O.Hero III: Using Proximity and Quantized RSS for Sensor Localization in Wireless Networks. WSNA 2003.

[15] M.L.Sichitiu and V.Ramadurai: Localization of wireless sensor networks with a mobile beacon. MAHSS 2004.

[16] E.Elnahrawy, X.Li; R.P.Martin: The limits of localization using signal strength: a comparative study. SECON 2004.

[17] J.W.Goodman: Introduction to Fourier Optics. Roberts and Company Publishers, 3rd Edition edition, December 10, 2004.

[18] K.Yedavalli, B.Krishnamachari, S.Ravula, and B.Srinivasan: Ecolocation: A sequence based technique for RF-only localization in wireless sensor networks. IPSN 2005.

[19] M.Maróti, P.Völgyesi, S.Dóra, B.Kusý, A.Nádas, Á.Lédeczi, G.Balogh, K.Molnár: Radio interferometric geolocation. SENSYS 2005.

[20] J.Lampe: Nanotron Chirp Spread Spectrum Proposal. IEEE P802.15 Working Group for Wireless Personal Area Networks (WPANs), 2005.

[21] N.Patwari: Location estimation in sensor networks. Thesis of Neal Patwari at University of Michigan, 2005.

[22] B.Kusý, Á.Lédeczi, M.Maróti, L.G.L.T.Meertens: Node density independent localization. In IPSN 2006.

[23] IEEE Standard. 802.15.4a-2007. http://standards.ieee.org/getieee802/download/802.15.4a-2007.pdf, 2012.

[24] K.Whitehouse, C.Karlof, D.Culler: A Practical Evaluation of Radio Signal Strength for Ranging-based Localization. Mobile Computing and Communications Review, Volume 11, Number 1, 2007.

[25] R.A.Malaney: Nuisance Parameters and Location Accuracy in Log-Normal Fading Models. IEEE Transactions on Wireless Communications, March 2007, Volume: 6, page(s): 937-947

[26] M.B.Kjyrgaard and C.V.Munk: Hyperbolic location fingerprinting: A calibration-free solution for handling differences in signal strength. PerCom 2008.

[27] E.Menegatti, A.Zanella, S.Zilli, F.Zorzi, E.Pagello: Range-only SLAM with a mobile robot and a Wireless Sensor Networks. In ICRA 2009.

[28] G.Chandrasekaran, M.A.Ergin, J.Yang, S.Liu, Y.Chen, M.Gruteser, R.P.Martin: Empirical Evaluation of the Limits on Localization Using Signal Strength. In SECON 2009.

[29] V.Honkavirta, T.Perala, S.Ali-Loytty, R.Piche: A Comparative Survey of WLAN Location Fingerprinting Methods. In WPNC 2009.

[30] B.J.Dil, P.J.M.Havinga: COM-LOC: A Distributed Range-Free Localization Algorithm in Wireless Networks. In: Proceedings of the 5th International Conference on Intelligent Sensors, Sensor Networks and Information Processing (ISSNIP), 7-12-2009, Mellbourne, Australia. pp. 457-462.

[31] Z.Xiuyuan, L.Hongbo, Y.Jie, C.Yingying, J.Francisco, R.P.Martin, L.Xiaoyan: Characterizing the impact of multi-frequency and multi-power on localization accuracy. In MASS 2010.

[32] B.J.Dil, P.J.M.Havinga: A Feasibility Study of RIP Using 2.4 GHz 802.15.4 Radios. MELT 2010, November 2010.

[33] K.Chintalapudi, A.Iyer, and V.Padmanabhan: Indoor localization without the pain. In MOBICOM 2010.

[34] B.J.Dil, P.J.M.Havinga: RSS-Based Localization with Different Antenna Orientations. Australian Telecommunication Networks and Applications Conference (ATNAC), 2010.

[35] B.J.Dil, P.J.M.Havinga: Calibration and Performance of RSS-based Localization Methods. Internet Of Things (IOT), 2010.

[36] B.Thorbjornsen, N.White, A.Brown, J.Reeve: Radio frequency (rf) time-of-flight ranging for wireless sensor networks. Measurement Science and Technology 21(3), 2010.

[37] B.J.Dil, P.J.M.Havinga: COM-LOC++ A distributed range-free localization algorithm in wireless networks. ISSNIP 2010, 7-10 December, Australia. pp. 157-162.

[38] B.J.Dil and P.J.M.Havinga: Stochastic Radio Interferometric Positioning in the 2.4 GHz Range. In SENSYS 2011.

[39] S.Lee, B.Kim, H.Kim, R.Ha, H.Cha: Inertial Sensor-Based Indoor Pedestrian Localization with Minimum 802.15.4a Configuration. IEEE Transactions on Industrial Informatics, 2011.

[40] B.J.Dil and P.J.M.Havinga: RSS-based Self-Adaptive Localization in Dynamic Environments. In IOT 2012.

[41] P.Pettinato, N.Wirström, J.Eriksson, T.Voigt: Multi-channel two-way time of flight sensor network ranging. In EWSN 2012.

[42] http://www.etsi.org, 2013.

[43] http://focus.ti.com/lit/ds/symlink/cc2430.pdf, 2013.

[44] http://www.jennic.com, 2013.

[45] http://www.aeroscout.com, 2013.

[46] http://www.nanotron.com, 2013.

CHAPTER 2

A Distributed Connectivity-Based Localization System

This chapter introduces a novel distributed connectivity-based localization system in wireless sensor networks. This novel system uses a flooding protocol that is commonly employed by distance-based localization systems to determine the shortest (hop) distance. We call this localization system COMLOC++. Our approach is new in that we optimize the localization performance for this communication protocol. We exploit a certain part of the information in the protocol that other localization systems consider as redundant or false. In addition, we process the information from all heard reference nodes to estimate the distance to one reference node. Our simulations show that this information increases the localization performance by 15% to 65% and increases the localization stability by 40% to 65% compared with existing connectivity- and RSS-based research using the same communication protocol.
[1]

2.1 Introduction and Related Work

In recent years, there is a growing interest in locating devices in wireless communication networks. Several of these localization systems are based on connectivity measurements ([5], [6], [8], [9], [11], [12], [13]). Connectivity information can be obtained with no additional hardware and minimum energy costs. Although other localization systems can be more accurate than connectivity-based localization systems, such localization systems often require specialized hardware or specialized network setups (e.g. TOF, AOA and TDOA) that are not commonly available in wireless communication networks. The localization

[1] This chapter is partially published in [17] and [19].

performance of these other techniques can be enhanced by processing connectivity information (as in [15]). Hence, connectivity-based localization is still an attractive field of research.

We compare our connectivity-based localization system to three types of RSS-based localization systems: range- ([13] and [16]), proximity- ([6] and [14]) and connectivity-based ([5], [9], [11] and [12]) localization. Existing connectivity-based localization systems assume that the transmission range is constant (so called unit disk model, [11]) or that the deployment distribution is a priori known ([5], [9] and [12]). This means that the performance depends on the difference between the expected and measured values of the transmission range and deployment distribution. We use the Log-Normal Shadowing Model to model connectivity.

Most existing localization systems in wireless networks are designed with the assumption that certain localization specific information is available. Afterwards, a communication protocol is designed to obtain this information. We do it the other way around. We design a distributed connectivity-based localization system on the basis of a communication protocol commonly employed by localization systems (as in [5], [9], [11], [12] and [15]). We construct the Maximum Likelihood Estimator (MLE) for localization on the basis of the communication protocol. Theoretically, this maximum likelihood estimator should provide optimum localization results for a given communication protocol. We present a new localization system called COM-LOC++. COM-LOC++ processes information that other systems consider as redundant or false information. In addition, it processes the information from all heard reference nodes to estimate the distance to one reference node.

This chapter is organized as follows. After the problem formulation in Section 2.2, Section 2.3 describes the propagation model to simulate connectivity. Section 2.4 shows how COM-LOC++ converts the information obtained during the communication phase into distance estimates and associated probability distributions. Section 2.5 provides a description of COM-LOC++. Section 2.6 numerically analyzes the localization performance of COM-LOC++. In addition, this section compares COM-LOC++ with ecolocation ([14]) and a modified version of the MLE described in [13]. Section 5.7 presents the conclusions.

2.2 Problem Formulation

This section provides a formal description of the connectivity-based localization problem using the flooding communication protocol. First consider a wire-

less network that consists of two types of nodes:

- *Reference nodes*: reference nodes know their position in advance.
- *Blind nodes*: blind nodes do not know their location and require localization.

We address the problem of blind node localization on the basis of connectivity measurements using a communication protocol called sum-dist ([7]). First, each reference node broadcasts a message with its position and hop distance set to one. Each receiving blind node stores the received reference node's position and hop count. The hop distance is increased by one and the message is forwarded. This ends the communication phase. We keep the communication costs at the minimum for localization functionality in mobile wireless networks ([11]). At the end of the communication phase, blind nodes have the following information:

1 A set of reference node positions that are one-hop-away (set S). We represent this set by: $S \subseteq R$. R is the set of heard reference nodes.

2 A set of reference node positions that are two-hops-away (set T). We represent this set by: $T \subseteq R$.

3 The number of received messages from other blind nodes per reference node (nr_{ref}). We represent this number by: nr_{ref} and ref $\in R$.

4 The number of received messages from other blind nodes. We represent this number by: nr_{total}.

We use these information components throughout this chapter. Most existing distributed connectivity-based localization algorithms, that use this communication protocol, only evaluate the shortest hop count for localization ([5], [9], [11] and [12]). Figure 2.1 shows an example of sum-dist. The black circles represent the nodes; r_1 represents a reference node and $b_1 \ldots b_4$ represent the blind nodes. The solid and broken lines represent the communication links. The text above the communication links shows whether the received messages are processed by existing algorithms. The number of hops indicates how many hops the blind node is away from the reference node. COM-LOC++ uses two types of messages that are not used by existing distributed connectivity-based algorithms:

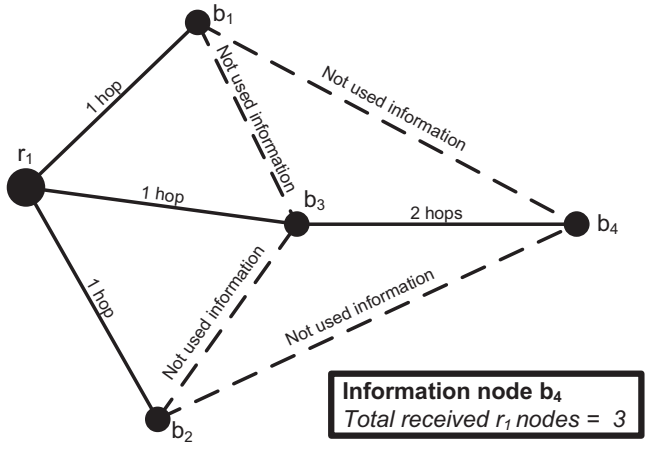

Figure 2.1: COM-LOC, communication phase

- "Redundant information": the messages from $b_1 \dots b_3$ all indicate that b_4 is two-hops-away from reference node r_1. Therefore, two of these messages are considered redundant. Note that $\text{nr}_{\text{ref}} = 3$.

- "False information": the messages from $b_1 \dots b_2$ to b_3 indicate that b_3 is two-hops-away from reference node r_1, while the shortest hop-distance is one-hop. Hence, these messages are considered as false information. Note that $\text{nr}_{\text{ref}} = 2$.

This means that many received messages are considered useless and are discarded. The main difference with shortest-hop localization algorithms is that COM-LOC++ processes these messages in order to increase the localization performance without increasing the communication costs. Figure 2.2 shows an example of what type of extra information COM-LOC++ processes for node b_4:

- $nr_1 = 3$: node b_4 receives messages from r_1 via nodes $b_1 \dots b_3$.

- $nr_2 = 3$: node b_4 receives messages from r_2 via nodes b_1 and $b_5 \dots b_6$.

- $nr_{total} = 5$: node b_4 receives messages from nodes $b_1 \dots b_3$ and $b_5 \dots b_6$.

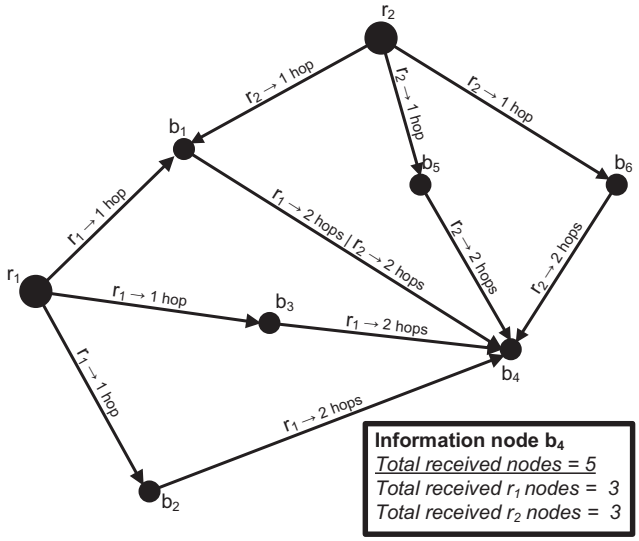

Figure 2.2: COM-LOC++, communication phase

This means that node b_4 does not receive messages from 2 nodes for reference nodes r_1 and r_2 ($nr_{total} - nr_1 = nr_{total} - nr_2 = 2$). In other words, b_4 is in transmission range of 5 blind nodes AND the reference nodes are NOT in transmission range of two of these nodes. COM-LOC++ uses this information to improve localization performance. Note that shortest-hop distance algorithms only process information components 1 and 2, COM-LOC++ also evaluates information components 3 and 4. Section 2.4 describes how this information is processed.

2.3 Connectivity Model

We adopt the Log-Normal Shadowing Model for modeling the signal strength over distance decay ([1]). Empirical studies support the application of this model in indoor and outdoor environments ([2] and [18]). In the next chapter, we numerically and experimentally verify that this model can be applied to our localization system. The following formula represents the Log-Normal

Shadowing Model:

$$P_d = P_{d_0} - 10 \cdot n \cdot \log_{10}(\frac{d}{d_0}) + X_{\sigma_{dBm}} \tag{2.1}$$

Here P_d represents the received signal power in dBm at distance d; P_{d_0} represents the received signal power in dBm at reference distance d_0; n represents the path loss exponent, representing the rate at which the path loss increases with distance; X_σ represents the error of the Log-Normal Shadowing Model and follows a zero-mean normal distribution with variance σ^2_{dBm}.

We use the Log-Normal Shadowing Model for estimating the packet delivery rate as a function of distance. Usually, connectivity is determined by an RSS threshold (like in [13]). The following formula computes the packet delivery rate as a function of distance:

$$P(\text{B hears A}|d_{A,B}) = 1 - \text{cdf}(thres, P_d, \sigma^2_{dBm}) \tag{2.2}$$

Here $P(\text{B hears A}|d_{A,B})$ represents the probability that receiver B receives a message from transmitter A at distance $d_{A,B}$. We calculate this probability using the cumulative distribution function of the normal distribution. The probability depends on the distance between transmitter A and receiver B. Therefore, the probability is a function of the coordinates of transmitter A and receiver B:

$$P(\text{B hears A}|d) = P\Big((x_A, y_A), (x_B, y_B)\Big) \tag{2.3}$$

Here (x_A, y_A) and (x_B, y_B) represent the x- and y-coordinates of transmitter A and receiver B. We use this notation throughout this chapter. Note that the parameter settings of the Log-Normal Shadowing Model (P_{d_0}, n and X_σ) influence the packet delivery rate over distance. For simplicity, we assume that these parameters are known a priori as in most connectivity-based algorithms. The values of these parameters could be determined by performing calibration measurements ([13]).

2.4 Estimating Distances and Probabilities

This section shows how COM-LOC++ converts the information obtained during the communication phase (Section 2.2) into distance estimates and associated probabilities using the Log-Normal Shadowing Model described in Sec-

tion 2.3. The estimates and associated probabilities are used for estimating the position of the blind node.

2.4.1 One- and Two-Hop-Away Reference Nodes

For completeness, we show how we convert information components 1 and 2 into a probability over distance distribution. We use Equation 2.3 to calculate the probability over distance distribution that blind node B hears reference node A:

$$P(\text{B hears A}|d_{A,B}) \tag{2.4}$$

We use Equation 2.4 to calculate the probability over distance distribution that blind node B does not hear reference node A (two-hop-away reference node information):

$$P(\text{B does not hear A}|d_{A,B}) = 1 - P(\text{B hears A}|d_{A,B}) \tag{2.5}$$

2.4.2 Communication via Blind Nodes

We are interested in the probability that reference node A can communicate indirectly with blind node B via nr_{ref} blind nodes as a function of the distance between reference node A and blind node B (information component 3 defined in Section 2.2):

$$P(B \text{ hears } A \text{ via } \text{nr}_{\text{ref}} \text{ nodes}|d_{A,B}) \tag{2.6}$$

Before we calculate the probability distribution associated with Equation 2.6, we first calculate the probability distribution involving one blind node. We call this blind node C:

$$P(B \text{ hears } A \text{ via 1 blind node}|d_{A,B}) = \int_{-\infty}^{\infty}\int_{-\infty}^{\infty} P\Big((x_A, y_A), (x_C, y_C)\Big) \cdot P\Big((x_C, y_C), (x_B, y_B)\Big) dx_C dy_C \tag{2.7}$$

Here (x_A, y_A) is the position of reference node A, (x_B, y_B) is the position of blind node B, (x_C, y_C) is the position of blind node C that forwards the broadcasted message of the reference node. For simplicity, we set the reference node position to $(x_A = 0, y_A = 0)$. We set the position of blind node B to $(x_B = d_{A,B}, y_B = 0)$. The position $((x_C, y_C))$ of blind node C is unknown, so we have to accumulate the probabilities over the localization space where blind node C resides. As nodes A and B can have arbitrary positions, this does

Figure 2.3: Monte Carlo Simulations: Position and Distance Distribution

not change the probability over distance distribution. Equation 2.7 does not normalize the probabilities, as we are only interested in the probability distributions and not in the absolute probabilities.

To our knowledge, Equation 2.7 does not have a closed-form solution. We approximate the probability over distance distribution using Monte Carlo Simulations (MCS). The MCS represent the position distribution of blind node C by drawing samples. We implement a grid-based sampling approach to ensure an uniform distribution and thus an equal influence per square meter on the final probability over distance distribution. Blind node C lies within transmission range from node A, so that we draw samples that lie within the transmission range from node A. We represent this set of possible blind node positions by: FORW. Figure 2.3 shows an example of an implementation of the MCS. The distance distribution of blind node B is represented by circles, and the position distribution of blind node C is represented by crosses.

We use Equation 2.2 for estimating probabilities between individual samples:

$$P(B \text{ hears } A \text{ via } C \in \text{FORW}|d_{A,B}) = \\ P(C \in \text{FORW hears } A|d_{A,C}) \cdot P(B \text{ hears } C \in \text{FORW}|d_{C,B}) \quad (2.8)$$

Here, C is a possible blind node position and an element in FORW. We use Equation 2.8 for estimating the probability that blind node B hears reference node A via one blind node (Equation 2.7):

$$P(B \text{ hears } A \text{ via } FORW|d_{A,B}) = \sum_{C \in \text{FORW}} P(B \text{ hears } A \text{ via } C \in \text{FORW}|d_{A,B}) \quad (2.9)$$

We use Equation 2.9 for estimating the probability that blind node B hears reference node A via nr_{ref} blind nodes (Equation 2.6):

$$P(B \text{ hears } C \text{ via } \text{nr}_{\text{ref}} \text{ nodes}|d_{A,B}) = \\ \prod_{i=1}^{nr} P(B \text{ hears } A \text{ via FORW}|d_{A,B}) \quad (2.10)$$

2.4.3 Heard and Not Heard Blind Nodes

Information component 4 is described by:

$$P(B \text{ did NOT hear } A \text{ via } nr_{\text{total}} - nr_{ref} \text{ nodes}|d_{a,b}) \quad (2.11)$$

Note that the probabilities defined in Equations 2.6 and 2.11 are independent. Hence, both information components are processed by multiplying the calculated probabilities. We use a similar method as described in the previous section to approximate this probability. We draw samples (Monte Carlo Simulations) as shown in Figure 2.3 to represent the position and distance distribution. We use Equation 2.2 for estimating probabilities between individual samples:

$$P(B \text{ did NOT hear } A \text{ via } C \in \text{FORW}|d_{A,B}) = \\ P(C \in \text{FORW did NOT hear } A|d_{A,C}) \cdot P(B \text{ hears } C \in \text{FORW}|d_{C,B}) \quad (2.12)$$

We use Equation 2.12 for estimating the probability that blind node B did not hear reference node A via one blind node:

$$P(B \text{ did NOT hear } A \text{ via FORW}|d_{A,B}) = \sum_{C \in \text{FORW}} P(B \text{ did NOT hear } A \text{ via } C \in \text{FORW}|d_{A,B}) \quad (2.13)$$

Note that we assume that blind node B hears blind node C via another reference node than reference node A. We use Equation 2.13 for estimating the probability that blind node B did not hear reference node A via $nr_{\text{total}} - nr_{ref}$ blind nodes (Equation 2.11):

$$P(B \text{ did NOT hear } A \text{ via } nr_{TOTAL} - nr_{ref} \text{ blind nodes}|d_{A,B}) = \prod_{i=1}^{nr} P(B \text{ did NOT hear } A \text{ via FORW}|d_{A,B}) \quad (2.14)$$

Hence, we assume that the calculated probabilities are independent. Figure 2.4 shows Equation 2.14 as a function of the distance between reference node A and blind node B for the following Log-Normal Shadowing Model parameter settings: $n = \{3.5\}$, $\sigma_{dBm} = \{6\}$ and $P_{d0} = \{-40\}$ and different nr_{TOTAL} and nr_{ref} settings.

2.4.4 Final Probability over Distance Distribution

We assume that the calculated probabilities associated with information components $1 \ldots 4$ are independent. Hence, the final probability over distance distribution is calculated by multiplying these probabilities:

- one-hop-away reference nodes ($s \in S$):

$$P(\text{B hears } s \in S|d_{s,B}) \cdot P(B \text{ hears } s \text{ via } nr_{ref} \text{ blind nodes}|d_{s,B}) \cdot P(B \text{ did NOT hear } s \text{ via } nr_{TOTAL} - nr_{ref} \text{ blind nodes}|d_{s,B}) \quad (2.15)$$

- two-hops-away reference nodes ($t \in T$):

$$(1 - P(\text{B hears } t \in T|d_{t,B})) \cdot P(B \text{ hears } t \text{ via } nr_{ref} \text{ blind nodes}|d_{t,B}) \cdot P(B \text{ did NOT hear } t \text{ via } nr_{TOTAL} - nr_{ref} \text{ blind nodes}|d_{t,B}) \quad (2.16)$$

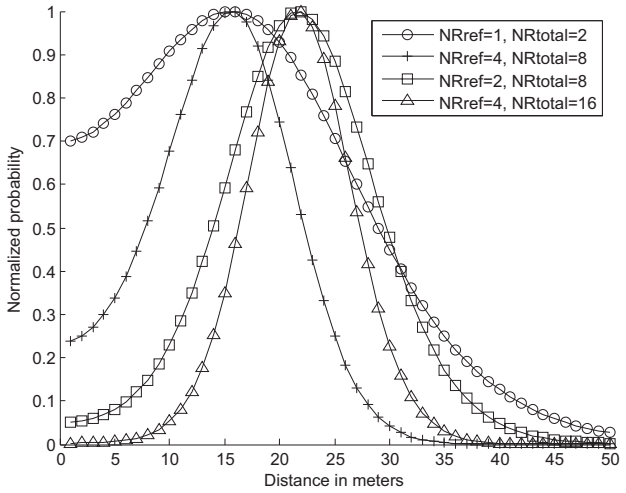

Figure 2.4: Example Probability over Distance Distribution

The required computations, described in Sections 2.4.1, 2.4.2 and 2.4.3 are too expensive to run on a blind node with limited computational capabilities. We calculate the outcome of Equations 2.4, 2.9 and 2.13 (for $nr_{ref} = 1$) before deployment. Blind nodes store the results of these calculations in a table with a user defined distance resolution. This implementation strategy significantly reduces the computational complexity, being linear for the required computations on the blind node. [16] calculates similar probabilities for an RSS range-based localization system. In this case, the blind nodes calculate the probabilities and the computational costs increase exponentially with an increasing number of heard nodes.

2.4.5 Numerical Analysis and Discussion

Increasing the number of heard and not heard nodes makes the probability over distance distribution steeper. Figure 2.4 shows two illustrations of this observation. A steeper probability distribution means that the distance estimate becomes more accurate. The number of heard and not heard blind nodes depends on the node density within a wireless network. Hence, the localization performance increases with increasing node density, which is verified in

Section 2.6.

2.5 Connectivity-based Localization Algorithm

This section describes how COM-LOC++ estimates a position using the probability over distance distributions described in Section 2.4. As in [11], COM-LOC++ implements a grid-based Monte Carlo Localization approach. An overview of Sequential Monte Carlo methods can be found in [4]. COM-LOC++ consists of two phases:

- The "prediction phase" draws samples that represent the position distribution.
- The "filtering phase" weights the samples drawn in the prediction phase in line with the observations.

COM-LOC limits the x- and y-coordinates of the position distribution on the basis of the calculated probability over distance distributions. We use this information to make a bounding box (as in [7]) and to keep the computational costs as low as possible. In the prediction phase we draw samples within the bounding box. After the prediction phase, we filter and weight the samples by multiplying the computed probabilities as described in Section 2.4.

2.6 Simulations

This section analyzes the localization performance of COM-LOC++. In addition, we compare COM-LOC++ with COM-LOC([17]), ecolocation ([14]) and a modified version of the MLE described in [13] and [17]. Ecolocation only processes one-hop information, so that it requires less communication than the other localization systems. We do not consider known connectivity-based localization systems such as DV-HOP ([5]), because they cannot cope with the varying transmission ranges introduced by the Log-Normal Shadowing Model ([17]).

2.6.1 Set-up

The set-up parameters are:

- The surface area is $100 \times 100\ m$.

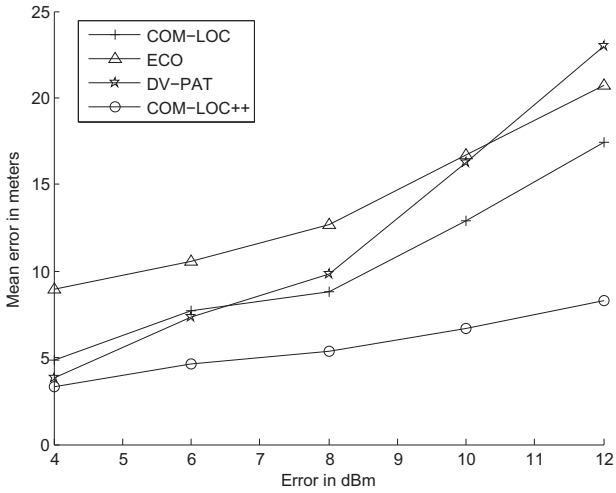

Figure 2.5: Mean error as a function of σ_{dBm}

- The simulations simulate RSS by using the model described in Equation 3.1. In general, the following parameter values are used: $\{P_{d_0} = -40$ dBm$, n = 3.5, \sigma_{dBm} = 6\}$.
- 36 reference nodes are randomly and uniformly placed over the surface area.
- 400 blind nodes are randomly and uniformly placed over the surface area.
- The localization performance is given as the mean over 25 runs.

2.6.2 Comparison with Other Localization systems

This subsection analyzes the performance as a function of σ_{dBm}, as σ_{dBm} defines the performance of RSS-based localization systems. We express the performance in terms of two statistical quantities:

- The average positioning error, which we define as the localization performance.

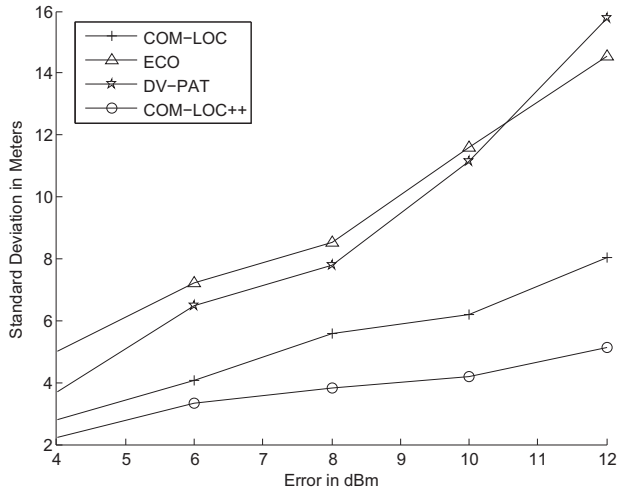

Figure 2.6: Standard deviation as a function of σ_{dBm}

- The standard deviation of the localization error, which we interpret as the localization stability.

Typical values of σ_{dBm} are between 6 and 12 dBm ([2]). For completeness, we evaluate the RSS-based localization systems with σ_{dBm} values between 4 and 12 dBm. Figures 2.5 and 2.6 show the localization error and stability as a function of σ_{dBm}. These figures show that COM-LOC++ outperforms COM-LOC and existing RSS-based localization systems in terms of localization performance and stability:

- COM-LOC++ increases the localization performance by $30 \ldots 50\%$ and the localization stability by $20 \ldots 40\%$ in comparison with COM-LOC. These results clearly show that the extra information processed by COM-LOC++ significantly increases the performance of COM-LOC.

- COM-LOC++ increases the localization performance by $15 \ldots 65\%$ and the localization stability by $40 \ldots 65\%$ in comparison with DV-PAT and ECOLOCATION. Note that DV-PAT and ECOLOCATION both use RSS measurements, while both COM-LOC++ and COM-LOC only use connectivity information.

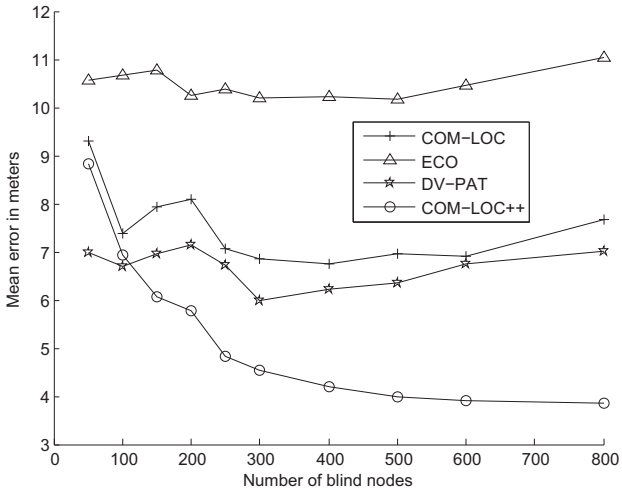

Figure 2.7: Mean error as a function of node density

Moreover, DV-PAT has 5 to 22% smaller localization error than COM-LOC with small values of σ_{dBm} ($\sigma_{dBm} = 4$ to 6 dBm), nevertheless COM-LOC has a significant better localization stability than DV-PAT with these small values of σ_{dBm} (25 to 50%).

2.6.3 Node Density

This subsection analyzes the localization performance as a function of the blind node density, as we expect that the node density influences the localization performance of COM-LOC++ (Section 2.4.5). Figure 2.7 and 2.8 show this functional dependence on the node density. These figures show that:

- The localization performance of COM-LOC++ increases with an increasing node density. We refer to Section 2.4.5 for an explanation.
- The localization stability of COM-LOC increases with an increasing node density.
- The localization performance of COM-LOC, DV-PAT and ECOLOCATION remain more or less equal with increasing node density.

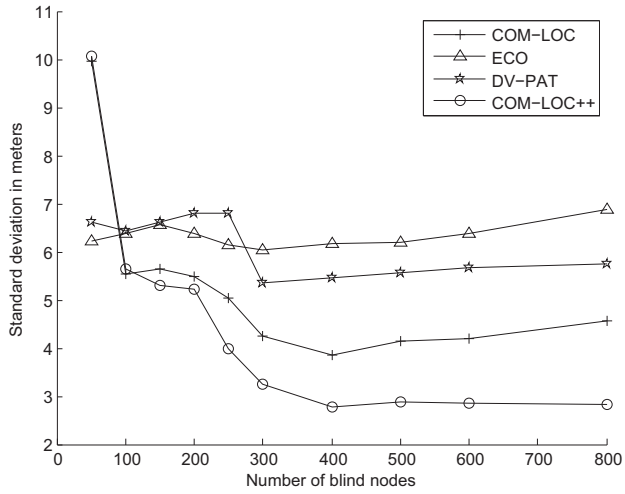

Figure 2.8: Standard deviation as a function of node density

- The localization stability of DV-PAT and ECOLOCATION remain more or less equal with increasing node density.
- DV-PAT performs slightly better than COM-LOC++ with a low node density (50 to 100 blind nodes).

In addition, these figures show that COM-LOC++ increases the localization performance by 45% and increases the localization stability by 40% in a wireless network with a high node density.

2.7 Conclusion

We introduced a new distributed connectivity-based localization system called COM-LOC++, which processes a new type of information. COM-LOC++ optimizes the localization performance for a communication protocol commonly employed by localization systems called sum-dist. Simulations show that the use of this new type of information increases the performance by 30% to 50% relative to its predecessor. In addition, comparative simulations of COM-LOC++

with two RSS-based localization systems show that COM-LOC++ performs 15 to 65% better than these localization systems over a wide range of conditions.

Bibliography

[1] Hashemi H.: The indoor radio propagation channel, Proc. IEEE, July 1993, pp. 943- 996.

[2] Rappaport T.S., Wireless Communication: Principles and Practice, Prentice Hall, ISBN 013 3755633, 1996.

[3] F.Dellaert, D.Fox, W.Burgard, S.Thrun: Monte Carlo Localization for Mobile Robots. IEEE International Conference on Robotics and Automation (ICRA). May 1999.

[4] A.Doucet, S.Godsill, C.Andrieu: On Sequential Monte Carlo Sampling Methods for Bayesian Filtering. Statistics and Computing. Volum 10, pp. 197-208. 2000.

[5] D.Niculescu, B.Nath: Ad hoc positioning systems. In: IEEE Globecom 2001, San Antonio. 2001.

[6] T.He, C.Huang, B.M.Blum, J.Stankovic, T.Abdelzaher: Range-free localization schemes for large scale sensor networks. MobiCom, San Diego, California, September 2003, pp. 81-95.

[7] Koen Langendoen and Niels Reijers: Distributed localization in wireless sensor networks: A quantitative comparison. In Computer Networks (Elsevier), special issue on Wireless Sensor Networks, 2003.

[8] Y. Shang, W. Ruml, Y. Zhang and M. Fromherz: Localization From Mere Connectivity. MobiHoc'03, Annapolis, Maryland, June 2003.

[9] R.Nagpal, H.Shrobe, J.Bachrach: Organizing a Global Coordinate System from Local Information on an Ad Hoc Sensor Network. 2nd International Workshop on Information Processing in Sensor Networks (IPSN). April 2003.

[10] Yi Shang and Wheeler Ruml: Improved MDS-based localization. In Infocom 2004

[11] L.Hu, D.Evans: Localization for Mobile Sensor Networks. Tenth Annual International Conference on Mobile Computing and Networking (MobiCom 2004), USA. 2004.

[12] S.Dulman, P.Havinga: Statistically enhanced localization schemes for randomly deployed wireless sensor networks. DEST International Workshop on Signal Processing for Sensor Networks, Australia. 2004.

[13] N.Patwari: Location estimation in sensor networks. Thesis of Neal Patwari at University of Michigan, 2005.

[14] K.Yedavalli, B.Krishnamachari, S.Ravula, and B.Srinivasan: Ecolocation: A sequence based technique for RF-only localization in wireless sensor networks. In IEEE IPSN 2005, April 2005.

[15] B.Dil, S.Dulman, and P.J.M.Havinga: Range-based localization in mobile sensor networks. In Third European Workshop on Wireless Sensor Networks, volume 3868 of Lecture Notes in Computer Science, Zurich, Switzerland, Feb. 2006. Springer.

[16] Rong Peng, Mihail L. Sichitiu: Probabilistic Localization for Outdoor Wireless Sensor Networks. ACM SIGMOBILE Mobile Computing and Communications, Volume 11, Issue 1, January 2007, pp. 53-64.

[17] B.J.Dil, P.J.M.Havinga: COM-LOC: A Distributed Range-Free Localization Algorithm in Wireless Networks. In: Proceedings of the 5th International Conference on Intelligent Sensors, Sensor Networks and Information Processing (ISSNIP), 7-12-2009, Mellbourne, Australia. pp. 457-462.

[18] B.J.Dil, P.J.M.Havinga: On the Calibration and Performance of RSS-based Localization Methods. Internet of Things 2010, Tokyo.

[19] B.J.Dil, P.J.M.Havinga: COM-LOC++ A distributed range-free localization algorithm in wireless networks. ISSNIP 2010, 7-10 December, Australia. pp. 157-162.

CHAPTER 3

RSS-based Self-Adaptive Localization in Dynamic Environments

This chapter focuses on optimal and automatic calibration of the propagation model of Received Signal Strength (RSS) based localization systems. Conventional RSS-based localization systems assume that optimal calibration of the propagation model is hardware- and space-invariant, so that the propagation model is identical for all nodes distributed over localization space. Such systems also assume that these calibration settings do not change between calibration rounds. Real environments are dynamic and continuously changing. In these environments, each individual node should estimate its own optimal propagation model settings dependent on the node's hardware and location. We call this process Self-Adaptive Localization (SAL). SAL systems estimate the parameter settings from available localization measurements. Such systems perform these localization measurements in the order of tens of milliseconds so that the environmental dynamics can be considered as static. We show that existing SAL systems can be significantly improved in terms of localization performance and stability. Our main contribution is that we determine the conditions under which SAL systems provide such optimal calibration settings each time an individual node localizes itself. Such conditions are shown to be constraints on the localization surface and radiation conditions on all nodes. As antenna orientations have a significant impact on RSS, we evaluate SAL in an environment where each node has an unknown antenna orientation. Our measurements and simulations show that our constrained SAL systems increase the localization performance by roughly 65% and the localization stability by about 75% compared to the conventional approach where each node has the same calibration settings.
[1]

[1] This chapter is partially published in [21], [22] and [25].

3.1 Introduction

In range-based RSS localization, the position estimate shows up as a parameter in the propagation model. These propagation models are mathematical representations of far-field solutions of the respective Navier-Stokes or Maxwell equations, depending on whether the network is based on the propagation of acoustic or electromagnetic waves. Mathematically, localization then reduces to calculating the field energies at the unknown location of the receiving antenna radiated from an antenna array at known positions. When the antenna array is large enough and the propagation model adequately represents the radiation in the environment, localization reduces to a set of non-linear equations for the position estimates and possible other parameters used in the propagation model. These other parameters are aimed to account for reflection, refraction, diffraction, and absorption effects in the environment. RSS-based localization usually employs the empirical Log-Normal-Shadowing model as the propagation model ([1]).

We identify the following four RSS-based localization systems: fingerprinting (e.g. [3]), range-based (e.g. [4]), range-free (e.g. [5]) and proximity-based (e.g. [10]) localization. Recent studies show that range-based localization outperforms other RSS-based localization systems in static LOS environments ([22]), and provides similar results in environments with an unknown antenna orientation ([21]). However, the current calibration approach cannot deal with unknown variables that influence RSS ([21]). This chapter aims to resolve that shortcoming.

3.1.1 Problem Description

This chapter deals with the general challenge of RSS-based localization systems to properly account for the dynamic influence of the changing environment on the signal strength. Propagation models used by RSS-based localization systems introduce parameters to capture environmental influences and hardware differences. The performance of localization systems depends on how well such parameters are able to capture these influences both locally and over time:

- How much do these calibration settings vary over localization space?
- How fast can calibration and localization measurements be taken relative to the time of change of the environment?

Several practical examples that show evidence of this influence on the propagation model show up in the literature and are given below:

- Antenna orientation: [21] reports that the received signal strength may vary a factor 32 under different antenna orientations (16 dBm).
- Elevation from ground: [15] reports that the signal strength may decay 17% faster at different elevated levels from the floor (6 to 30 cm elevation).
- Materials in environment: [15] reports that the signal strength may decay 32% faster with higher grass (6 to 30 cm grass).

Other examples that influence the signal strength are reflections, moving obstacles, temperature and humidity. In this chapter, we focus on capturing the influence of unknown antenna orientations. We expect that other space-varying influences, as mentioned in [15], can be captured in a similar matter. We assume that these influences are static during the localization measurements as the measurement time is in the order of tens of milliseconds.

In general, it is difficult to estimate the optimal parameter settings in an automated way for each time a node localizes itself. In theory, the optimal values of these parameters depend on the locally varying electromagnetic permittivity and permeability of localization space. In other words, the propagation model needs to account for local changes in the localization environment. Conventional RSS-based localization systems assume that there exists one optimal propagation model that is identical for all nodes. In principle, such a uniform propagation model cannot account properly for the local spatial influences in the environment.

In a more realistic model, each node should estimate its own optimal parameter settings dependent on the node's hardware and location. We call this process Self-Adaptive Localization. SAL applies multivariate propagation models, so that it adapts to the local spatial influences in the environment. This chapter reviews and improves several new and existing distributed Self-Adaptive Localization systems.

3.1.2 Conventional Versus Self-Adaptive Localization Approach

Conventional localization systems estimate the optimal values of the propagation model parameters by performing calibration measurements (see Figure 3.1). The parameters calculated from calibration measurements are usually called "nuisance parameters" as they only serve to help estimating the

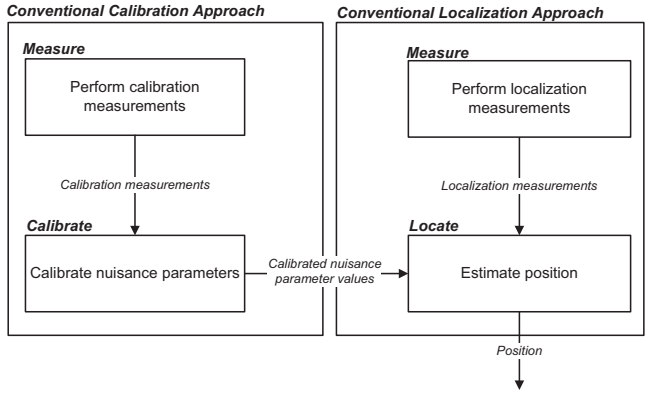

Figure 3.1: Conventional Approach

unknown positions of the blind nodes. This calibration is said to take place in the "Conventional Calibration Approach" phase. During the second phase, the "Conventional Localization Approach" phase, the position of the blind node is estimated using the calibrated nuisance parameters as well as the localization measurements. The conventional localization approach characterizes itself by the clear distinction between these two phases. Calibration measurements are only used for calibrating the nuisance parameters; localization measurements are only used for estimating the position. The clear separation of these two phases implies that:

In conventional localization approaches, the optimal calibration settings do not change locally and over time until the next calibration round.

Hence, the optimal calibration settings are assumed to be equal for each node and static between calibration rounds. This holds in *static environments*.

In this chapter, we propose the "Self-Adaptive Localization (SAL) Approach" (see Figure 3.2) that continuously adapts to a dynamic environment. The main difference with the "Conventional Localization Approach" is that the "SAL Approach" uses localization measurements for both estimating the "nuisance parameters" as well as for estimating the position of the nodes (see "Estimate nuisance parameter values" in Figure 3.2). This implies that the "SAL Approach" updates the calibration settings every time a node estimates its position. As a result:

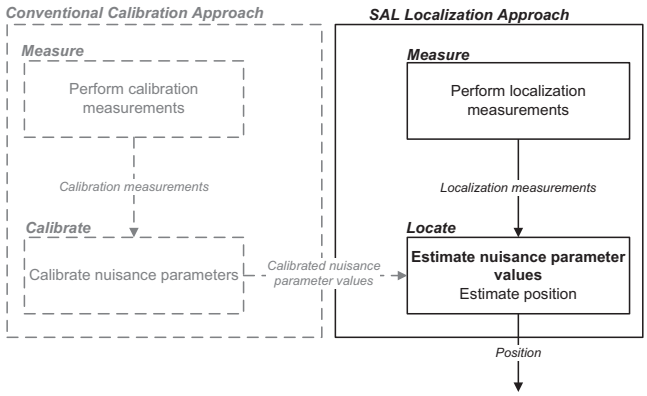

Figure 3.2: SAL Approach

The SAL approach allows that the optimal calibration settings vary over space and time, and are assumed to be static during the localization measurements.

The idea of estimating nuisance parameters on the basis of localization measurements is not new in the field of RSS-based localization using radio signals ([13] and [16]) or acoustic signals ([9] and [17]). However, it has not been applied in dynamic environments. RSS-based localization measurements only take milliseconds. Compared to the conventional approach, SAL requires less or no online/offline calibration measurements. The broken grey line in Figure 3.2 indicates this improvement.

3.1.3 Contributions

The three main contributions of this chapter are:

1. This chapter contains a short review of existing RSS-based conventional ([8]) and SAL localization systems ([9], [13], [16], [17], [18] and [19]). We analyze these localization systems and show their similarities and differences.

2. SAL systems estimate the propagation model settings using localization measurements. In other words, SAL increases the number of unknowns

while evaluating the same amount of measurements as conventional localization systems. We show that this decreases the localization performance and stability. We analyze the behavior of existing SAL systems and determine under which conditions these localization systems provide the best and most reliable results. We then apply these conditions as constraints on the localization systems. These constraints limit the boundaries of the localization surface by assuming that the blind nodes are located within the convex hull of the reference node positions. This constraint increases the localization performance by roughly $\sim 40\%$ and the localization stability by about $\sim 65\%$ in static environments.

3. We evaluate the performance of existing and our constrained conventional and SAL systems in an environment with unknown antenna orientations. These measurements show that our constrained SAL systems increase the localization performance by 65% and stability by 75% in comparison with an optimally calibrated conventional localization system. In addition, our constrained SAL systems increase the localization performance by 45% and stability by 70% in comparison with existing SAL systems.

This chapter is organized as follows. After formalizing the localization setup in Section 3.2, Section 3.3 classifies the conventional and SAL systems. Section 3.4 describes how the constraints significantly improve the performance of existing SAL systems. In addition, Section 3.4 compares the performance of conventional and SAL systems. Section 3.5 summarizes the results.

3.2 Model Formulation and Setup

This section first provides a formal description of the localization setup. The second section describes the model of the signal strength over distance decay and its limitations. In addition, it describes the measurement setup used throughout this chapter. The last section describes the model of the signal strength over distance decay used in the field of acoustic signal-based localization ([9] and [17]) and its similarity with the model used in radio signal-based localization ([13], [16] and [19]).

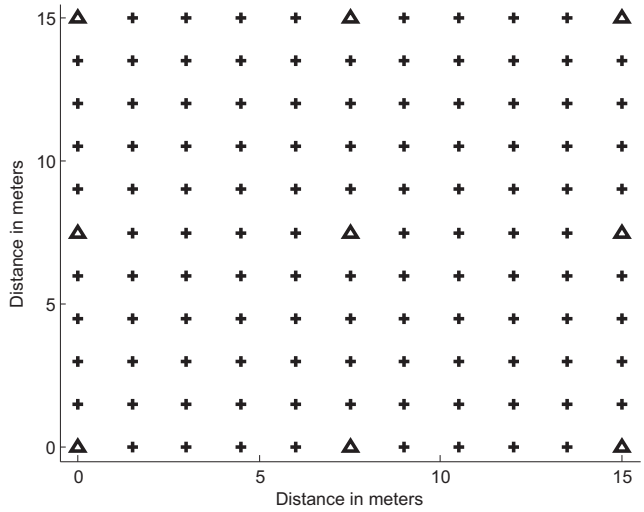

Figure 3.3: Measurement setup

3.2.1 Localization Definition

Consider a wireless network that consists of N reference nodes and M blind nodes:

- **Reference nodes** know their positions in advance. We identify the positions of the N reference nodes by: $(x_1, y_1) \dots (x_N, y_N)$.
- **Blind nodes** do not know their locations and require localization. We identify the positions of the M blind nodes by: $(x_{N+1}, y_{N+1}) \dots (x_{M+N}, y_{M+N})$.

Our aim is to position blind nodes using signal strength measurements from several reference nodes. We do not evaluate signal strength measurements between blind nodes (like in [4] and [12]). We use the following variables to identify individual nodes and RSS measurements:

- j represents the identification number of the jth blind node.
- i represents the identification number of the ith reference node.
- $P_{i,j}$ represents the RSS measurement between reference node i and blind node j.

- H_j represents the set of reference nodes heard by blind node j. This set consists of the identification numbers of these reference nodes.

Figure 3.3 shows the measurement setup. The nine triangles represent the reference nodes ($N = 9$); the 112 crosses represent the blind nodes ($M = 112$).

3.2.2 Log-normal Shadowing Model and Measurement Setup

We adopt the Log-Normal Shadowing Model (LNSM) for modeling the signal strength over distance decay. This empirical model is widely used by RSS-based localization estimators (e.g. [4], [12] and [14]) and has shown to be a reasonable representation of reality ([2]). The Log-Normal Shadowing Model assumes that RSS follows a log-normal distribution. A log-normal distribution is a continuous distribution in which the logarithm of the variable follows a normal distribution. This means that:

- The average received signal strength decreases logarithmically over distance.
- The received signal strength follows a normal distribution at a certain distance.

The following formula represents the Log-Normal Shadowing Model ([1]):

$$P_d = P_{d_0} - 10 \cdot n \cdot \log_{10}(\frac{d}{d_0}) + X_\sigma \tag{3.1}$$

Here:

- P_d represents the received signal strength in dBm at distance d.
- P_{d_0} represents the received signal strength in dBm at reference distance d_0, which we call the "Reference RSS". In general, d_0 is relatively small. For simplicity, we assume that d_0 equals 1 meter (see [2]).
- n represents the Path Loss Exponent (PLE). The path loss exponent represents the rate at which the path loss increases with distance.
- X_σ represents the standard deviation of the received signal strength due to shadowing effects and is invariant with distance ([2]). X follows a zero-mean normal distribution with standard deviation σ:

$$X \sim N(0, \sigma^2) \tag{3.2}$$

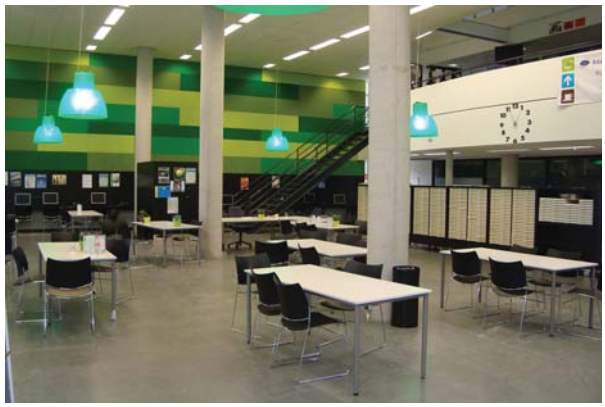

Figure 3.4: Measurement environment

Figure 3.5: radios

Even though this empirical model is widely accepted and has shown to be useful, it is important to note that it has some limitations. Three major sources of error are interfering effects, shadowing ([1]) and hardware inaccuracies ([6] and [7]). Multiple signals with different amplitudes and phases add constructively or destructively to the RSS, causing frequency-selective destructive and constructive interference. The error caused by such interfering effects is usually minimized by performing RSS measurements over a relatively large frequency band. The remaining errors in RSS measurements are caused by shadowing. Shadowing is the attenuation of a signal due to obstructions, also called medium-scale fading ([1]).

We performed two sets of measurement rounds on each blind node location (Figure 3.3) in which the blind node had a vertical or a horizontal antenna orientation. Figure 4.13 shows the measurement environment. Figure 4.14 shows two CC2430 radios, equipped with standard 2.4 GHz dipole antennas (e.g. [24], which shows a typical radiation pattern). One radio has a horizontal antenna orientation and the other radio has a vertical antenna orientation. In this measurement setup, the reference nodes have a vertical antenna orientation, and the blind node measures the RSS with a vertical and a horizontal antenna orientation at the 112 blind node positions shown in Figure 3.3. Parallel antenna orientations (vertical/vertical) optimize reception and perpendicular or crossed antenna orientations (vertical/horizontal) minimize reception. During each measurement round, the blind node performs 100 consecutive RSS measurements at 38 different frequencies in the $2406 \ldots 2480$ MHz band. The

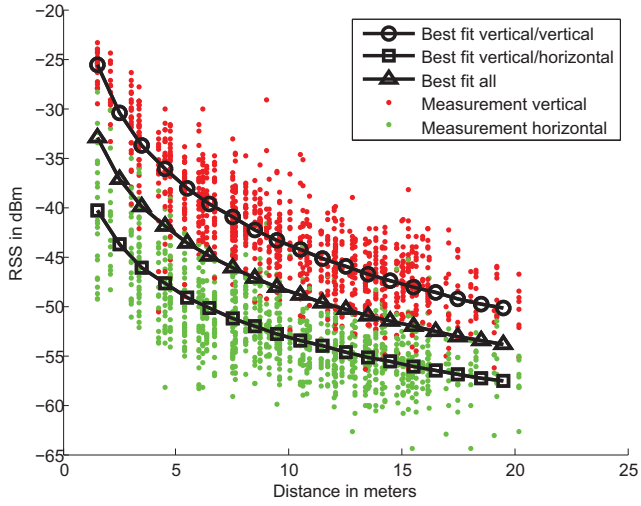

Figure 3.6: RSS over distance distribution

mean RSS over these 38 frequencies is used as input for the calibration phase and localization systems. We perform RSS measurements over the total available free bandwidth in the 2.4 GHz to ensure optimal localization performance (e.g. [20]). Figure 3.6 shows the Log-Normal Shadowing Model fitting these RSS measurements. The red dots represent individual RSS measurements with a vertical/vertical antenna orientation (best reception); the green dots represent individual RSS measurements with a vertical/horizontal antenna orientation (worst reception). There are three fits that minimize the squared residual between the measured and estimated RSS using the Log-Normal Shadowing Model:

- The curve that fits the measurements made with parallel antenna orientations (vertical/vertical). The parameter values of this fit are: $\{P_{d_0} = -21.6 \text{ dBm}, n = 2.2, \sigma_{dBm} = 3.2 \text{ dBm}\}$.
- The curve that fits the measurements made with perpendicular antenna orientations (vertical/horizontal). The parameter values of this fit are: $\{P_{d_0} = -37.6 \text{ dBm}, n = 1.5, \sigma_{dBm} = 3.4 \text{ dBm}\}$.
- The curve that fits all measurements. The parameter values of this fit are: $\{P_{d_0} = -29.6 \text{ dBm}, n = 1.9, \sigma_{dBm} = 5.9 \text{ dBm}\}$.

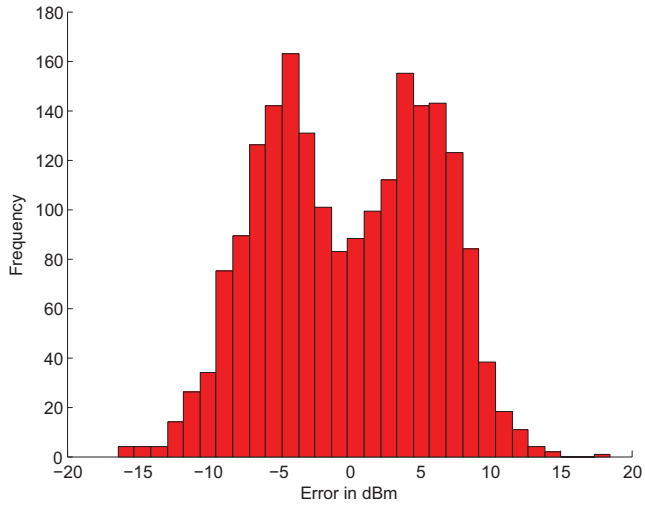

Figure 3.7: Error distribution, log-normal shadowing model

These parameters settings are used as the reference calibration settings throughout this chapter.

Figure 3.7 shows the error distribution of the graph that fits all measurements. Figure 6 shows that the error distribution consists of two normal distributions. This is because the graph that fits all measurements fits two different Log-Normal Shadowing models, each of which is identified by a certain antenna orientation. The measurements verify that RSS is significantly decreased by perpendicular antenna orientations, the reference RSS (P_{d_0}) is decreased by a factor 32 (from -21.6 to -37.6 dBm). Moreover, the measurements show that the path loss exponent is decreased by 30% (from 2.2 to 1.5).

3.2.3 Acoustic Signal Propagation

For comparison, we present the acoustic signal strength over distance decay function used by SAL systems described in [9], [11] and [17]. The following formula represents the acoustic power decay model:

$$P_d = 10 \log \left(\frac{g \cdot S}{d^n} + \varepsilon_\sigma \right) \tag{3.3}$$

Here:

- S represents the transmission power in mW.
- g represents the gain of the microphones.
- ε_σ represents the error of the model. ε follows a μ-mean normal distribution with standard deviation σ:

$$\varepsilon \sim N(\mu, \sigma^2) \tag{3.4}$$

- [9], [11] and [17] assume that the path loss exponent equals $n = 2$.

For comparison, we rewrite the formula of the Log-Normal Shadowing Model:

$$P_d = 10 \log \left(\frac{10^{\frac{P_{d_0}}{10}}}{d^n} \cdot 10^{\frac{X_\sigma}{10}} \right) \tag{3.5}$$

We assume that $10^{\frac{P_{d_0}}{10}} = g \cdot S$. Hence, the main difference between the models is the error distribution. In the next section, we compare the acoustic-based SAL systems with the radio-based ones.

3.3 Maximum Likelihood Estimators

This section describes the Maximum Likelihood Estimators (MLE) of range-based localization systems. We first formulate a general MLE using the Log-Normal Shadowing Model ([4]). The MLE of a position estimate equals the position estimate that maximizes the probability using the probability density function of Equation 3.1. The MLE for blind node j equals:

$$\max_\theta \prod_{i \in H_j} \frac{1}{\sigma\sqrt{2\pi}} e^{\frac{(P_{i,j} - \hat{P}_{i,j})^2}{2\sigma^2}} \tag{3.6}$$

Here $\hat{P}_{i,j}$ represents:

$$\begin{aligned} \hat{P}_{i,j} &= P_{d_0} - 10 \cdot n \cdot \log_{10}(\frac{d_{i,j}}{d_0}) \\ d_{i,j} &= \sqrt{(x_i - \widehat{x_j})^2 + (y_i - \widehat{y_j})^2} \end{aligned} \tag{3.7}$$

In Equation 3.6 and 3.7:

- $d_{i,j}$ represents the distance between reference node i and the position estimate of blind node j.
- θ is the set of parameters that maximizes the optimization function (Equation 3.6). Note that θ always contains the position estimate, this means that: $\widehat{x_j} \in \theta$ and $\widehat{y_j} \in \theta$.

The Log-Normal Shadowing Model assumes that the variance remains constant over distance ([2]). Hence, after some algebra, Equation 3.6 reduces to:

$$\begin{aligned} &\min_{\theta} \sum_{i \in H_j} \left(P_{i,j} - \left(P_{d_0} - n \cdot 10 \cdot \log_{10}(\frac{d_{i,j}}{d_0}) \right) \right)^2 \\ =&\min_{\theta} \sum_{i \in H_j} (P_{i,j} - \widehat{P}_{i,j})^2 \end{aligned} \tag{3.8}$$

This equation represents the MLE in its most general form using the Log-Normal Shadowing Model. Note that it does not define:

- The values of the reference RSS (P_{d_0}) and the path loss exponent (n). This paper focuses on the calibration of these parameters.
- θ. In SAL implementations, the different definitions of θ define the difference between the conventional and SAL approach.

The following enumeration describes the MLEs of the conventional localization approach and six implementations of the SAL approach:

The **Conventional Localization Approach (LN-CON)** assumes that the optimal values of the reference RSS (P_{d_0}) and the path loss exponent (n) are known before minimizing Equation 3.8 (as in [4]):

$$\min_{\theta=\{\widehat{x}_j,\widehat{y}_j|P_{d_0}=\alpha,n=\beta\}} \sum_{i \in H_j} \left(P_{i,j} - \left(P_{d_0} - n \cdot 10 \cdot \log_{10}(\frac{d_{i,j}}{d_0}) \right) \right)^2 \tag{3.9}$$

α ($= P_{d_0}$) and β ($= n$) are the calibrated values of the Log-Normal Shadowing Model.

Reference RSS Self-Adaptive Localization (RR-SAL) estimates the reference RSS (P_{d_0}) on the basis of the localization measurements. Contrary to the conventional localization approach, RR-SAL assumes that the value of the reference RSS (P_{d_0}) is not known before minimizing Equation 3.8:

$$\min_{\theta=\{\widehat{x}_j,\widehat{y}_j,\widehat{P_{d_0}}|n=\beta\}} \sum_{i \in H_j} \left(P_{i,j} - \left(\widehat{P_{d_0}} - n \cdot 10 \cdot \log_{10}(\frac{d_{i,j}}{d_0}) \right) \right)^2 \tag{3.10}$$

Path Loss Exponent Self-Adaptive Localization (PLE-SAL) estimates the path loss exponent (n) on the basis of the localization measurements (as in [13]). Contrary to the conventional localization approach, PLE-SAL assumes that the value of the path loss exponent (n) is not known before minimizing Equation 3.8:

$$\min_{\theta=\{\widehat{x}_j,\widehat{y}_j,\widehat{n}|P_{d_0}=\alpha\}} \sum_{i\in H_j} \left(P_{i,j} - \left(P_{d_0} - \widehat{n} \cdot 10 \cdot \log_{10}(\frac{d_{i,j}}{d_0}) \right) \right)^2 \tag{3.11}$$

Log-Normal Self-Adaptive Localization (LN-SAL) estimates the reference RSS (P_{d_0}) and the path loss exponent (n) on the basis of the localization measurements (as in [16]). Contrary to the conventional localization approach, LN-SAL assumes that the value of the reference RSS (P_{d_0}) and the path loss exponent (n) are not known before minimizing Equation 3.8:

$$\min_{\theta=\{\widehat{x}_j,\widehat{y}_j,\widehat{P_{d_0}},\widehat{n}\}} \sum_{i\in H_j} \left(P_{i,j} - \left(\widehat{P_{d_0}} - \widehat{n} \cdot 10 \cdot \log_{10}(\frac{d_{i,j}}{d_0}) \right) \right)^2 \tag{3.12}$$

Path Loss Exponents Self-Adaptive Localization (PLEs-SAL) estimates the path loss exponents ($n_1 \ldots n_N$) on the basis of the localization measurements ([19]). Contrary to the conventional localization approach, PLEs-SAL assumes that the value of the path loss exponents ($n_1 \ldots n_N$) are not known before minimizing Equation 3.8:

$$\min_{\theta=\{\widehat{x}_j,\widehat{y}_j,\widehat{n}_1 \ldots \widehat{n}_N|P_{d_0}=\alpha\}} \sum_{i\in H_j} \left(P_{i,j} - \left(P_{d_0} - \widehat{n}_i \cdot 10 \cdot \log_{10}(\frac{d_{i,j}}{d_0}) \right) \right)^2 \tag{3.13}$$

Equation 3.13 does not define a unique position estimate, because the number of unknowns is larger than the number of measurements. Therefore, localization systems that estimate a different path loss exponent value per link require more information than the available measurements. [19] solves this problem by putting constraints on the estimated path loss exponents and changing the optimization function.

Self-Adaptive Fingerprinting-based Localization uses RSS differences between reference node pairs ([18]), instead of using RSS measurements from individual reference nodes. [18] shows that this approach copes with hardware differences between blind nodes. This is similar to calibrating the reference RSS every time the blind node localizes itself, as in RR-SAL. The difference is that [18] bases itself on fingerprints instead of a propagation model that describes

Type	Article	θ	Calibrated parameters
LN-CON	[4]	$\{x, y\}$	$\{P_{d_0}, n\}$
RR-SAL	This	$\{x, y, P_{d_0}\}$	$\{n\}$
PLE-SAL	[13]	$\{x, y, n\}$	$\{P_{d_0}\}$
LN-SAL	[16]	$\{x, y, P_{d_0}, n\}$	$\{\}$
PLEs-SAL	[19]	$\{x, y, n_1 \dots n_m\}$	$\{P_{d_0}\}$
Acoustic	[9]	$\{x, y, 10^{(P_{d_0}/10)}\}$	$\{n\}$

Table 3.1: Summary Conventional and SAL systems

the signal strength over distance decay (RR-SAL). We expect that Self-Adaptive fingerprinting systems require similar constraints as range-based SAL systems, because the Log-Normal Shadowing Model has shown to be a reasonable representation of reality (e.g. [2]).

Acoustic Self-Adaptive Localization calibrates the transmission power (S) on the basis of the localization measurements ([9], [11] and [17]):

$$\min_{\theta=\{\widehat{x}_j,\widehat{y}_j,\widehat{S}|n=\beta,g=\gamma\}} \sum_{i\in H_j} \left(p_{i,j} - \left(\frac{g \cdot S}{d^n}\right)\right)^2 \tag{3.14}$$

Here $p_{i,j} = 10^{\frac{P_{i,j}}{10}} - \mu$. Equation 3.14 calculates the transmission power ($\widehat{S}$) that minimizes the residual for a given position estimate, path loss exponent and antenna gain ($(\widehat{x}_j, \widehat{y}_j)$, n and g). This is similar to RR-SAL (Equation 3.10), however the error distributions are different (see Section 3.2.3).

Table 3.1 summarizes the characteristics of the MLE of the conventional and SAL approaches. The table columns represent the following:

- The "*type*" column contains the type of localization system.
- The "*Article*" column contains the references to the articles that describe these localization systems.
- The "θ" column contains the set of parameters that are estimated by the localization measurements.
- The "*Calibrated parameters*" column contains the set of parameters that are calibrated before localization.

LN-CON and RR/PLE/LN-SAL all use the propagation model in the same way. These localization systems assume that the reference RSS and the path loss exponent are equal for all links.

3.4 Constrained and Unconstrained Localization System Behavior

This section first analyzes the performance of RR/PLE/LN-SAL and compares them with their conventional counterpart (LN-CON). We use this analysis to determine the conditions under which these localization systems provide the best and most reliable results. We apply these conditions as constraints on the SAL systems. The last subsection evaluates the unconstrained and constrained conventional and SAL systems in a environment with unknown antenna orientations.

3.4.1 Measurement Setup

The measurement setup is equal to the setup described in Section 3.2.2, and we use the same parameter values for the Log-Normal Shadowing Model as determined in Section 3.2.2 for our simulations. We use the same measurements for calibration and localization, which ensures the best localization performance for the localization systems evaluated. We minimize Equations 3.9, 3.10, 3.11 and 3.12 using a brute force grid-based Monte-Carlo localization approach. Other approaches can be used, but this approach avoids local minima. We evaluate our localization systems by:

- **Simulations** provide a way to analyze the localization performance. We perform 1000 simulation runs per blind node position in Matlab.
- **Real Measurements** provide an indication for the localization performance in a real-world application. We perform two sets of localization measurements per blind node position (one set per antenna orientation).

We define the localization performance and stability as follows:

- The average positioning error, which we define as the localization performance.
- The standard deviation of the positioning errors, which we define as the localization stability.

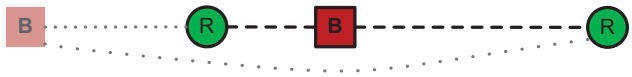

Figure 3.8: LN-CON and RR/PLE-SAL in one dimension

3.4.2 Performance and Behavior of Unconstrained Localization Systems

This section analyzes the costs of calibrating the nuisance parameters with localization measurements by first analyzing the behavior and then the performance of the unconstrained conventional and SAL systems. First, we analyze the behavior in the one-dimensional case and secondly, we analyze the two-dimensional case.

Consider the one-dimensional setup shown in Figure 3.8. In this setup, the blind node measures RSS from two reference nodes. The green circles represent reference nodes, the solid red box represents the blind node. Figure 3.8 shows that:

- LN-CON (Equation 3.9) calculates a unique position estimate represented by the solid red box.
- RR- and PLE-SAL (Equation 3.10) calculate two unique position estimates represented by the solid box and the transparent red box. Note that these two position estimates have different estimated propagation model settings. In the one dimensional case, one position estimate is always inside the convex hull of the reference nodes, and one position estimate is always outside the convex hull of the reference nodes.

This ambiguity is easily solved by measuring RSS from several reference nodes. In a real measurement setup, the number of available reference nodes is scarce and the ranging error is exponential (Equation 3.1). This means that SAL systems could pick the "wrong optimum", which decreases the performance significantly.

Figures 3.9 and 3.10 show the typical probability distribution of the position estimates over the localization surface at blind node position $(x = 3, y = 12)$ in a two dimensional case. The triangles represent the reference nodes; the black cross represents the real blind node position. White represents a probability of zero; blue represents a relatively low probability; red represents a relatively high probability. These figures show that the probability distribution of the

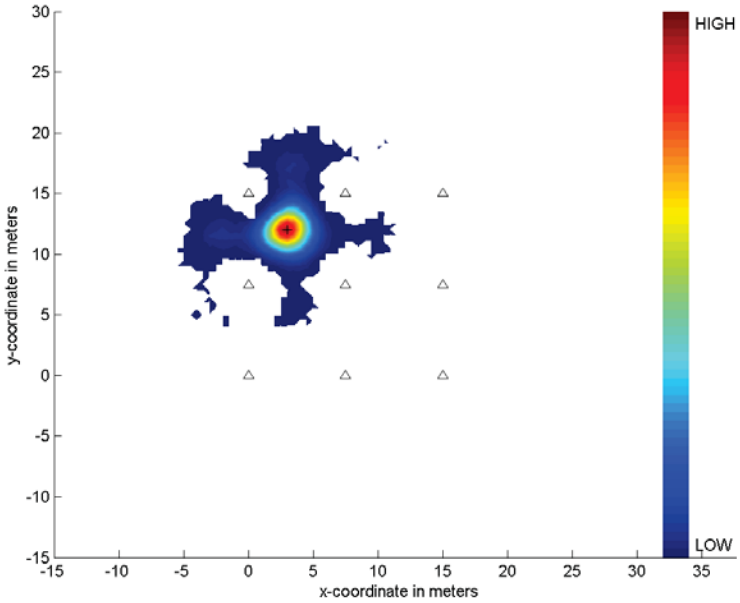

Figure 3.9: Position distribution of LN-CON calculated by simulations

position estimates of LN-SAL differs significantly from LN-CON. In addition, LN-SAL increases the localization error from 1.7 meters to 5.2 meters at blind node position $(x = 3, y = 12)$. We made two observations by analyzing an extensive amount of probability distributions of blind node positions that have a relatively high localization error:

1. The blind node positions within the convex hull tend to have large error slopes outside the convex hull, especially when estimated by the SAL systems. In Figure 3.10 the error slope is located at the north-west corner of the localization surface.

2. LN-SAL tends to have an asymptotic position distribution. Figure 3.10 shows that the asymptotic position distribution is located at the south-east corner of the localization surface. The estimated path loss exponents in the asymptotic position distribution have a negative value.

These observations in 2D localization space show that position estimates that are relatively far away from the actual position are located outside the convex

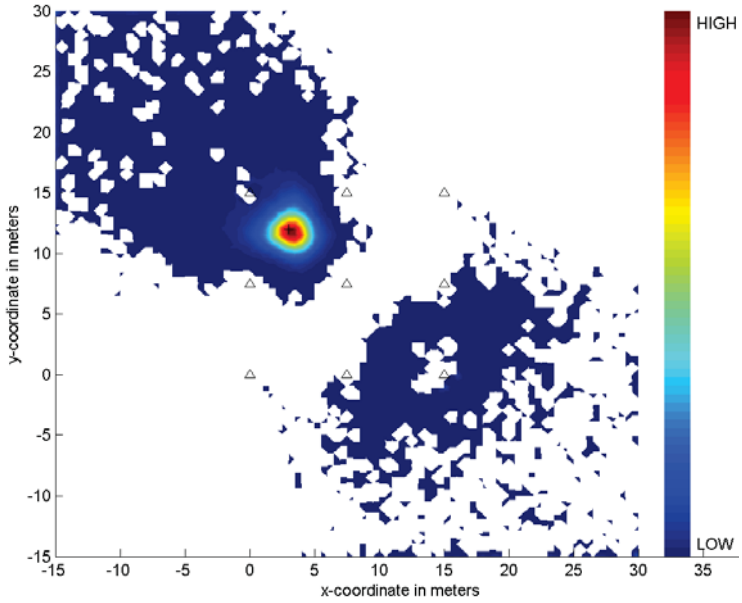

Figure 3.10: Position distribution of LN-SAL calculated by simulations

hull or have a negative path loss exponent. This is a similar finding that we observed in the one-dimensional case. We use these observations in the next subsection to constrain the conventional and SAL systems.

Tables 3.11 and 3.12 show the performance of the unconstrained conventional and unconstrained SAL systems, calculated by the simulations and observed by the real measurements. SIM is an abbreviation for simulations; REA is an abbreviation for real measurements; UNC is an abbreviation for unconstrained and CON is an abbreviation for constrained. These tables show that the localization performance decreases significantly as the number of unknowns increases, which is in line with the observations. Note that the performances obtained by simulations and real measurements are similar.

3.4.3 Performance of Constrained Localization Systems

In line with our empirical findings, we set constraints on the MLEs of the conventional and SAL systems. We diminish the error causes recognized in Section

Figure 3.11: Performance results simulations, unconstrained and constrained systems in static environment

Approach	**Approach Number**	**Antenna Orientation**	**MEAN SIM** UNC/CON	**STD SIM** UNC/CON
LN-CON	1	VER	1.59/1.37 m.	1.06/0.93 m.
RR-SAL	2	VER	2.14/1.42 m.	2.36/0.95 m.
PLE-SAL	3	VER	2.37/1.40 m.	2.98/0.93 m.
LN-SAL	4	VER	2.95/1.50 m.	4.14/0.97 m.
LN-CON	1	HOR	2.44/2.09 m.	1.71/1.47 m.
RR-SAL	2	HOR	3.53/2.12 m.	4.31/1.46 m.
PLE-SAL	3	HOR	3.22/2.14 m.	3.52/1.49 m.
LN-SAL	4	HOR	5.17/2.26 m.	6.51/1.59 m.

Figure 3.12: Performance results real measurements, unconstrained and constrained systems in static environment

Approach	**Approach Number**	**Antenna Orientation**	**MEAN REA** UNC/CON	**STD REA** UNC/CON
LN-CON	1	VER	1.53/1.39 m.	1.18/0.91 m.
RR-SAL	2	VER	1.98/1.40 m.	2.00/0.90 m.
PLE-SAL	3	VER	2.27/1.41 m.	2.60/0.89 m.
LN-SAL	4	VER	3.70/1.51 m.	5.65/0.97 m.
LN-CON	1	HOR	2.64/2.38 m.	1.73/1.40 m.
RR-SAL	2	HOR	3.43/2.42 m.	2.76/1.41 m.
PLE-SAL	3	HOR	3.32/2.47 m.	2.40/1.47 m.
LN-SAL	4	HOR	3.74/2.46 m.	4.09/1.43 m.

3.4.2 by assuming that:

- the blind node is positioned within the convex hull of the reference nodes.

- the path loss exponent is positive.

These assumptions are presented by the following constraints:

$$\begin{aligned}(\widehat{x}_j, \widehat{y}_j) &= \sum_{i \in H_j} \alpha_i \cdot (x_i, y_i) \\ \sum_{i \in H_j} \alpha_i &= 1 \\ n &\geq 0\end{aligned} \tag{3.15}$$

Note that these constraints ensure that the position estimate is within the convex hull, even when the true position may lie outside the convex hull. Our approach imposes requirements on the reference node setup relative to the blind node locations. Note that this is similar to applying a spatial filter on the blind node positions, a terminology used in the field of optics that spatially filters noise from unwanted sources. In this section we use box constraints instead of a set of inequality constraints defined by the convex hull, as this significantly lowers the computation costs.

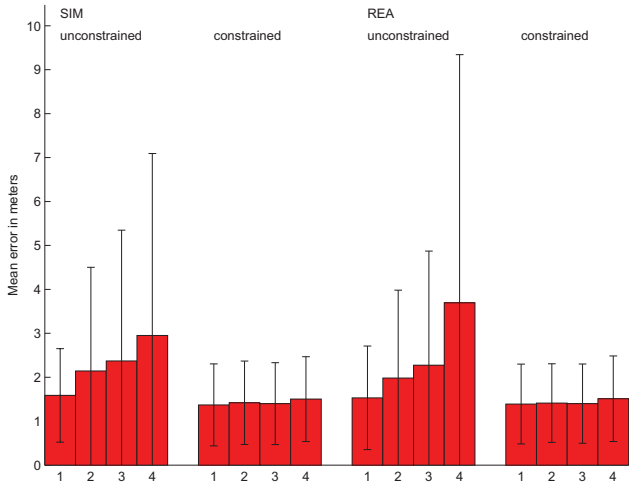

Figure 3.13: Performance of unconstrained and constrained localization systems in static environment with vertical antenna orientation

Figure 3.13 shows the performance of the unconstrained and constrained conventional and SAL systems. On the x-axis, we use the approach numbers as indicated by the localization approach numbering in Figures 3.11 and 3.12.

Table 3.2: Performance in environment with two unknown antenna orientations

Approach	MEAN REA UNC/CON	STD REA UNC/CON
LN-CON	5.58/2.34 m.	4.67/1.65 m.
RR-SAL	3.13/1.94 m.	3.40/1.25 m.
PLE-SAL	4.13/2.12 m.	5.19/1.21 m.
LN-SAL	3.72/1.99 m.	4.92/1.31 m.

Figure 3.13 shows the results of the simulations (SIM) and real measurements (REA). Figures 3.11 and 3.12 show the raw numbers represented in Figure 3.13. Figures 3.11, 3.12 and 3.13 show that:

- *The constrained localization systems increase the localization performance by roughly* 40% *and the localization stability by about* 65% *(in average).*

- *The constrained SAL systems provide similar results as their optimally calibrated constrained conventional counterpart.*

We expect that the SAL systems provide similar results as their conventional counterpart in wireless networks with a uniform reference node setup, as simulations with other uniform reference node setups show similar results. Simulations with 1000 random reference node setups show that the constrained RR-SAL and PLE-SAL provide similar results (mean error = 1.6 m) as their conventional counterpart (mean error = 1.5 m). These simulations also show that LN-SAL is more dependent on the reference node setup than the other constrained SAL systems (mean error = 1.9 m). The random reference node setups contain 9 reference nodes, with four reference nodes located at the corners of the localization area (15×15 m^2) in order to comply with the constraints.

We expect that the SAL systems provide similar results as their conventional counterpart with other Log-Normal Shadowing Model parameter settings. Hence, the Log-Normal Shadowing Model parameter settings only determine the magnitude of the mean error (e.g. [8]). Simulations with other parameter settings verify this observation. For instance, simulations with the following parameter settings $\{P_{d_0} = -10$ dBm, $n = 3.5$, $\sigma_{dBm} = 8dBm\}$ show that the constrained SAL systems provide similar results (mean error = $2.5/2.5$ $/2.8$ m) as their conventional counterpart (mean error = 2.3 m).

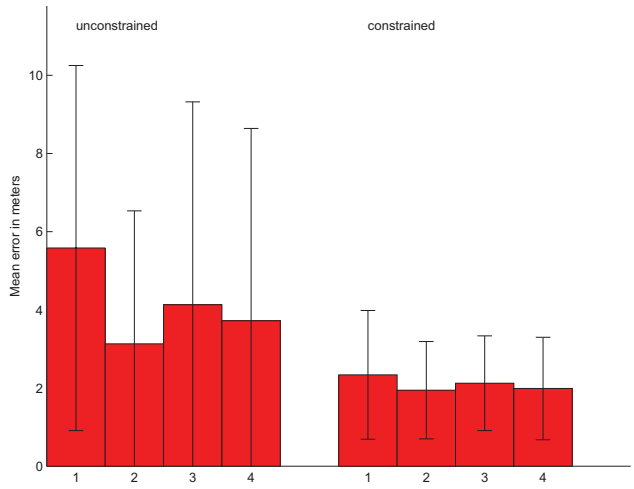

Figure 3.14: Performance in environment with two unknown antenna orientations

3.4.4 Performance with Different Antenna Orientations

This section analyzes the performance of unconstrained and constrained conventional and SAL systems in an environment using the measurements described in Section 3.2.2. In these measurements, we assume that the antenna orientation of the blind node is not known. In other words, the localization systems use the propagation model settings that fit all the measurements (vertical and horizontal antenna orientation described in Section 3.2.2). Table 3.2 shows the numbers that are represented by Figure 3.14 using a similar format as Figure 3.13. This table and figure show that on average:

- Our constrained SAL systems increase the localization performance by roughly 45% and stability by about 70% in comparison with the existing unconstrained SAL systems.
- Our constrained SAL systems increase the localization performance by roughly 65% and stability by about 75% in comparison with the unconstrained conventional localization systems.
- The constrained conventional localization system increases the localization performance by roughly 60% and localization stability by about 65% in comparison with the unconstrained conventional localization system.

These measurements show that SAL outperforms the conventional localization system when the antenna orientation is unknown. In a more realistic setup, there are more spatial factors that influence the RSS in a similar way. Therefore, we expect that in a spatially varying environment the difference in performance will be larger between SAL and conventional localization systems.

Finally, these measurements show that constraining the conventional localization system increases the performance in a similar way as with SAL systems.

3.5 Conclusion

Conventional RSS-based localization estimators assume that the propagation model is static and identical for all nodes. This limits the applications to environments in which the optimal calibration settings are independent of space or hardware. Realistic environments are dynamic and the optimal propagation model settings are dependent on the node's hardware and location. Self-Adaptive Localization systems only use milliseconds for their calibration and localization measurements, which is too short to be influenced by dynamic changes of the environment. We showed that constraining these SAL systems is necessary to provide optimal and reliable results in static and dynamic environments.

3.6 Acknowledgements

This chapter describes work in part undertaken in the context of the TSP and SALOC project.

Bibliography

[1] Hashemi H.: The indoor radio propagation channel, Proc. IEEE, July 1993, pp. 943- 996.

[2] Rappaport T.S., Wireless Communication: Principles and Practice, Prentice Hall, ISBN 013 3755633, 1996.

[3] P. Bahl and V. N. Padmanabhan: RADAR: An In-Building RF-Based User Location and Tracking System. In Proceedings of the 19th IEEE International Conference on Computer Communications (INFOCOM), March 2000.

[4] N.Patwari, R.J.O'Dea, Y.Wang: Relative Location in Wireless Networks. Presented at IEEE Vehicular Technology Conference, Spring, Rhodes, Greece, May 2001.

[5] D.Niculescu, B.Nath: Ad hoc positioning systems. In: IEEE Globecom 2001, San Antonio. 2001.

[6] J.Hightower, C.Vakili, G.Borriello, R.Want: Design and calibration of the spoton ad-hoc location sensing system. August 2001.

[7] K.Whitehouse, D.Culler: Calibration as Parameter Estimation in Sensor Networks. In ACM International Workshop on Wireless Sensor Networks and Applications, Atlanta, GA, USA, September 2002.

[8] N. Patwari, A.O. Hero, M.Perkins, N.S.Correal, R.J.O'Dea: Relative Location Estimation in Wireless Sensor Networks. IEEE Transactions on Signal Processing, special issue on Signal Processing in Networks, vol. 51, no. 8, August 2003, pp. 2137-2148.

[9] D.Li and Y.H.Hu: Energy based collaborative source localization using acoustic micro-sensor array. J.EUROSIP Applied Signal Process., vol. 4, 2003.

[10] K.Yedavalli, B.Krishnamachari, S.Ravula, and B.Srinivasan: Ecolocation: A sequence based technique for RF-only localization in wireless sensor networks. In IEEE IPSN 2005, April 2005.

[11] X.Sheng and Y.Hu: Maximum Likelihood Multiple-Source Localization Using Acoustic Energy Measurements with Wireless Sensor Networks. IEEE Transactions on Signal Processing, January 2005.

[12] J.A.Costa, N.Patwari, A.O.Hero: Distributed Weighted Multidimensional Scaling for Node Localization in Sensor Networks. ACM Transactions on Sensor Networks, Feb. 2006, vol. 2, no. 1, pp. 39-64.

[13] X.Li: RSS-based location estimation with unknown pathloss model. IEEE Transactions on Wireless Communications, vol. 5, no. 12, pp. 3626-3633, December 2006.

[14] Rong Peng, Mihail L. Sichitiu: Probabilistic Localization for Outdoor Wireless Sensor Networks. ACM SIGMOBILE Mobile Computing and Communications, Volume 11, Issue 1, January 2007, pp. 53-64.

[15] K.Whitehouse, C.Karlof, D.Culler: A Practical Evaluation of Radio Signal Strength for Ranging-based Localization. Mobile Computing and Communications Review, Volume 11, Number 1, 2007.

[16] F.Gustafsson, F.Gunnarsson: Localization based on observations linear in log range. IFAC World Congress, Seoul, 2008.

[17] C.Meesookho, U.Mitra and S.Narayanan: On Energy-Based Acoustic Source Localization for Sensor Networks. In IEEE Transactions on Signal Processing, vol. 56, no. 1, January 2008.

[18] M.B.Kjyrgaard and C.V.Munk: Hyperbolic location fingerprinting: A calibration-free solution for handling differences in signal strength. PerCom 2008.

[19] S.Mazuelas, A.Bahillo, R.M.Lorenzo, P.Fernandez, F.A.Lago, E.Garcia, J.Blas, E.J.Abril: Robust Indoor Positioning Provided by Real-Time RSSI Values in Unmodified WLAN Networks. IEEE journal of selected topics in signal processing, october 2009.

[20] Z.Xiuyuan, L.Hongbo, Y.Jie, C.Yingying, J.Francisco, R.P.Martin, L.Xiaoyan: Characterizing the impact of multi-frequency and multi-power on localization accuracy. In MASS 2010.

[21] B.J.Dil, P.J.M.Havinga: RSS-Based Localization with Different Antenna Orientations. Australian Telecommunication Networks and Applications Conference (ATNAC), 2010.

[22] B.J.Dil, P.J.M.Havinga: Calibration and Performance of RSS-based Localization Methods. Internet Of Things (IOT), 2010.

[23] CC2430. http://focus.ti.com/lit/ds/symlink/cc2430.pdf, 2012.

[24] http://www.pulseelectronics.com/download/2962/w1030pdf, 2012.

[25] B.J.Dil and P.J.M.Havinga: RSS-based Self-Adaptive Localization in Dynamic Environments. In IOT 2012.

CHAPTER 4

Stochastic Radio Interferometric Positioning in the 2.4 GHz Band

This chapter presents a novel Radio Interferometric Positioning System (RIPS), which we call Stochastic RIPS (SRIPS). Although RIPS provides centimeter accuracy, it is still not widely adopted due to (1) the limited set of suitable radio platforms and (2) the relatively long measurement and calibration times. SRIPS overcomes these practical limitations by (1) omitting the calibration phase of the existing RIPS and by (2) applying a novel positioning algorithm. SRIPS exploits the phenomenon of the small but stable difference between two transmitted frequencies that often exists when two radios are tuned to the same frequency. We obtain an experimental measure for this stability. This approach enables the implementation of RIPS on commonly available radio platforms, such as the CC2430, because fine-tuning in small steps relative to the beat frequencies for calibration is not required. In addition, we show that SRIPS calculates the position that provides the best fit to the set of measurements, given the underlying statistical and propagation models. Therefore, SRIPS converges more accurately to the true locations in a variety of situations of practical interest. Experiments in a $20 \times 20m^2$ set-up verify this and show that our SRIPS CC2430 implementation reduces the number of required measurements by a factor of three, and it reduces the measurement time to less than 0.1 seconds, while providing accuracy similar to that of the existing RIPS implementation on the CC1000 platform, which requires seconds.

1

[1]This chapter is partially published in [17] and [25]

4.1 Introduction

This chapter describes a novel approach for Radio Interferometric Positioning of devices in wireless networks that we call Stochastic RIPS, or SRIPS. Localization in wireless networks is the process of finding a physical location in an automated manner using wireless communication.

Radio Interferometric Positioning does not depend on the received signal strength as a measure for the location of unknown nodes as in standard RSS-based localization. Rather, it depends on the stability of two slightly different frequencies of a pair of carrier waves and on the nonlinear permittivity of a pair of receiving antennas to generate beat signals. Electromagnetic Interferometric Positioning was first developed with the same propagation models in the optical regime with the advent of Zeeman Lasers ([1]). The Zeeman Laser Interferometer generates two laser frequencies relatively close to each other, generating a frequency beat at the detector. The stability of the frequency beat is a direct measure for the positioning accuracy ([1]). As this frequency beat is derived from the same source, you can obtain nanometer accuracy over a range of one meter ([3]).

RIPS ([8]) relies on two independent sources. These sources, called sender pairs, simultaneously transmit unmodulated carrier waves at slightly different frequencies that must be stable during the measurement time of one frequency beat signal. Receiving node pairs that are within transmission range measure the energy of the frequency beat signal. The phase offsets of the beat signals are a function of the distances between the nodes involved relative to the carrier wavelengths. These phase offset measurements are performed for all sending and receiving node pairs over a range of discrete carrier frequencies. This set of phase offset measurements serves to calculate the unique geometrical path differences between each sending and receiving node pair. Each path difference is called a q-range ([9]). RIPS calculates the position estimate by fitting it to the q-ranges. [8] shows that RIPS can achieve centimeter accuracy over a range of 100 meters.

[8] calculates each q-range separately, by fitting the phase offset measurements of each sending and receiving pair separately. Then it fits the position estimate to these calculated q-ranges. This approach does not always provide the best fit given the set of phase offset measurements and underlying statistical and propagation models. A more rigorous approach is to fit all phase offset measurements together, rather than fitting the phase offset measurements of each sending and receiving pair separately. That approach should converge to the best fit of all phase offset measurements, and that is what SRIPS does. It

fits all the phase offset measurements by evaluating the q-ranges as stochastic functions instead of deterministic ones.

RIPS achieves its centimeter accuracy at the cost of (1) a strict requirement on the radio platform that limits the set of suitable radio platforms and (2) relatively long measuring and calibration times. SRIPS overcomes these practical limitations by (1) omitting the calibration phase and by (2) applying its new algorithm. The RIPS calibration phase requires that the radio tune its frequency in steps smaller than the desired frequency beat, so that the frequency beat can be calibrated. Most Commercial-Off-The- Shelf (COTS) radios do not comply with this tuning requirement. As a result, RIPS can be implemented only on a few radio platforms, such as the CC1000 ([8]-[16]). To our knowledge, there are no IEEE $802.15.4$ radios in the 2.4 GHz range that comply with the frequency tuning requirement of the original RIPS implementation (e.g. [21]-[24]).

One of the reasons we implemented SRIPS on a CC2430 radio platform is that it operates in the 2.4 GHz range. The CC1000 platform ([20]) operates in the 400 and $800/900$ MHz range. The allocated bandwidth (ISM band) within these frequencies is non-overlapping for different regions in the world. For instance, in Europe the allocated bandwidths are limited to 433.05-434.79 MHz and $868.0-868.6$ MHz. The existing RIPS implementation uses a bandwidth of 60 MHz ($[400, 460]$ MHz, [8]), which is outside the allocated bandwidth below the 1 GHz range.

The contributions of this chapter are as follows:

- The accuracy of Electromagnetic Interferometric Positioning depends on the stability of the generated frequency beat ([1]). This chapter experimentally verifies that the stability of the generated frequency beat signal is sufficient for at least 80 milliseconds, which provides the required stability for a position accuracy of centimeters.

- We introduce a novel Radio Interferometric Positioning System called SRIPS. Measurements on a CC2430 platform in a 20×20 m^2 outdoor environment show that SRIPS provides an accuracy of ~ 0.3 meters. We show that our SRIPS CC2430 implementation provides results similar to those of the existing RIPS CC1000 implementation, while reducing the measurement time from 1 to 0.06 seconds and reducing the number of measurements by a factor of 3.

- We compare the performance of our SRIPS algorithm with a typical RSS-based localization algorithm ([6]). Measurements on a CC2430 platform

in a 20×20 m^2 outdoor environment show that SRIPS improves the accuracy from ~ 6 to ~ 0.3 meters compared with a typical RSS-based positioning algorithm.

Section 4.2 of this chapter reviews the existing work in the field of Optical and Radio Interferometric Localization. Section 4.3 describes how we implemented the Radio Interferometric Position System on the CC2430 platform. In addition, it shows that the CC2430 platform provides the required stability for a position accuracy of centimeters. Section 4.4 describes the SRIPS positioning algorithm and shows how our algorithm copes with the varying distance estimate accuracies. Section 4.5 evaluates RIPS and SRIPS on a CC2430 platform. In addition, it compares our CC2430 SRIPS implementation with the existing CC1000 RIPS implementation. Section 5.7 provides a conclusion.

4.2 Background

This section presents a brief summary on Interferometric Positioning. Because the propagation models for Optical and Radio Interferometric Positioning are essentially the same, and because the former was developed thirty years earlier, we start with positioning based on Optical Interferometry. Then we describe the measurement set-up we use throughout this chapter. Section 4.2.3 provides the theoretical background on Radio Interferometric Positioning. At the end of this section, we compare the process flows of RIPS and SRIPS.

4.2.1 Interferometric Positioning in the Optical Regime

In Optical Interferometric Positioning Systems, the two interference signals are generated by one coherent laser source that is split into two Zeeman modes ([1]). These two modes are split by a special beam splitter into a reference and signal mode, with the signal mode reflected by a moving target that must be positioned. The frequency beat (Δf) of these two modes is on the order of a few hundred MHz. The positioning is derived from the Doppler shifted phase difference between the two modes. The resolving power of this positioning device is directly related to the stability of the beat signal: $\frac{\delta(\Delta f)}{\Delta f}$ ([1]). Hence, the error increases linearly with the distance: $(d_{BC} - d_{BD}) \cdot \frac{\delta(\Delta f)}{\Delta f}$ ([1]). The Zeeman Laser provides a high frequency beat stability because both modes are derived from the same source. Inherent instabilities in the source are canceled

out at the detector. This results in nanometer resolving power on a range of one meter ([3]). RIPS uses two independent radio transmitters with two independent receiving pairs, and this seriously limits the stability of the resulting beat signals compared to the Optical Interferometer. As we see later, the resulting resolving power is on the order of $10^{-2} \dots 10^{-3}$ as compared with 10^{-9} in the optical case. In this chapter, we empirically measure the resolving power of our radio platform by determining the stability of the beat signals (see Section 4.3.2).

4.2.2 Radio Interferometric Positioning Set-up

This chapter focuses on Radio Interferometric Positioning of a target node using a network infrastructure. This set-up distinguishes two types of nodes: the infrastructure nodes and the target nodes. The infrastructure nodes know their location and support the target nodes to position themselves. In general, this set-up provides decimeter accuracy in a measurement time of one second (see Section 4.5.5). The target node can be either a transmitter or receiver. We implement the target-as-receiver implementation, so that we can position multiple target nodes in parallel without increasing the measurement time. This scalability is not possible with the target-as-sender implementation, because in that set-up the measurement time increases with the number of target nodes ([11] and [12]). We consider the scalability of increasing the number of target nodes without affecting the measurement time as an important aspect in wireless positioning systems.

Figure 4.1 shows the RIPS/SRIPS set-up used throughout this chapter. The circles represent the infrastructure nodes (A/B/C/E) and the triangle (D) represents the target node. Red indicates transmitting nodes and green receiving nodes. The diagram in Figure 4.2 shows which measurements are performed to estimate the position of one or several target nodes:

- **Phase Offset Measurements**
  Two infrastructure nodes form a sender pair and generate a beat signal; two or more receivers sample the beat signal with 'O' sample points. RIPS uses 256 sample points. We vary this amount for analysis (see Section 4.5). The CC1000 has a sampling frequency of 9 kHz, and the CC2430 has a sampling frequency of 62.5 kHz. The beat frequency and phase offset is then calculated from these sampled beat signals for each receiver pair. Each receiver pair includes one infrastructure node and one target

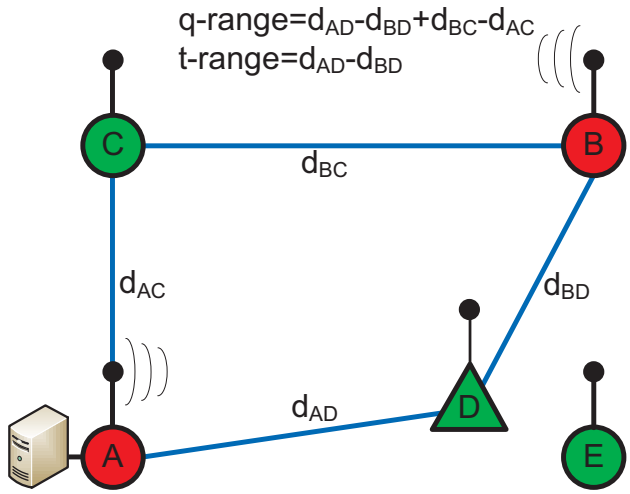

Figure 4.1: Measurement set-up: red = transmitting, green = receiving, circle = infrastructure node, triangle = target node

node. Note that all participating nodes must be accurately synchronized (microsecond synchronization, [8]).

- **Measurement round**
  This phase consists of performing N phase offset measurements at N different frequencies to calculate the q-range between the sending and receiving node pair (see Section 4.2.3). However, calculating q-ranges is computationally intensive. Therefore, the calculated phases and frequencies are sent to a computer for post-processing at the end of each measurement round ([8]-[13]). Each measurement round is identified by a unique sender pair.

- **Positioning of the target node**
  The position of the target node is calculated on a central computer on the basis of the data of two or more measurement rounds (independent q-ranges).

The table in Figure 4.2 shows which nodes are sending/receiving during each measurement round in the measurement set-up shown in Figure 4.1. For

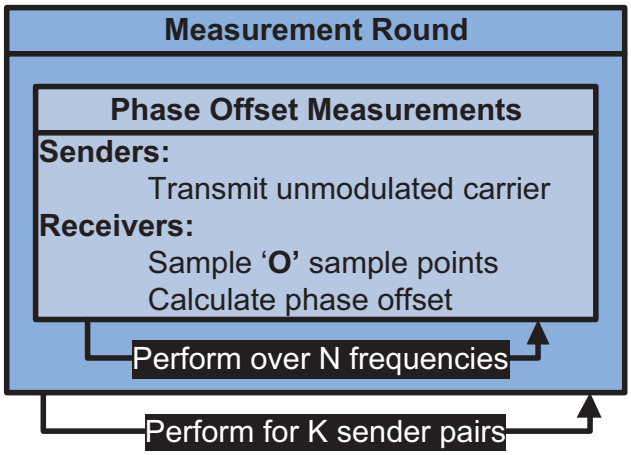

Measurement Round (K)	Senders	Receivers	Frequencies (N)
1	A / B	C / E / D	38
2	A / C	B / E / D	38
3	A / E	B / C / D	38
4	B / C	A / E / D	38
5	B / E	A / C / D	38
6	C / E	A / B / D	38

Figure 4.2: Measurement phases

instance in the first measurement round, infrastructure nodes A and B are transmitting unmodulated carriers. Nodes C, E and D measure the beat signal ($R = 3$ Receivers). Each beat signal is measured over 38 frequencies in our set-up. Figure 4.2 shows that there are $K = 6$ measurement rounds, each allowing for two receiver pairs. In this example, we assume that the receivers sample the beat signal with $O = 500$ sample points. Then the total number of sample points used to position the target node equals:

$$K \cdot R \cdot N \cdot O = 6 \cdot 3 \cdot 38 \cdot 500 = 342000 \tag{4.1}$$

The total measurement time to position the target node does not depend on the number of receivers:

$$\text{Total measurement time} = K \cdot N \cdot O \cdot \frac{1}{f_s} \tag{4.2}$$

Here f_s is the sampling frequency of the hardware used. Therefore, increasing the number of receiving infrastructure nodes increases the total number of sample points used to position the target node. This increases the positioning accuracy (e.g. [12]), without increasing the total measurement time, and therefore energy consumption of the target nodes.

4.2.3 Radio Interferometric Positioning

Nodes A and B in Figure 4.1 transmit an unmodulated carrier signal with frequencies f_A and f_B. Receivers C and D measure the energy of the composite signal with a frequency beat of $\Delta f = |f_A - f_B|$. The measured phase offset is a function of the distances between sender pair A/B and receiver pair C/D, assuming that $f_A > f_B$:

$$\Delta\varphi_i = 2\pi \left(\frac{d_{AD} - d_{AC}}{\lambda_A} - \frac{d_{BD} - d_{BC}}{\lambda_B} \right) \mod (2\pi) \tag{4.3}$$

$$\approx 2\pi \left(\frac{d_{ABCD}}{\lambda_i} \right) \mod (2\pi)\,. \tag{4.4}$$

Here:

$$\text{q-range} = d_{ABCD} = d_{AD} - d_{BD} + d_{BC} - d_{AC}\,, \tag{4.5}$$

and:

$$\text{t-range} = d_{ABCD} - d_{BC} + d_{AC} = d_{AD} - d_{BD}\,. \tag{4.6}$$

Here $\Delta\varphi_i$ is the relative phase offset; d_{AD} is the distance between node A and D; [8] defines λ_i as $\lambda_i = \frac{2c}{f_A + f_B}$ with c representing the speed of light. We define d_{ABCD} as the q-range, as in [9]. The locations of infrastructure nodes A, B and C are known, so the distances between these nodes are also known (d_{BC} and d_{AC}). We use this information to transform the q-range into the t-range, so that all the values of the variables on the left side of the equation are known. Throughout this chapter, we use the q-range in the equations and the t-range in

the figures, because the t-range is independent of the location of the receiving infrastructure node. This is useful for comparing q-ranges of the same sender pair, as we show in Section 4.4.3.

Equation 4.3 does not define a unique solution for the q-range (d_{ABCD}) due to $\mod(2\pi)$-related ambiguity of the q-range. Therefore, RIPS implementations perform phase offset measurements over N frequencies for the same sender pair: $f_1 \dots f_N$. The squared error of a q-range estimate is given by ([9]):

$$\text{ERROR}(\text{q-range}_j) = \sum_{i=1}^{N} (\text{q-range}_j - d_{i,j})^2 \tag{4.7}$$

Where:

$$d_{i,j} = \text{round}\left(\frac{\text{q-range}_j - \gamma_{i,j}}{\lambda_{i,j}}\right) \cdot \lambda_{i,j} + \gamma_{i,j}$$

minimizes Equation 4.7 for a given q-range; $\gamma_{i,j}$ represents the phase offset relative to the wavelength $\gamma_{i,j} = \lambda_{i,j} \frac{\Delta\varphi_{i,j}}{2\pi}$. Figure 4.3 shows the t-range error distribution calculated by Equation 4.7 as a function of the t-range.

The Most-Likelihood-Estimator of the q-range is the global minimum of the q-range error distribution, minimizing the squared error between the calculated and measured phase offsets:

$$\begin{aligned} \text{q}_{\text{est},j} &= \arg \min_{\text{q-range}_j} \sum_{i=1}^{N} (\Delta\varphi_{i,j} - \widehat{\Delta\varphi_{i,j}})^2 \\ &= \arg \min_{\text{q-range}_j} \sum_{i=1}^{N} (\text{q-range}_j - d_{i,j})^2 \\ &= \arg \min_{\text{q-range}_j} \text{ERROR}(\text{q-range}_j) \end{aligned} \tag{4.8}$$

Most RIPS algorithms use this deterministic approach for estimating one q-range on the basis of the calculated q-range distribution (e.g. [8]). Figure 4.3 shows an example of a t-range error distribution of one sending pair. It shows that the real t-range is located in a local minimum instead of the global minimum. Such error distributions seriously limit the accuracy of RIPS but can be handled by SRIPS. We discuss this further in Section 4.4.

The position is estimated by minimizing the squared difference between the calculated and estimated q-ranges:

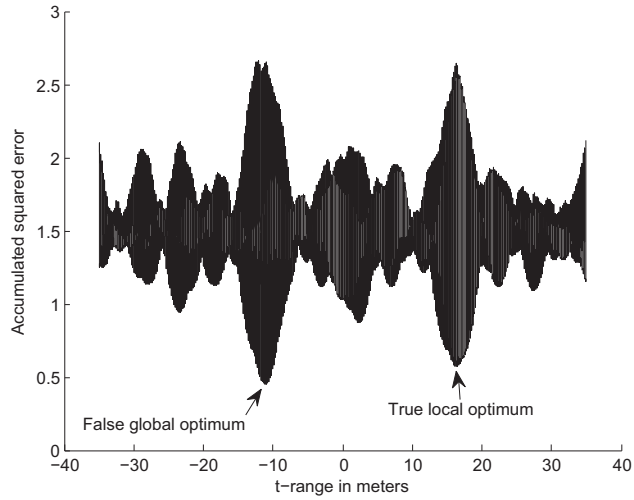

Figure 4.3: t-range error distribution, local optimum

$$\{\hat{x}, \hat{y}\} = \arg\min_{\hat{x},\hat{y}} \sum_{j=1}^{M} (q_{\text{est},j} - \widehat{\text{q-range}}_j)^2 \tag{4.9}$$

Here, M is the number of q-range estimates; $\widehat{\text{q-range}}_j$ is the calculated q-range as a function of the estimated position $(\hat{x}, \hat{y})$. Although the present literature shows that Equation 4.9 converges with increasing N (phase offset measurements over different frequencies) and M (q-range estimates), they don't necessarily converge to the true positions, as shown in Section 4.4.

4.2.4 Process flow of RIPS and SRIPS

Figure 4.4 shows the individual phases of the CC1000 RIPS and the CC2430 SRIPS implementations:

- **Calibration Phase**
  The calibration phase ensures that the frequency beat is measurable given the user-defined sample time ($28 \ldots 40$ ms) and the hardware-defined sampling rate (9 KHz). However, the calibration phase requires that the

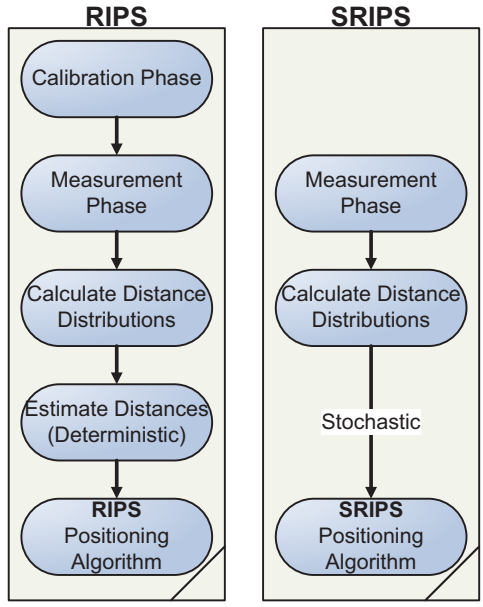

Figure 4.4: RIPS vs SRIPS

radio set the frequency in small steps relative to the desired beat frequencies. The CC1000 can tune its frequency in steps of 65 Hertz, which is sufficient for a frequency beat of 300 to 400 Hertz ([8]). The CC2430 does not comply with this tuning requirement; therefore, SRIPS follows another approach (see Section 4.3.1).

- **Measurement Phase**
  In this phase, the receivers measure the phase and frequency of the beat signals. RIPS and SRIPS use a simple threshold-crossing technique ([2]) for estimating the phase offset between the receivers, to keep the computational costs low.

- **Calculate Distance Distributions**
  The q-range error distribution is calculated using Equation 4.7.

- **Estimate Distances (Deterministic)**
  In this phase, the q-range is estimated on the basis of the calculated q-range error distribution. Figure 4.3 shows an example where the real

Platform	CC1000	CC2430
Calibration	Yes	Not available
Sample time	28.4 . . . 40 ms	0.8 . . . 8 ms
RSS sampling rate	9 kHz	62.5 kHz
Frequency beat	200 . . . 800 Hz	0.2 . . . 14 kHz
Frequency range	400 - 800/900 MHz	2.4 GHz
Positioning algorithm	RIPS	SRIPS

Table 4.1: Platform characteristics

q-range lies in a local minimum, which is a known problem of RIPS (e.g. [9]). Most RIPS algorithms assume that the real q-range is determined by this global minimum (Equation 4.8). [9] and [11] try to solve this problem, however they are dependent on parameter settings that can only be determined empirically. SRIPS does not estimate q-ranges, but evaluates the q-range error distribution directly for estimating the position. Therefore, it does not have this distance estimation phase (for details we refer to Section 4.4).

- **RIPS and SRIPS Positioning Algorithms**
  In this phase, RIPS estimates the position on the basis of the q-range estimates (Equation 4.9). SRIPS estimates the position on the basis of the calculated q-range error distributions.

Figure 4.4 shows that the only difference between RIPS and SRIPS is the omitted calibration phase and the localization algorithm. Otherwise, RIPS and SRIPS perform the same measurements and use the same input for localization.

4.3 SRIPS Measurement Phase and Error Characterization

In this section, we focus on the measurement phase. In addition, we empirically verify whether the CC2430 hardware is suitable for radio interferometric positioning.

4.3.1 CC2430 Measurement Phase

A typical target-as-receiver RIPS and SRIPS set-up is shown in Figure 4.1. Although our SRIPS implementation tunes each sender pair to the same frequency, in practice these frequencies are never exactly the same. There is often a small but stable difference between the transmitted frequencies caused by small and stable differences between the crystal oscillators. We measure the beat frequencies at receiver pairs in our user-defined measurement time of 8 ms per frequency at the hardware-defined sampling rate of 62.5 KHz.

The measurement time per frequency determines the lower bound of the measurable frequency beat: $\frac{1}{0.008} \approx 125$ Hz. The Nyquist frequency determines the upper bound of the measurable frequency beat: $\frac{62.5}{2} \approx 30$ KHz. Measurements with 48 different sender pairs show that 85% of these pairs generate measurable frequency beat signals.

Our CC2430 SRIPS test bed contains a master node, which controls and collects the SRIPS measurements. The master node can be a transmitter or receiver. Our SRIPS implementation consists of the following steps in order to perform one phase offset measurement:

1. The master node sends a synchronization message, which synchronizes the nodes and identifies the transmitters and receivers. We use the CC2430 MAC controller in order to obtain at least 208 ns synchronization accuracy at the reception of the synchronization message ([21]). The time (1.4 ms) between the synchronization message and sampling the beat signal introduces an additional error. This error depends on the accuracy of the crystal oscillator and the 1.4 ms waiting time. [17] shows that this introduces an extra error of approximately 60 ns.

2. 1 ms after receiving the synchronization message, the transmitters start sending unmodulated carrier signals.

3. 1.4 ms after receiving the synchronization message, the receivers start sampling the beat signal. We use the CC2430 DMA controller to perform the measurements with clock tick accuracy. This means that the accuracy of the crystal oscillator determines the measurement jitter. [17] shows that the maximum measurement jitter is on the order of 320 ns when sampling 500 consecutive sample points over 8 ms.

4. At the end of each phase offset measurement, the master node collects the 500 sample points from each receiver for analysis.

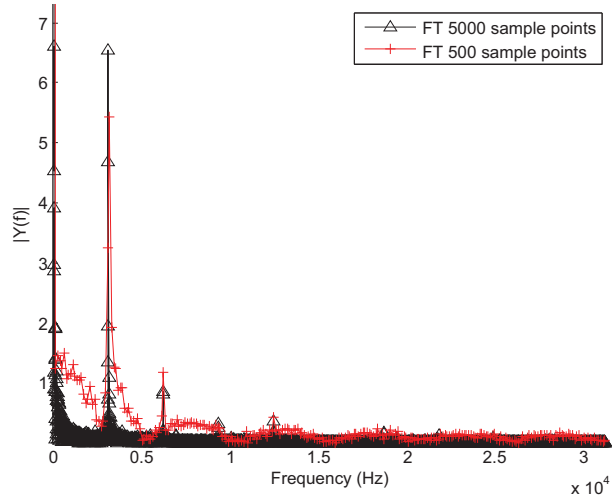

Figure 4.5: Single-Sided Amplitude Spectrum, FT stands for Fourier Transform

RIPS and SRIPS use the same methodology to obtain the required phase offset measurements. The only difference is that in our current SRIPS implementation, we send the raw sample points to a computer for analysis. In a commercial implementation, these computations can be distributed to the local processors of the nodes. Table 4.1 compares the characteristics of the CC1000 and CC2430 platform.

4.3.2 CC2430 Error Characterization

Before we further analyze SRIPS and its performance in a practical localization set-up, we perform several frequency beat measurements in a limited set-up to show that our CC2430 hardware with a 20 ppm crystal oscillator is suitable for radio interferometric positioning. This limited set-up consists of four nodes placed in the corners of a 1×1 m^2 square. The short-range and line-of-sight measurements minimize the influence of the environment on the received signals, so that we practically measure the performance of the CC2430 hardware. We place all radios on tripods at the same height of 1.5 meters, and we do not place objects in the vicinity of the radios, to minimize the influence of interfering reflections ([9]). The conditions during the measurements are static (tem-

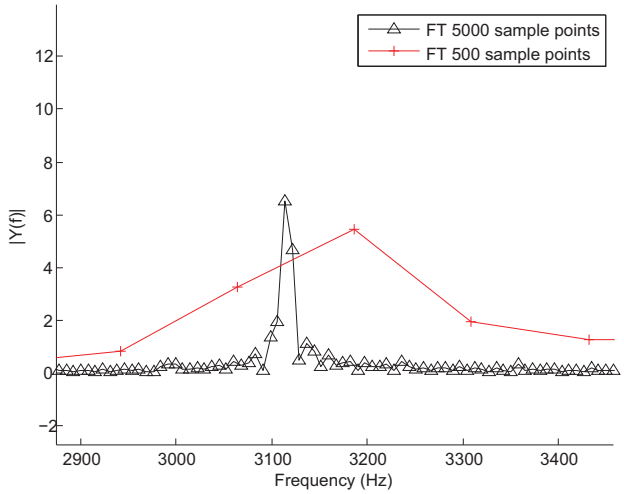

Figure 4.6: Zoomed in Single-Sided Amplitude Spectrum, FT stands for Fourier Transform

perature, humidity, no moving objects). Receiving nodes sample the beat signals with 5000 sample points at a sample rate of 62.5 KHz. All nodes are tuned over 38 frequencies in a bandwidth of $2.406 \ldots 2.480$ GHz. The frequency beat signals are measured with all possible sender and receiver pairs (6). Each node is equipped with a widely used omnidirectional dipole antenna with a vertical orientation.

Minimum bandwidth is the inverse of the maximum coherence time or stability of the beat signals. Therefore, increasing the measurement time beyond the coherence time does not provide reliable phase measurements as expressed by Equation 4.3. We calculate the bandwidth of the first 500 sample points and over all 5000 sample points. Figures 4.5 and 4.6 show the Fourier transform of the corresponding frequency beat signals. In each figure, the red curve represents the Fourier transform of the first 500 sample points and the black curve represents the Fourier transform of the 5000 sample points. These figures clearly show that the bandwidth of the spectrum of the black curve (~ 20 Hz) is a factor of 10 smaller than the corresponding bandwidth of the red curve (~ 200 Hz). Only coherent signals reduce the frequency bandwidth proportional to the measurement time. This is a direct result of the Heisenberg-Pauli-

Weyl inequality, because the product of the variance of time and frequency remains constant. This means that the stability of our beat signals is at least 80 ms.

[8] states that the interferometric range of the CC1000 carrier waves is on the order of a few hundred meters. Our SRIPS algorithm measures a frequency stability of at least 80 ms, which corresponds to a theoretical coherence length of at least 2400 km for the plane waves of our propagation model that have an infinite range in free space. However, the energy transmitted from the antenna is not concentrated into a narrow beam, so that in the far field this energy decreases inversely proportionally to the square of the distance from the radio transmitters. This path loss in free space limits the application of RIPS and SRIPS to localization areas with a diagonal of a few hundred meters. Therefore, both RIPS and SRIPS can determine the positions with a relative accuracy of roughly $(d_{BC} - d_{BD}) \cdot \frac{\delta(\Delta f)}{\Delta f} \approx (d_{BC} - d_{BD}) \cdot 10^{-3}$ when the measurement times are adapted to approach the coherence times of the radio transmitters. In principle, it is possible to work with an array of sending emitters that relay the carrier waves at the points of maximum decay, so that the localization space can be extended by several orders of magnitude. This is a subject for future research.

4.4 Stochastic Radio Interferometric Positioning

This section describes our novel SRIPS positioning algorithm. It first analyzes and compares the optimization functions of RIPS and SRIPS. Then it describes the implementation of the localization algorithm of SRIPS. In the last subsection, it provides a typical example of the performance of RIPS and SRIPS.

4.4.1 RIPS versus SRIPS

RIPS ([8], [12] and [14]) estimates the position by sequentially minimizing two cost functions. First it calculates the q-ranges by minimizing the cost function described in Equation 4.8. This equation calculates the q-range that minimizes the squared difference between the phase offsets measured at N frequencies associated with one sender and receiver pair. This minimum is equal to the global minimum of the q-range error distribution. Then RIPS calculates the position by minimizing the cost function described in Equation 4.9. This latter cost function calculates the position by minimizing the squared difference between the calculated and estimated q-ranges. RIPS ([8], [12] and [14]) uses a

Least Squares Method to calculate the position that best fits the measurements. In Radio Interferometric Positioning, the measured values are the phase offset measurements. However, the position calculated by Equations 4.8 and 4.9, does not minimize the squared difference between all measured and estimated phase offsets. The best fit to all measurements is obtained by:

$$\{\hat{x}, \hat{y}\} = \arg\min_{\hat{x},\hat{y}} \sum_{j=1}^{M} \sum_{i=1}^{N} (\Delta\varphi_{i,j} - \widehat{\Delta\varphi_{i,j}})^2 \tag{4.10}$$

Here, $\widehat{\Delta\varphi_{i,j}}$ is the estimated phase offset calculated by the position estimate. In other words, Equation 4.10 calculates the best position (fit) given the set of measurements and underlying propagation and statistical models, rather than first taking the minimum of a subset and substituting it in the total. Note that Equation 4.10 corresponds to the Maximum Likelihood Estimator when the phase offset measurements follow a normal distribution. This results in the following practical differences between RIPS and SRIPS:

- The original RIPS algorithm cannot cope with false global optimums and q-ranges located in local optimums in the q-range error distribution (e.g. [9]). This is because Equation 4.8 calculates each q-range separately on the basis of the phase offset measurements associated with that q-range. Equation 4.10 can cope with false global optimums and local optimums when the other phase offset measurements (those not associated with that specific q-range) can discriminate between the true and false optimums.

- The original RIPS algorithm cannot cope with varying q-range estimate precisions. It implicitly assumes that the precisions are equal for the estimated q-ranges, because it minimizes the equally weighted squared difference between the calculated and fitted q-ranges (Equation 4.9). SRIPS discriminates against such less precise or wider q-range error distributions, because these provide a constant contribution to the squared errors of Equation 4.10.

The advantage of Equations 4.8 and 4.9 over Equation 4.10 is that Equations 4.8 and 4.9 require significantly fewer computations using the analytic solver ([10]), while providing the required localization performance on the CC1000 (e.g. [12]).

4.4.2 SRIPS implementation

This section describes the implementation of the localization algorithm of SRIPS. Equation 4.10 is rewritten as:

$$\{\hat{x},\hat{y}\} = \arg\min_{\hat{x},\hat{y}} \sum_{j=1}^{M}\sum_{i=1}^{N}(\Delta\varphi_{i,j} - \widehat{\Delta\varphi_{i,j}})^2 \tag{4.11}$$

$$= \arg\min_{\hat{x},\hat{y}} \sum_{j=1}^{M}\sum_{i=1}^{N}(d_{i,j} - \widehat{\text{q-range}}_j)^2 \tag{4.12}$$

$$= \arg\min_{\hat{x},\hat{y}} \sum_{j=1}^{M}\text{ERROR}(\widehat{\text{q-range}}_j) \tag{4.13}$$

SRIPS minimizes Equation 4.13. However, Equation 4.13 has a rapidly oscillating behavior as can be seen from the t-range error distribution shown in Figure 4.3 ($\sum_{j=1}^{M}\text{ERROR}(\widehat{\text{q-range}}_j)$). Therefore, the calculated errors for a given position estimate become unpredictable. SRIPS solves this problem by taking the envelope of the minimum of the q-range error distribution:

$$\text{ERROR}_{SRIPS}(\widehat{\text{q-range}}_j) = \min\Big(\text{ERROR}([\widehat{\text{q-range}}_j - W, \widehat{\text{q-range}}_j + W])\Big) \tag{4.14}$$

Here W is a constant dependent on the frequency band used of the radio, in our case 2.4 GHz; $[\widehat{\text{q-range}}_j - W, \widehat{\text{q-range}}_j + W]$ is an interval; $\min\Big(\text{ERROR}([\widehat{\text{q-range}}_j - W, \widehat{\text{q-range}}_j + W])\Big)$ is the minimum value of Equation 4.7 over the specified interval. We numerically determine the value of W as 12.5 centimeters. We rewrite Equation 4.13 with the aid of Equation 4.14 as:

$$\{\hat{x},\hat{y}\} = \arg\min_{\hat{x},\hat{y}} \sum_{j=1}^{M}\text{ERROR}_{SRIPS}(\widehat{\text{q-range}}_j) \tag{4.15}$$

Figure 4.7 shows an example of the smoothed t-range error distribution using Equation 4.14. Figure 4.8 shows this smoothed t-range error distribution over the localization surface using Equation 4.15. In Figure 4.8, the cross is the true location of the target node; red represents large errors and blue represents

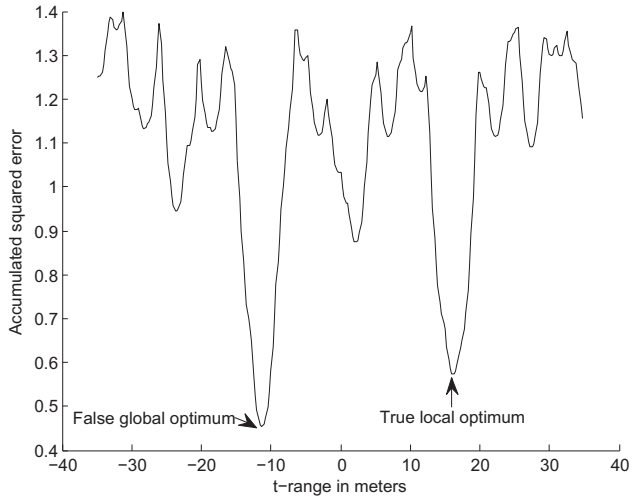

Figure 4.7: Smoothed t-range error distribution

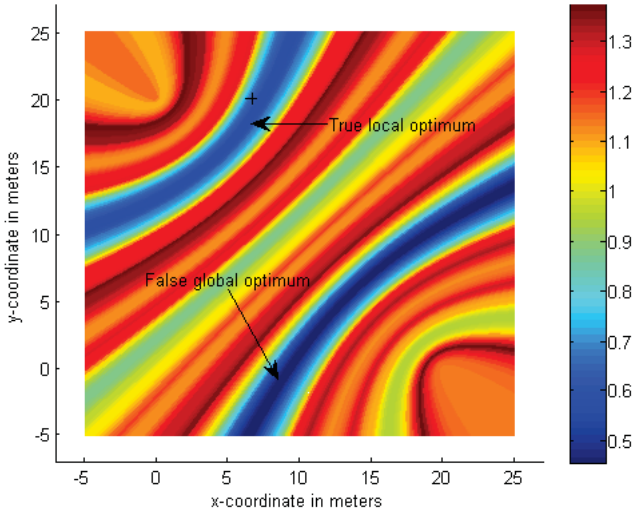

Figure 4.8: Smoothed t-range error distribution over the localization surface

small errors. Note that the two minimums shown in Figure 4.7 are represented by the two darker blue lines in Figure 4.8.

The SRIPS localization algorithm uses a grid-based Monte Carlo approach to minimize Equation 4.15. It accumulates the M smoothed q-range error distributions over the localization area represented by the Monte Carlo samples. In other words, it treats the q-ranges as stochastic variables to minimize Equation 4.15. We implemented SRIPS in Matlab, which post-processed all the data obtained by the CC2430 test bed. The main purpose of this implementation is to provide a tool for analysis; therefore, it does not minimize the computational or memory costs.

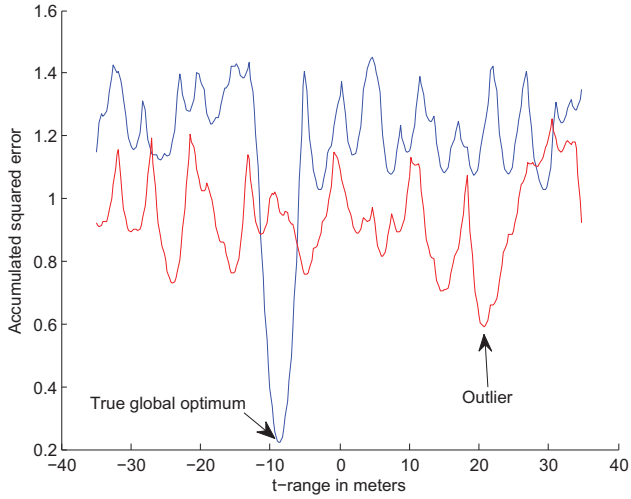

Figure 4.9: Two separate smoothed t-range error distributions (blue curve and red curve)

4.4.3 Typical Example of RIPS versus SRIPS

For reasons discussed in Section 4.5.5, our CC2430 platform test bed produces roughly 25% outliers in estimating the q-range, even at relatively long measurement times. Figure 4.9 shows an example where a t-range with a clear distinct minimum in its smoothed error distribution (blue curve) is combined with an outlier that has its global minimum about 30 meters away. These two

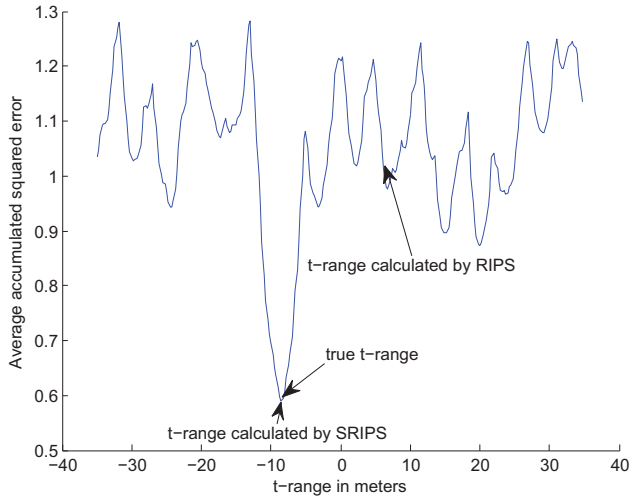

Figure 4.10: Average accumulated smoothed t-range error distribution as calculated by SRIPS

t-range measurements belong to the same sender pair but have different receiver pairs. In other words, they share the same t-range (see Section 4.2.3). RIPS calculates the t-range based on these two measurements as the average of the global minimums of the two t-ranges, which is about $\frac{30}{2} \approx 15$ meters away from the true t-range. SRIPS averages the two error distributions as in Equation 4.15. This average is represented by the blue curve in Figure 4.10 and still has its global minimum at the true location.

Figure 4.10 shows an example in one dimension (error as a function of the t-range). Note that SRIPS discriminates between true and false minimums in a similar way when all t-range error distributions are summed over the localization surface as defined in Equation 4.15. Figure 4.11 shows that SRIPS discriminates between the two minimums shown in Figures 4.7 and 4.8 by including the t-range error distributions from the other sender and receiver pairs. In this particular case, the resulting positioning error is 3 centimeters.

Figure 4.12 illustrates the sensitivity of SRIPS to the total measurement time as defined by Equation 4.2. When reducing the total measurement time by a factor of 20, the error plot of Figure 4.12 becomes less discriminating. The positioning error increases to 60 centimeters. The advantage of these error distribution plots is that, at a glance, they give a quick impression of the accuracies

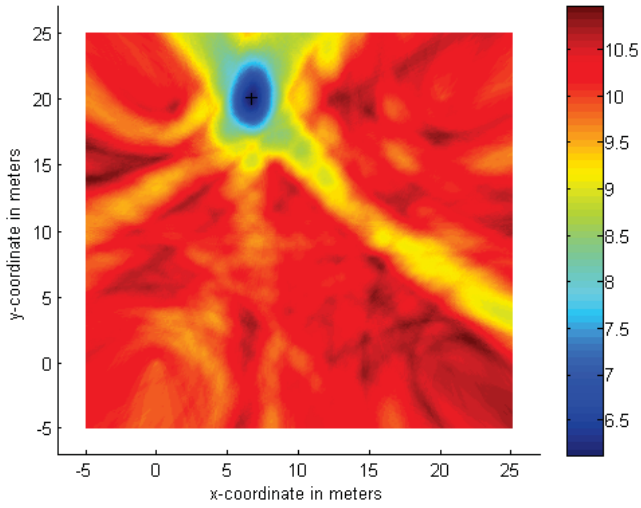

Figure 4.11: 2 s. total measurement time, error distribution over localization surface

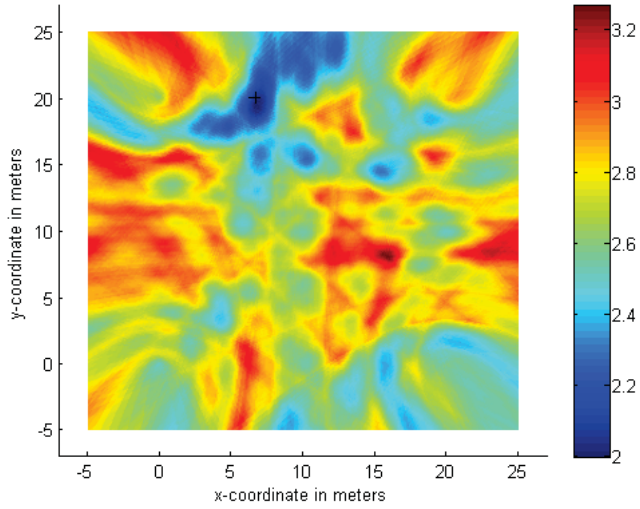

Figure 4.12: 100 ms. total measurement time, error distribution over localization surface

of the position estimates.

4.5 Performance Evaluation

Section 4.5.1 describes the measurement set-up. Section 4.5.2 presents the performance evaluations of the RIPS and SRIPS positioning algorithms on the CC2430 platform with the various measurement settings of interest. Section 4.5.3 briefly discusses the amplitude filtering as applied by RIPS on the CC1000 platform. Section 4.5.4 compares the SRIPS results with ranged-based RSS results in a similar set-up. Section 4.5.5 summarizes the differences between SRIPS and RIPS on the CC2430 platform, and Section 4.5.6 compares the RIPS and SRIPS results on the different platforms. Finally, Section 4.5.7 discusses the performance of SRIPS in indoor environments.

Figure 4.13: Measurement environment

4.5.1 Measurement Set-up

The measurements were conducted in a 20×20 m^2 outdoor environment, shown in Figure 4.13, with six CC2430 radios (Figure 4.14). We used four CC2430 radios as reference nodes, which were located at the corners of the localization area; these reference nodes were fixed during and between measurement rounds. We used two CC2430 radios as target nodes; these target nodes measured the frequency beat signals at 12 different locations in a 4×4

Figure 4.14: CC2430 radio

grid. We determined the locations of the reference and target nodes with a measuring tape. We estimate the accuracy of the node placements as 10 cm. The receiving nodes measured 500 sample points per phase offset measurement in 8 ms per frequency over a total of 38 frequencies in a range of 2406 to 2480 MHz. All of the radios were placed at the same height of 1.5 m to minimize reflection noise (e.g. [9]). All individual sample points were sent to a computer and logged for post-processing. These measurements were performed over a period of two days with changing weather conditions. We used this set-up because it is similar to the set-up described in [8].

This measurement set-up also performed 500 RSS measurements at the same 38 frequencies using individual sender rather than paired senders to compare the performance of RIPS and SRIPS with a typical RSS-based localization algorithm.

4.5.2 Performance Evaluation

This section analyzes the performance of SRIPS as a function of the total number of sample points to position one target node. We calculate this number and the measurement time using Equations 4.1 and 4.2. Figures 4.15 and 4.16 show the performance of the RIPS and SRIPS positioning algorithms as a function of the number of sample points per phase offset measurement. The horizontal axis represents the number of measured sample points per phase offset measurement. The four curves show the performance of the RIPS positioning algorithm using a different number of frequency measurements ($N = 38/19/13/10$)

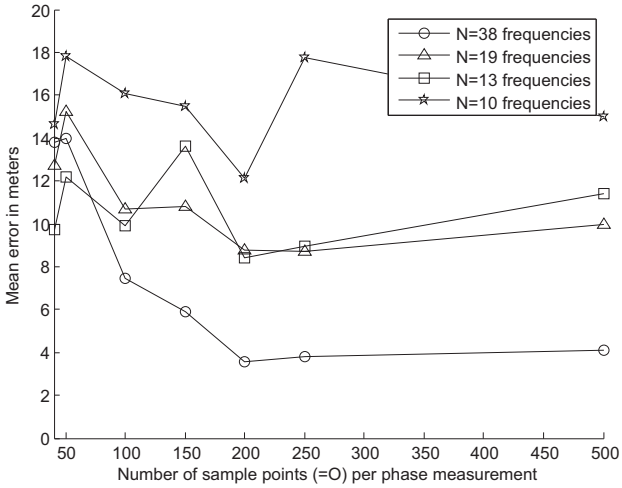

Figure 4.15: RIPS performance as a function of sample points (O) per phase measurement

per sender pair ($M = 6$) and using the full frequency bandwidth of the available frequency band ($2.406 \ldots 2.480$ GHz). This means that we increase the frequency hop length to $\{2, 4, 6, 8\}$ MHz instead of decreasing the frequency bandwidth. We use this strategy because experiments show that it provides better results than the frequency-bandwidth strategy.

Figures 4.15 and 4.16 show that SRIPS converges faster and more accurately to the true locations than RIPS. These empirical numerical results indicate that beat signals on the CC2430 platform can be roughly collected over 0.8 ms (50 sample points) at 19 different frequencies and 6 sender pairs to have SRIPS yield reliable results on the order of 50 cm accuracy.

Figure 4.17 shows the number of measurable phase offset measurements as a function of the number of measured sample points per phase offset measurement. Not every measurement provides a measurable phase offset measurement due to noise or due to the fact that not every frequency beat is measurable given the measurement time and sampling rate (see Section 4.3.1). Figure 4.17 shows that the number of measurable phase offsets decreases when the number of sample points per phase offset measurement decreases below 200, especially from 100 to 50 sample points. Two sender pairs do not generate measurable frequency beats given the measurement time per phase offset

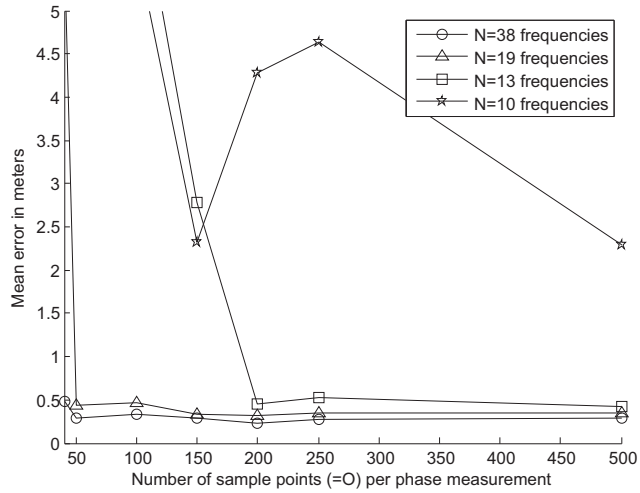

Figure 4.16: SRIPS performance as a function of sample points (O) per phase measurement

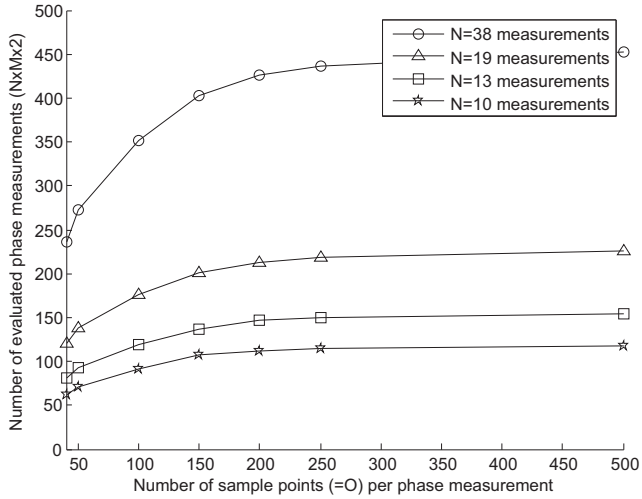

Figure 4.17: Number of valid phase measurements

measurement (50 samples, 0.8 ms), because one period of the generated beat signals is larger than the measurement time per phase offset measurement. So the effective total measurement time reduces from 0.09 to 0.06 s when sampling the beat signal with 50 sample points. This then implies that our nodes and environment must be static during the total measurement time of all beat signals, which is on the order of 0.1 seconds.

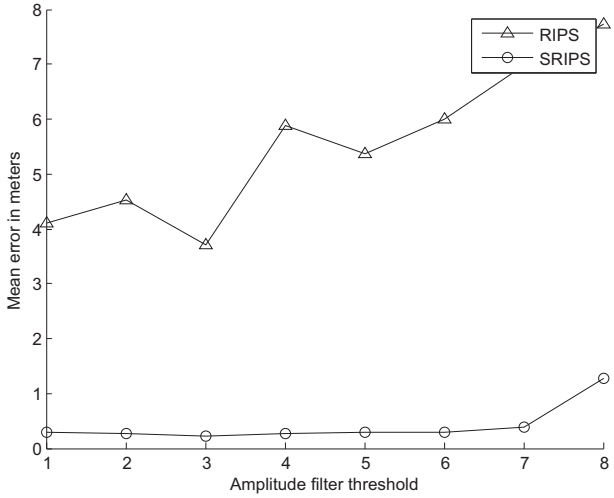

Figure 4.18: Performance as a function of the amplitude filter threshold

4.5.3 Amplitude Filtering

In this section we analyze whether the amplitude filter implemented on the CC1000 RIPS platform provides similar results on the CC2430 platform. The amplitude filter filters frequency beat signals with an amplitude smaller than a certain threshold ([8]). Figure 4.18 shows the performance of the RIPS and SRIPS positioning algorithms as a function of this threshold. It shows that the amplitude filter does not significantly affect the performance of both algorithms on our platform, and that it can decrease the performance when it is set too high. This decreasing performance with increasing threshold filtering appears to be logical because increasing the threshold decreases the amount of evaluated phase measurements, which in turn decreases the localization performance.

4.5.4 Performance of Typical RSS-based Localization Technique

Recent studies ([18] and [19]) show that range-based localization ([6]) outperforms or provides similar results to other typical localization methods in line-of-sight environments (e.g. [5], [7]). Therefore, we evaluated the performance of the range-based localization algorithm described in [6]. First, we calibrated the propagation model ([4]) by the localization measurements. Then we used the same localization measurements for evaluating the performance. This ensures that [6] provides the best performance. [6] provides a mean error of ~ 6 meters, so SRIPS outperforms ranged-based RSS localization by an order of magnitude in this measurement set-up.

4.5.5 Discussion of CC2430 RIPS versus CC2430 SRIPS Results

Figures 4.15 and 4.16 show that:

- RIPS provides a localization accuracy of several meters rather than centimeters reported on the CC1000 platform.
- SRIPS outperforms the RIPS positioning algorithm in all cases investigated.

As described in Section 4.4.3, these differences are mainly caused by the fact that RIPS uses a least-squares method, which does not cope well with the 25% outliers produced in the q-range error distributions by our test bed.

As a first candidate for the cause of these outliers, we eliminated multipath effects, which is further explained in Section 4.5.7. Except for random spontaneous hardware effects, it is unlikely that the cause can be traced to the hardware. It is unlikely because the same hardware produces reliable measurements and outliers in the same locations at different times without any noticeable changes in the environment. As a possible cause for these outliers, we suspect the busy 2.4 GHz band, which carries a lot of traffic. All sorts of interferences, such as those from a nearby WiFi network, might have produced outliers in our test bed at unexpected times. The real world always has outliers and the good thing is that our localization algorithm dealt with them in an adequate way.

RIPS uses a least-squares method, which is known to be susceptible to outliers. If we use a Least-Absolute Deviation (LAD) rather than a least-squares optimization algorithm:

References	Measurement time	Total sample points	Error	Area
[8]	88747 ms	NA	3 cm	324 m^2
[9]	69518 ms	NA	10 cm	8000 m^2
[11]	440 ms	43560	61 cm	7200 m^2
[12]	1252 ms	33972	70 cm	780 m^2
[14]	1024 ms	46080	70 cm	100 m^2
SRIPS	60 ms	11400	50 cm	400 m^2
RIPS	730 ms	136800	410 cm	400 m^2
RIPS(LAD)	365 ms	68400	50 cm	400 m^2
TYPICAL	2000 ms	76000	620 cm	400 m^2

Table 4.2: CC1000 RIPS and CC2430 SRIPS performance 1

References	Frequencies	Sender Pairs	Platform
[8]	13	240	CC1000
[9]	13	188	CC1000
[11]	11	1	CC1000
[12]	22	2	CC1000
[14]	18	2	CC1000
SRIPS	19	4	CC2430
RIPS	38	6	CC2430
RIPS(LAD)	38	6	CC2430
TYPICAL	38	4 senders	CC2430

Table 4.3: CC1000 RIPS and CC2430 SRIPS performance 2

$$\{\hat{x}, \hat{y}\} = \arg\min_{\tilde{x},\tilde{y}} \sum_{j=1}^{M} \left| q_{\text{est},j} - \text{q-}\widehat{\text{range}}_j \right| \ ,$$

it adequately manages the 25% outliers ($\sim$ 30 cm accuracy when evaluating all measurements). However, the performance of LAD decreases rapidly when decreasing the total number of sample points. LAD still provides decimeter accuracy when sampling 100 sample points per phase measurement at 38 frequencies. The error increases directly to several meters when we further de-

crease the total number of sample points. For example, when sampling 50 sample points per phase measurement at 38 frequencies, the localization accuracy decreases to ~ 9 meters while SRIPS still provides a localization accuracy of ~ 30 cm. Moreover, LAD needs a factor of six more measurements than SRIPS for providing decimeter accuracy, as we show in the next section.

4.5.6 CC1000 RIPS versus CC2430 SRIPS Results

Tables 4.2 and 4.3 summarize the results obtained by the CC1000 RIPS implementation and our CC2430 SRIPS implementation. These tables consist of eight columns:

- **References** is the reference used or the name of the positioning algorithm evaluated.
- **Measurement time** is the total measurement time of one target node. We use Equation 4.2 to calculate the total measurement time.
- **Total sample points** is the total number of sample points used to position one target node. We use Equation 4.1 to calculate the total number of sampling points.
- **Error** is the mean of the positioning error.
- **Area** is the surface area of the localization surface.
- **Frequencies** is the number of frequencies used per sender pair.
- **Sender pairs** is the number of sender pairs used by RIPS and SRIPS.
- **Platform** is the radio platform used.

The first two rows show the performance of the RIPS network localization ([8] and [9]). This set-up characterizes itself by the relatively long sampling time (minutes) and high accuracy (centimeters). The remaining rows represent the performance using the infrastructure approach as described in Section 4.2.2. The difference between the two approaches clearly shows that the performance improves with increasing sampling time. [8]/[9] increase the performance by a factor of 10 compared to [11]/[12]/[14]/SRIPS at the cost of an increased sampling time by a factor of 250.

[11] differs from [12]/[14]/SRIPS in that it implements the target-as-sender instead of the target-as-receiver approach. It is difficult to compare the results between these two implementations because [11] calculates 55 q-ranges on the basis of one measurement round. The disadvantage of this approach is that the measurement time increases linearly with the number of target nodes, which is not the case with the target-as-receiver approach. In addition, [11] estimates positions of mobile nodes, while [12]/[14]/SRIPS estimate the positions of static nodes. Note that [12] and [14] also estimate the position of mobile nodes, but we leave these results out of the table. For completeness, we added the results of the Least-Absolute Deviation method described in Section 4.5.5.

Tables 4.2 and 4.3 show that SRIPS provides comparable results as reported by [11]/[12]/[14], while reducing the sampling time by a factor of 15 compared with a target-as-receiver implementation. A factor of 7 is explained by the seven times faster sampling rate of the CC2430. In general, SRIPS requires a factor of 3 fewer measurements compared with the CC1000 implementation. This is because RIPS requires q-range measurements with a relatively high precision (the global minimum is required to be at the true q-range). This high precision is obtained by increasing the measurement time per sender pair ([12] and [14]). SRIPS does not have this requirement as we have seen. Therefore, SRIPS can reduce the required measurement time per sender pair significantly, while increasing the number of sender pairs. This finally results in requiring a factor of 3 fewer measurements, excluding the seven times higher sampling rate available with our CC2430 radio platform.

4.5.7 Radio Interferometric Positioning in Indoor Environments

Both RIPS and SRIPS use the same propagation model that models the electromagnetic energy as scalar plane waves. This scalar approach neglects the polarization effects that start to play a role when the dimensions of the obstacles that meet these propagating waves become of the order of the wavelengths of the carrier waves. In addition, the propagation model does not account for multiple reflections, such as those that are commonly modeled in the area of image reconstruction. Hence, both RIPS and SRIPS cannot reliably localize in such environments. Our preliminary set of indoor measurements in a hall with metal frames confirms this. The results were especially unreliable when the nodes were near these metal frames. But we did obtain decimeter accuracy in those cases where only a few nodes suffered from interfering reflections. Hence, when multiple reflections are not dominating the measurements, SRIPS holds the promise of the ability to discriminate between those reflections.

4.6 Conclusion

In this study, we experimentally verified that it is possible to perform Radio Interferometric Positioning on commonly available radio platforms, such as the CC2430. Such radio platforms do not comply with the frequency tuning requirements of the existing RIPS implementation on the CC1000 platform.

Experiments on the CC2430 platform showed that the RIPS positioning algorithm does not provide decimeter accuracy, because it cannot cope with the outliers generated by the CC2430 platform. This chapter introduced a novel RIPS algorithm, which we call Stochastic Radio Interferometric Positioning (SRIPS). SRIPS was shown to cope with the varying accuracies of the distance estimates without any calibration and with relatively short measurement times compared with the existing CC1000 RIPS implementation. Experiments in a 20×20 m^2 set-up showed that our SRIPS CC2430 implementation reduces the measurement time to less than 0.1 seconds, while providing an accuracy similar to the existing RIPS implementation on the CC1000 platform.

4.7 Acknowledgements

We would like to thank our shepherd Ákos Lédeczi for his comments and guidance, and the anonymous reviewers for their constructive criticism. We are very grateful to Cindy Kleinfeld for editing the chapter.

This chapter describes work in part undertaken in the context of the TSP project. The TSP project has joint funding from the European Regional Development Fund of the European Union and the Dutch Provinces of Gelderland and Overijssel.

Bibliography

[1] M.Sargent, E.Willis Lamb, R.L.Fork: Theory of a Zeeman Laser I. Physical Review, vol. 164, Issue 2, pp. 436-449, December 1967.

[2] D.Rife, R.Boorstyn: Single tone parameter estimation from discrete-time observations. IEEE Transactions on Information Theory, Volume 20, Issue 5, September 1974.

[3] Yi Xie and Yi-zun Wu: Zeeman laser interferometer errors for high-precision measurements. Applied Optics, Vol. 31, Issue 7, pp. 881-884 (1992)

[4] Hashemi H.: The indoor radio propagation channel, Proc. IEEE, July 1993, pp. 943- 996.

[5] P. Bahl and V. N. Padmanabhan: RADAR: An In-Building RF-Based User Location and Tracking System. In Proceedings of the 19th IEEE International Conference on Computer Communications (INFOCOM), March 2000.

[6] N.Patwari: Location estimation in sensor networks. Thesis of Neal Patwari at University of Michigan, 2005.

[7] K.Yedavalli, B.Krishnamachari, S.Ravula, and B.Srinivasan: Ecolocation: A sequence based technique for RF-only localization in wireless sensor networks. In IEEE IPSN 2005, April 2005.

[8] M.Maróti, P.Völgyesi, S.Dóra, B.Kusý, A.Nádas, Á.Lédeczi, G.Balogh, K.Molnár: Radio interferometric geolocation. SenSys 2005: pp. 1-12.

[9] B.Kusý, Á.Lédeczi, M.Maróti, L.G.L.T.Meertens: Node density independent localization. IPSN 2006: 441-448.

[10] B.Kusý, J.Sallai: Analytical solution for radio-interferometric localization of mobile sensors. ISIS technical report, ISIS-06-710. May 2006.

[11] B.Kusý, G.Balogh, J.Sallai, Á.Lédeczi, M.Maróti: InTrack: High Precision Tracking of Mobile Sensor Nodes. EWSN 2007: 51-66.

[12] B.Kusý, J.Sallai, G.Balogh, Á.Lédeczi, V.Protopopescu, J.Tolliver, F.DeNap, M.Parang: Radio interferometric tracking of mobile wireless nodes. MobiSys 2007: 139-151.

[13] B.Kusý, Á.Lédeczi, X.D.Koutsoukos: Tracking mobile nodes using RF Doppler shifts. SenSys 2007: 29-42.

[14] H.Wu, H.Chang, C.You, H.Chu, P.Huang: Modeling and optimizing positional accuracy based on hyperbolic geometry for the adaptive radio interferometric positioning system. International Symposium on Location- and Context-Awareness (LOCA 2007), Oberpfaffenhofen, Germany, September 2007, pp 228-244.

[15] J.Tian, H.Chang, T.Lai, H.Chu: SpinTrack: Spinning Infrastructure Nodes for Precise Indoor Localization. In the poster session of UBICOMP, September 2008.

[16] H.Chang, J.Tian, T.Lai, H.Chu, P.Huang: Spinning Beacons for Precise Indoor Localization. ACM SENSYS 2008, November 2008.

[17] B.J.Dil, P.J.M.Havinga: A Feasibility Study of RIP Using 2.4 GHz 802.15.4 Radios. MELT 2010, November 2010.

[18] B.J.Dil, P.J.M.Havinga: RSS-Based Localization with Different Antenna Orientations. Australian Telecommunication Networks and Applications Conference (ATNAC), 2010.

[19] B.J.Dil, P.J.M.Havinga: Calibration and Performance of RSS-based Localization Methods. Internet Of Things (IOT), 2010.

[20] CC1000. http://focus.ti.com/lit/ds/symlink/cc1000.pdf, 2011.

[21] CC2430. http://focus.ti.com/lit/ds/symlink/cc2430.pdf, 2011.

[22] MRF24J40. http://ww1.microchip.com/downloads/en/DeviceDoc/DS-39776b.pdf, 2011

[23] Low Power 2.4 GHz Transceiver for ZigBee, IEEE 802.15.4, 6LoWPAN, RF4CE and ISM Applications. http://www.atmel.com/dyn/resources/prod_documents/doc5131.pdf, 2011

[24] JN5148 Module. http://www.jennic.com/files/product briefs/JN5148-MO-PB 1v1.1.pdf, 2011.

[25] B.J.Dil and P.J.M.Havinga: Stochastic Radio Interferometric Positioning in the 2.4 GHz Range. In SENSYS 2011.

CHAPTER 5

Space-based RSS localization

This chapter introduces a novel approach to Received Signal Strength (RSS) radio localization. We call this approach space-based RSS. It derives its idea from spatial image reconstruction in Fourier Optics. We show that the resolving power of signal reconstruction determines the localization performance bound. In the far field, this resolving power is independent of whether sampling is performed in space, time or frequency domains as long as the effective number of measurements is equal. Space-based RSS samples RSS over space and can be designed to provide the same resolving power and performance as TOF- and phase-based localization. In our space-based RSS implementation, the far fields from an array of multiplexed fixed transmitters are sampled over localization space with a mobile node. In one-dimension, we experimentally show that the performance of space-based RSS approaches the lower bound of one wavelength of the carrier signal (12.5 cm) in a range of 50 m. In a two-dimensional Line-Of-Sight(LOS) outdoor environment, we obtain a similar localization performance (0.6 m in an area of 20×20 m^2) as the more complicated techniques of TOF and phase measurements, all performed by us for validating this comparison. In a Non-Line-Of-Sight(NLOS) indoor environment, our localization performance is shown to be significantly better (1 m in an area of 40×15 m^2).

5.1 Introduction

This chapter focuses on RSS-based localization and compares its localization performance to TOF- and phase-based localization systems. The advantage of RSS measurements is the relatively low energy consumption, simplicity and widespread availability. Existing papers on the performance bound of RSS-based localization focus on static networks ([4] and [14]). In such studies, the

localization performance is assumed to increase with the number of measurements to fixed nodes with known and unknown positions ([4] and [14]), including calibration measurements. In a practical set-up with a limited amount of fixed nodes, this results in a localization performance of several meters ([7] and [15]). In general, more complicated techniques like TOF- and phase-based localization offer better performances in these set-ups (e.g. [4] and [18]). For example, [18] describes that phase measurements perform a factor of 20 better than RSS measurements in a 20×20 m^2 outdoor environment with four fixed nodes with known positions.

This chapter theoretically and experimentally shows that RSS-based localization can provide similar results as TOF- and phase-based systems by measuring RSS over space. We call this approach space-based RSS. Our experiments over a one-dimensional trajectory show that the performance of space-based RSS approaches the theoretical bound of roughly one wavelength (12.5 cm over a range of 50 m) as determined by the Rayleigh Criterion ([5]). Outdoor experiments in an ideal 20×20 m^2 LOS environment, with four nodes with known positions, show that our new approach provides similar performances (0.6 m) as existing TOF- and phase-based approaches ([23] and [18]). Indoor experiments in a 40×15 m^2 NLOS office environment, with six nodes with known positions, show that our space-based RSS localization system increases the performance to 1 m, compared to 5 m achieved by existing TOF- and phase-based localization systems.

5.1.1 Contributions

We see three contributions in this research:

- We compare theoretical performance bounds of RSS-, TOF- and phase-based localization. This analysis shows that RSS-based localization can obtain similar results as TOF- and phase-based localization by measuring RSS over space.

- Our experiments over one and two dimensions in an ideal LOS outdoor environment show (1) that the theoretical performance bound of roughly 1.22 wavelengths can be obtained over a linear trajectory of 50 m, and (2) that space-based RSS provides similar performances (0.6 m) as the more complex TOF- and phase-based localization systems in a two-dimensional LOS set-up of 20×20 m^2.

- Our experiments in a 40×15 m^2 indoor NLOS office environment show that space-based RSS is more robust to fading effects than TOF- and phase-based localization and increases the performance by a factor of five to roughly 1 m.

5.1.2 Fundamentals of localization

Radio localization describes the process of obtaining a physical location in an automated manner using radio communication. The wave parameters like time, position, temporal frequency and spatial frequency are represented in the propagation model. Propagation models are mathematical representations of far-field solutions of the Maxwell equations. Mathematically, localization then reduces to fitting the measured signals at the unknown location to the appropriate propagation model. We analyze the performance bounds of the various ranging methods by applying the Uncertainty Principle on the wave parameters of the radio waves. Like the Cramer-Rao-Lower-Bound, the Uncertainty Principle is an expression of the Cauchy-Schwartz inequality, and both take on the same form for signals with a wave character. Our analysis shows that the effective number of measurements in time, temporal frequency band and space domain determine the resolving power of the measured ranges. This effective number of measurements is interchangeable in the three domains due to the general wave character of the signals in their far fields. In other words, phase-, TOF- and RSS-based localization systems provide similar performance bounds when the effective number of measurements is the same.

5.1.3 Space-based RSS

The idea of space-based RSS has its origin from image reconstruction in Fourier Optics ([5]). In Fourier Optics, a signal is sampled over space to reconstruct the transmitted signal at a given position. The optimal resolving power is provided when the signal is sampled with the maximum effective resolution over the entire localization space. Space-based RSS samples signal intensities (RSS) over space with a mobile node (with unknown position) to reconstruct the signal and the position of a transmitter (with unknown position). The mobile node estimates its position by measuring signal intensities to an array of fixed transmitters with known positions. The maximum resolving power is obtained when the localization surface is sampled with the resolution defined by the Rayleigh Criterion for incoherent signals. As already stated

above, we experimentally apply this space-based RSS localization to a one-dimensional trajectory, to a two-dimensional LOS outdoor environment, and to a two-dimensional NLOS indoor environment. We find general agreement between theory and experiments.

5.1.4 Overview

This chapter is arranged in the following way. Section 5.2 briefly reviews the underlying physics of the uncertainties or lower and upper performance bounds on signals with a periodic wave character. Section 5.3 describes the setup and results for one-dimensional ranging and Section 5.4 for the new two-dimensional approach. Section 5.5 evaluates our space-based RSS implementation and compares it to other localization systems. Section 5.6 discusses the results and relates it to existing work in this field. Finally, Section 5.7 gives the conclusions.

5.2 Analysis of Performance Bounds

In this section, we theoretically compare the resolving power and performance of phase-, TOF- and RSS-based localization techniques. We use the fact that these techniques are based on signals with a periodic wave character measured in the far field. In order to reconstruct such signals with optimal resolving power, we compute the minimum number of required sample points. For a thorough analysis on scalar wave propagation, we refer to [5].

The amplitude, V, of a wave radiating from a point source at the origin measured in the far field at position, $\vec{r}$, is represented by:

$$V\left(\vec{k},\vec{r},f,t,\varphi\right) = V_{ref} \cdot \frac{\sin\left(\vec{k}\cdot\vec{r}+2\pi ft+\varphi\right)}{(\vec{k}\cdot\vec{r})} \tag{5.1}$$

Here, $\vec{k}$ is the wave vector, f is the temporal frequency, t is the time, and φ is the phase. Time and traveling distance, $d = |\vec{r}|$, are connected by the constant speed of light, c, as are temporal frequency and wavelength, $\lambda = \frac{c}{f} = \frac{2\pi}{|\vec{k}|}$. In the far field, $\vec{k}\cdot\vec{r} >> 1$, traveling distance, d, and spatial frequency, $\frac{1}{\lambda}$, are Fourier conjugates as are time, t, and temporal frequency, f. The fundamental upper and lower bounds on the bandwidths (FWHM, Full Width at Half Maximum) of these pairs of wave parameters can be simultaneously estimated by

the respective Uncertainty Principles that hold for Fourier conjugates of wave parameters. The lower bounds on the bandwidths of these respective parameters are estimated by:

$$\Delta t \cdot \delta f \gtrsim 1 \tag{5.2}$$

$$\delta t \cdot \Delta f \gtrsim 1 \tag{5.3}$$

$$\Delta \frac{1}{\lambda} \cdot \delta d \gtrsim 1 \tag{5.4}$$

$$\delta \frac{1}{\lambda} \cdot \Delta d \gtrsim 1 \tag{5.5}$$

Here, δf, δt, $\delta \frac{1}{\lambda}$ and δd represent the lower bounds or smallest measurable quantity of the wave parameters. The upper bounds or measuring ranges of the wave parameters are represented by Δf, Δt, $\Delta \frac{1}{\lambda}$ and Δd. For example, δf equals the FWHM of the carrier wave during a given measurement time, Δt. It follows directly from Equations 5.2, 5.3, 5.4 and 5.5 that the resolving power of the respective wave parameters is connected to each other through:

$$\frac{\delta t}{\Delta t} = \frac{\delta f}{\Delta f} = \frac{\delta \frac{1}{\lambda}}{\Delta \frac{1}{\lambda}} = \frac{\delta d}{\Delta d} = \frac{1}{N} \tag{5.6}$$

In Equation 5.6, N, is the minimum number of required measurement points on Δd. For coherent signals this minimum number is determined by the Nyquist sampling rate, which corresponds to two sample points per temporal period, $\frac{1}{f}$. For incoherent signals, this minimum is determined by the Rayleigh Criterion which corresponds to one sample point per 1.22 wavelengths. Such minimum numbers are called the effective number of sample measurements. Increasing the number of samples beyond this number does not increase the resolving power (so-called empty magnification). The effective number of sample measurements follows from the Uncertainty Principles as the ratio of lower and upper bounds as expressed by Equation 5.6. In the time domain, the upper bound is limited by the coherence time of the carrier waves. In space, the upper bound is determined by the longest diagonal cross-section of the sampled localization space and leads to the diffraction limit as given by the Rayleigh criterion. This latter upper bound should be smaller than the product of the coherence time of the carrier wave and the speed of light.

The carrier frequency cannot be determined beyond its natural bandwidth or spread, δf, of the transmitted and received signals. This means that increasing the measurement time beyond the coherence time, $\frac{1}{\delta f} = \Delta t_c$, does not further increase the resolving power (or decrease the bandwidth). We assume that the natural bandwidth of the transmitted signals is determined by the Q-factor of the crystal oscillator, or $\delta f = \frac{f}{Q}$. To make a fair comparison, this stability is assumed to be equal for all localization techniques. We follow the $802.15.4$ guidelines ([3]), so that our crystal oscillators transmit in the 2.4 GHz range ($f = 2.4 * 10^9\ Hz$) and have a Q-factor of 10^4 ($\sigma = 40$ ppm, FWHM $\approx 2.4 \cdot 40 \approx 100$ ppm). The coherence time is given by $\frac{1}{\delta f} = \Delta t = \Delta t_c \approx 4.2 \cdot 10^{-6}$ s (FWHM). We assume that the localization techniques sample each signal within the coherence time.

The following three sections analyze the resolving power in existing phase-, TOF- and RSS-based localization techniques. The fourth subsection analyzes the resolving power of space-based RSS. The last subsection compares these four resolving powers.

5.2.1 Phase-Based Localization

Phase-based localization determines the distance or range, Δd, on the basis of phase difference measurements, $\Delta\varphi$, between transmitter-receiver pairs as given by:

$$\Delta d = (n_\lambda + \Delta\varphi)\lambda \tag{5.7}$$

Here, n_λ is an integral number of wavelengths in Δd, $n_\lambda = \lfloor \frac{\Delta d}{\lambda} \rfloor$, and is assumed to be known. For further analysis of phase-based localization we refer to [1]. The natural bandwidth of the beat signal, δf_b, translates into a wavelength deviation as:

$$\delta\lambda_b \approx -\frac{\delta f_b}{f_b}\lambda_b \tag{5.8}$$

Using Equations 5.2, 5.3, 5.4 and 5.5 and using the Q-factor of our oscillators gives the following resolving power:

$$\frac{\delta d}{\Delta d} \approx \frac{\delta f_b}{f_b} \approx \frac{\delta f}{f} = \frac{\delta t}{\Delta t} = 5 \cdot 10^{-5} \tag{5.9}$$

Equation 5.9 shows that the resolving power is about equal to the natural bandwidth relative to the carrier frequency ($\frac{\delta f}{f}$), which amounts to the inverse

of the effective number of samples over time ($\frac{\delta t}{\Delta t}$). Here δt is determined by the Nyquist sampling rate. The theoretically attainable resolving power of 0.005%, calculated for $802.15.4$ radios, is a factor of 10 better than the resolving power measured in [11] (~ 5 centimeter performance on 100 meters). We expect that this difference is caused by that the localization in [11] assumes that n_λ is not known, which increases the error significantly. In principle, further interpolation of phases beyond the Nyquist limit is possible using, for instance, Doppler shifts. This falls outside the scope of this chapter.

5.2.2 TOF-Based Localization

TOF-based localization determines the distance on the basis of a Time-Of-Flight measurement. We analyze the resolving power of the distance estimate of TOF measurements between one sender - receiver pair. In TOF-based localization, the resolving power depends on how well the time-of-flight can be measured given a pulse of Δt seconds with a bandwidth of Δf and a crystal oscillator with a natural bandwidth of δf. TOF systems modulate the temporal frequency with time, like chirps or wavelets (e.g. [10]). The number of measured or distinguishable temporal frequencies determines the resolving power. For our radios, this resolving power can be derived from Equation 5.6 with $\Delta f = 80$ MHz as given by ([10]):

$$\frac{\delta f}{\Delta f} = \frac{1}{N_f} = 3 \cdot 10^{-3} = \frac{\delta d}{\Delta d} \tag{5.10}$$

Here N_f represents the number of measured or distinguishable temporal frequencies. Equation 5.10 shows that the localization performance directly relates to the natural bandwidth of the carrier wave and the bandwidth of the pulse. Note that Equation 5.10 implies that the resolving power of TOF measurements is constant, independent of range and is approximately 0.3% of the measurement distance. This resolving power, calculated for $802.15.4a$ radios, is roughly equal to the resolving power estimated in [10] (~ 60 centimeter over 100 meters with $\Delta f = 40$ MHz).

5.2.3 Existing RSS-based Localization

The Received Signal Strength is the power or intensity of the received signal, which equals to the accumulated squared magnitudes of the frequency components of the received signal amplitudes (Equation 5.1). The distance between one sender and one receiver is given by:

$$\sqrt[n]{\frac{P_{d_0}}{RSS}} = \Delta d \tag{5.11}$$

Here, RSS is given in milliWatt (mW). P_{d_0} is the "reference RSS" received at reference distance d_0. For sake of simplicity, we assume that $d_0 = 1$ m. The reference RSS is a function of the antenna gains and transmission power ([2]). The path loss exponent, n, represents the rate at which the power decreases with increasing distance. In general, the power is given in dBm (Decibel Milliwatt, e.g. [2]):

$$10 \log_{10}(RSS) = 10log_{10}(P_{d_0}) - 10n \log_{10}(\Delta d) \tag{5.12}$$

Note that Equation 5.12 represents the well-known Log-Normal Shadowing Model. In this empirical model, the path loss exponent is a variable parameter. In existing RSS-based localization, the resolving power depends on how well RSS can be measured with a pulse of Δt seconds, a bandwidth of Δf, and a crystal oscillator with a natural bandwidth of δf:

$$\frac{\delta f}{\Delta f} = \frac{1}{N_f} = \frac{\delta d}{\Delta d} \tag{5.13}$$

However, in practical RSS setups, scanning a frequency band of Δf is not performed with resolving power determined by the natural bandwidth of the carrier wave and the bandwidth combined of all carrier waves. As we shall see later in Sections 5.3.1 and 5.5, this seriously limits the attainable resolving power.

5.2.4 Space-based RSS

In this analysis, we assume that the receiver is moving relative to the transmitter over a range of Δd meters. Equation 5.6 then gives:

$$\frac{\delta \frac{1}{\lambda}}{\Delta \frac{1}{\lambda}} \approx \frac{\lambda}{\Delta d} = \frac{1}{N_d} \tag{5.14}$$

Equation 5.14 implies that the resolving power of RSS measurements is not constant but varies with the measuring range when we keep the number of sample points constant per wavelength. This is similar to the phase-based localization case. However, the resolving power depends on the number of measured wavelengths over the measuring range ($N_d = \frac{\Delta d}{\lambda}$) instead of the number

Table 5.1: Performance bounds

Method	Resolving Power	Resolving power in 802.15.4 in 2.4 GHz	Bandwidth
Phase-based localization	$\frac{\delta f}{f}$	$5 \cdot 10^{-5}$	80 MHz
TOF-based localization	$\frac{\delta f}{\Delta f}$	$3 \cdot 10^{-3}$	80 MHz
Space-based RSS	$\frac{\lambda}{\Delta d}$	$\frac{0.125}{\Delta d}$	5 MHz

of periods over time ($N_p = f \cdot \Delta t$). As we shall see later, sampling the signal intensities over space does not have to be performed within the coherence time to obtain the theoretically attainable resolving power of Equation 5.14, which is roughly λ. The smallest measurable position difference (δd) is defined by the Rayleigh Criterion for two incoherent sources and amounts to roughly 1.22 wavelengths.

5.2.5 Comparison

Table 5.1 shows the resolving power of the localization techniques considered. For comparison, we set the resolving power of the various localization techniques equal to the TOF technique ($\frac{\delta f}{\Delta f}$). Phase-based localization provides the same resolving power by reducing the measuring time (Δt) by a factor of ($\frac{f}{\Delta f}$ =)60 to 70 nanoseconds. Space-based RSS provides the same resolving power when RSS is measured over a distance of Δd =42 meters.

The advantage of space-based RSS is that the resolving power does not depend on (1) the Q-factor of the crystal oscillator (δf) as long as $\Delta d < c\Delta t_c$, and on (2) the available temporal frequency bandwidth Δf. This means that space-based RSS can be implemented on any COTS narrowband radio that measures RSS (e.g. [22]). Moreover, free temporal frequency bandwidth is sparse. For instance, in the 2.4 GHz there is 80 MHz available that has to be shared between all radios.

Space-based RSS in an NLOS indoor office environment is more robust to spatial influences than existing TOF and phase-based solutions in the 2.4 GHz range (see Section 5.5), without increasing the required bandwidth. The disadvantage of space-based RSS is that it requires a mobile radio to measure RSS over space.

5.3 Experimental Analysis in one Dimension

In this section, we experimentally investigate the theoretical RSS results obtained in Section 5.2 in one dimension. First, we describe the experimental set-up used throughout this section. In the first series of measurements, we analyze the resolving power of RSS measurements by adding and averaging RSS measurements over time and temporal frequencies like is done in the existing literature (e.g. [16]) and in line with Section 5.2.3. In the second series of measurements, we analyze the resolving power of RSS measurements in the space-domain in line with Section 5.2.4. We use the JN5148 platform ([22], 802.15.4 [3]) for measuring RSS. [22] uses 5 MHz O-QPSK signals. All measurements are performed in the same outdoor environment as in [18].

5.3.1 RSS Measurements in One Dimension

We measure RSS between one fixed transmitter and one receiver over a distance of 50 m. The transmitter is main powered, has a power amplifier and broadcasts messages with the maximum power allowed by ETSI ([20]). The receiver is battery powered and does not have a power amplifier ([22]). Both transmitter and receiver have an external dipole antenna. While measuring RSS, we ensure that the antennas have the same vertical orientation and are in line-of-sight for best reception. Both radios are attached to tripods for stability. Both radios are placed at a height of 0.35 m in order to eliminate interference with ground reflections over a range of 50 m.

The transmitter broadcasts a message every 1.6 ms with an incrementing message count. After each transmitted message, the transmitter changes its operating frequency, rotating between eight frequencies. These frequencies are equal to the following IEEE 802.15.4 channels ([3]): {11,13,15,17,19,21,23,25}, and are uniformly distributed over the frequency interval [2.405 GHz, 2.475 GHz]. The receiver starts logging when it receives the first message and stores the message counts and associated RSS measurements. The receiver synchronizes to the transmitter by the received messages and it rotates through the same frequencies. At the end of a measurement round, the receiver flushes the logged data over a serial cable. The logged data are analyzed centrally with Matlab. We start and end a measurement round manually.

We calibrate the Log-Normal Shadowing model parameters (See Section 5.2.3, Equation 5.12) by fitting all RSS measurements over the total range of 50 m. This fit is assumed to represent the true signal strength decay over space.

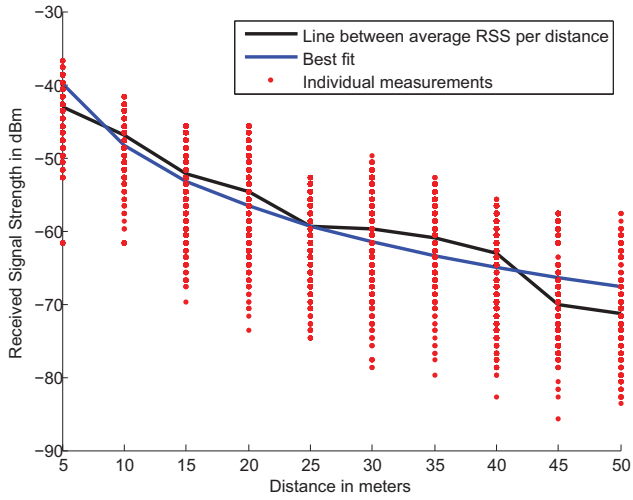

Figure 5.1: Individual RSS measurements with fixed radios

One Dimensional RSS with Fixed Radios

In our first series of measurements, we analyze the influence of time and temporal frequencies on the resolving power. In this experimental set-up, the transmitter and receiver are fixed during the measurement rounds. We only change the position of the receiver between the measurement rounds. The receiver measures RSS at 10 different distances in steps of 5 m ($5, 10 \ldots 50$ m) at 8 different frequencies during 10 s (~ 6000 RSS measurements).

Figure 5.1 shows the results of these RSS measurements. The "Best fit" (blue curve) has the following Log-Normal Shadowing Model parameters (Equation 5.12 in Section 5.2.3, $P_{d_0} = -20\ dBm$ and $n = 2.7$). The black curve in Figure 5.1 represents the average RSS decay over distance.

The experiment shows that:

- The individual measurements provide a resolving power of 0.35 (35% of measurement distance is error), without averaging RSS measurements over time and temporal frequencies.

- Averaging $\sim$ 1000 RSS measurements over a time span of 10 seconds per measurement distance increases the resolving power to 0.33 (33% of

measurement distance is error). In this averaging, we did not include RSS measurements over temporal frequencies.

- Averaging 8 consecutive RSS measurements over 8 temporal frequencies per measurement distance increases the resolving power to 0.18 (18% of measurement distance is error).
- Averaging RSS over time and 8 temporal frequencies increases the resolving power to 0.18 (18% of measurement distance is error).

In conclusion, averaging RSS measurements over time has a relatively small influence on the resolving power (increasing resolving power from 0.35 to 0.33), while averaging RSS measurements over different temporal frequencies has a limited influence on the resolving power (increasing resolving power from 0.35 to 0.18). These measurements show that the maximum resolving power in the 2.4 GHz band is equal to 0.18 (9 m localization performance at 50 m), if we average RSS measurements over time and temporal frequencies at one point in space like is done in the existing literature (e.g. [16]).

One Dimensional RSS with Moving Receiver

In our second series of measurements, we analyze the influence of space on the resolving power. In this experimental set-up, the transmitter is fixed and the receiver is carried by a moving person. The person holding the receiver starts walking in a straight line towards the transmitter. We manually start the measurements when the distance between the receiver and the transmitter equals 50 m. We manually stop the measurement when the receiver is five meters away from the transmitter ensuring we stay in the far field. We assume that the person holding the receiver walks with a constant speed. Therefore, the message count determines the time, speed, distance to the transmitter, and the temporal frequency. Note that the possible variation in speed of the receiver and manually starting and stopping the measurement introduce ranging errors (reduces resolving power). We performed seven measurement series.

The receiver measures RSS (RSS_i) at fixed time intervals ($i = 1 \dots M$) over a certain distance interval (Δd). We are interested in the distances, d_i, corresponding to the RSS_i measurements. The distances between the individual RSS measurements are assumed to be known ($\forall i$, $\forall j$,$d_i - d_j$ is known). Figure 5.2 illustrates this sliding-window method. The measured RSS over the distance interval, Δd, are fitted to the expected RSS decay over distance as represented by the equation:

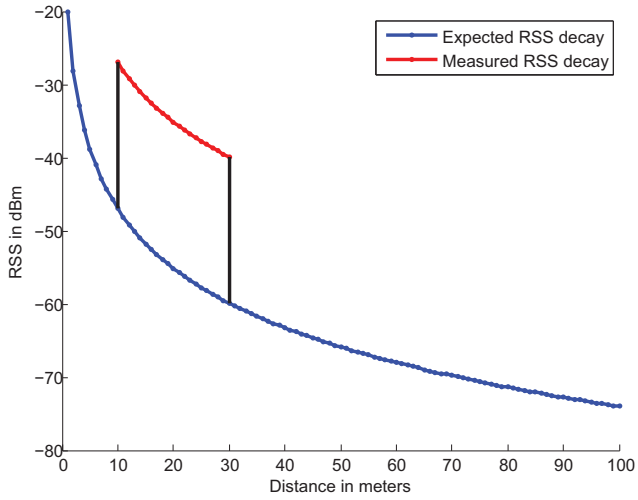

Figure 5.2: Cross correlating RSS over space

$$\min_{\bar{d}} \sum_{i} \left(P_{d_0} - 10 \cdot n \cdot \log_{10}(\bar{d} + o_i) - RSS_i \right)^2 \tag{5.15}$$

Here $\bar{d}$ is the average distance between the transmitter and the receiver; o_i is the distance offset between the average distance and the actual distances (which are known); RSS_i is RSS measured at distance $\bar{d} + o_i$. We minimize Equation 5.15 by sliding a window of distance interval Δd (see insert in Figure 5.2) over the total range of 200 m using a brute force optimization technique with a resolution of 0.01 m. Note that Equation 5.15 is similar to cross-correlating a measured signal with the expected signal over space. TOF measurements cross-correlate the measured signal with the expected signal over time ([10]). In that case, the peak of the cross-correlation function is the measured time of arrival.

Figure 5.3 shows the localization performance of four different number of temporal frequencies ($N_f = \{1, 2, 4, 8\}$) as a function of the distance interval ($\Delta d = \{0.75, 1.5, 3, 6, 12, 24\}$ m). The measurements show that:

- The influence of the number of temporal frequencies decreases with an increasing distance interval.

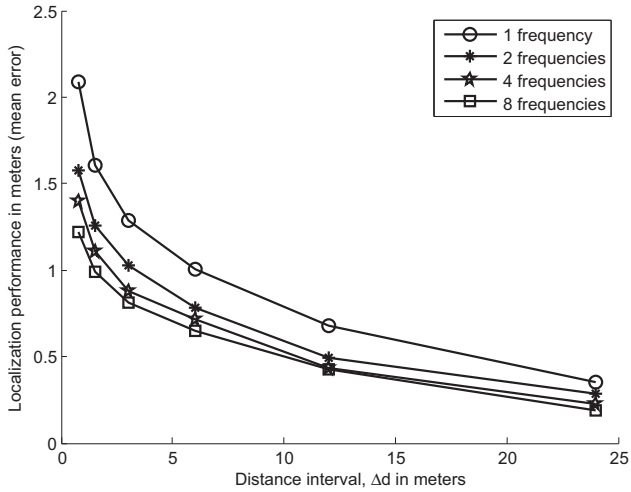

Figure 5.3: Error as a function of the distance interval

- The localization performance converges to 18 cm and approaches the theoretical limit determined by the Rayleigh Criterion of 1.22λ=15 cm (see Section 5.2.4). Note that a localization performance of 18 cm is equal to a resolving power of 0.0065 ($\approx 1.22\frac{\lambda}{\Delta d} = 1.22\frac{0.125}{24}$).

Increasing the distance interval decreases the influence of the number of measured temporal frequencies. Hence, space-based RSS does not require additional measurements over temporal frequencies to improve its resolving power. This significantly reduces the implementation and network complexity.

In conclusion, we showed that it is possible to experimentally approach the theoretical limit by measuring RSS over a distance interval of at least 24 m in one dimension. In addition, this section experimentally showed that measuring RSS in the space-domain increases the resolving power from 0.18 (Section 5.3.1) to 0.0065 (0.33 m localization performance at 50 m).

In our measurement set-up, we assumed that the distances between the measurements were known by assuming that the receiver is moving with a constant speed towards the transmitter. A practical implementation of this set-up would involve inertial sensors in combination with a network of transmitters (e.g. [13]). However, in this chapter we focus on an RSS-only solution. Section 5.4 describes our implementation of a two-dimensional space-based

RSS localization system.

5.4 Space-based RSS Localization

We now describe the network set-up of our space-based RSS localization system. First, we describe the network set-up and how the nodes perform the required measurements and communication. Secondly, we describe how the obtained information is used for localization.

5.4.1 Network Set-up

Section 5.2.4 theoretically showed that the resolving power increased with an increasing measuring space. The measurements in Section 5.3.1 experimentally verified this increase. In this section, we describe our implementation of a two-dimensional space-based RSS localization system. It derives its idea from spatial signal reconstruction in Fourier Optics [5]. In Fourier Optics, a signal is sampled over space to reconstruct the transmitted signal at a given position. Our space-based RSS localization system samples RSS over the localization surface with a mobile node to reconstruct the signal and the position of a fixed transmitter at unknown position. The mobile node and the transmitter do not know their locations and thus require localization. We call these two types of nodes mobile and fixed blind nodes. The mobile nodes position themselves by measuring RSS to transmitters with known positions, which we call reference nodes. The optimal resolving power is provided when RSS is sampled by a mobile node with the required resolution over the entire localization space (see Section 5.2.4). However, this is not a realistic scenario as this would require too many measurements. Therefore, in most cases the maximum resolving power is not obtained. Section 5.5 experimentally verifies this resolution issue. Figure 5.4 shows the network set-up of our localization system. We distinguish two basic types of nodes:

- **Reference nodes** know their position. We distinguish two types of reference nodes: (1) infrastructure nodes ('I' in Figure 5.4) and (2) gateways ('G' in Figure 5.4). The infrastructure nodes form the backbone of the network and transmit all measurements to the gateway. The gateway connects the wireless network to a server for centralized data processing.
- **Blind nodes** do not know their position and require localization. We distinguish two types of blind nodes based on their mobility characteristics:

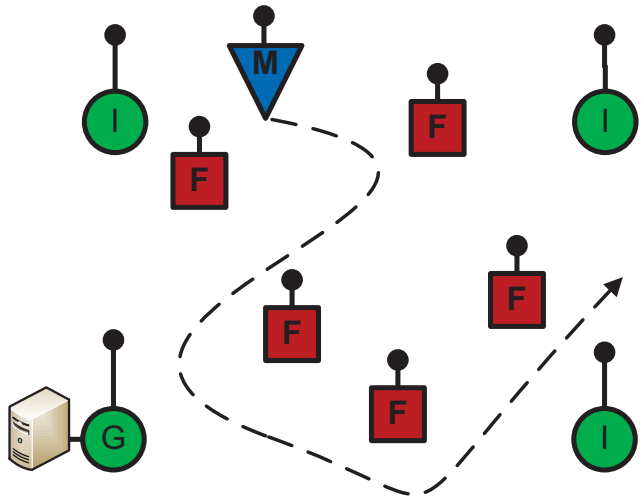

Figure 5.4: Our space-based RSS set-up

(1) fixed blind nodes ('F' in Figure 5.4) and (2) mobile blind nodes ('M' in Figure 5.4). Fixed blind nodes are fixed during the localization process. Mobile blind nodes are mobile and require real-time localization.

Figure 5.5 shows the communication direction and which nodes perform the required RSS measurements for localization:

- The reference nodes broadcast their ID and the mobile nodes listen to these messages and perform RSS measurements.
- The fixed blind nodes broadcast their ID and the reference nodes and mobile blind nodes listen to these messages and perform RSS measurements.

All RSS measurements performed by the reference nodes and mobile nodes are forwarded to the localization server. The server processes this information to estimate the position of all blind nodes. The next section describes how the nodes obtain the required measurements and forward this information to the server.

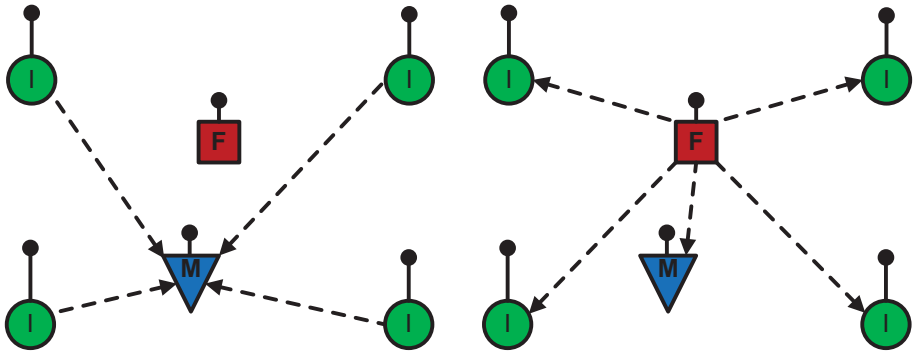

Figure 5.5: Communication and measurement direction

5.4.2 Communication Protocol

Our communication protocol uses two different channels; one for performing the RSS measurements (Broadcast Channel) and one for forwarding the RSS measurements (Data Channel):

- The Broadcast Channel is used by the reference and fixed blind nodes to broadcast their ID's every 100 ms. These messages are used for (1) RSS measurements for localization and (2) Network establishment. Every hundred milliseconds, the reference and fixed blind nodes broadcast their ID. The reference nodes also broadcast their current hop count for updating their node neighborhood list and for determining the shortest path to the gateway. Only robust links are stored in the neighborhood list. Robust links are links that have an RSS above a certain threshold. The mobile blind node transmits its messages to the reference node that has the most robust link (highest RSS).

- The Data channel is used for forwarding the localization measurements to the server. We ensure that communication in the data channel is reliable by using the automatic ACK's in the IEEE 802.15.4 standard ([3]).

Our network operates as follows. The mobile blind nodes listen to the messages in the broadcast channel. When a mobile blind node receives a message, it stores the ID, relative time of arrival, and measured signal strength. After a short period (in our system set to one second), the mobile blind node switches

to the data channel and forwards the collected localization measurements via the reference nodes to the localization server.

The reference nodes form the wireless infrastructure and establish a mesh network to the nearest gateway. The routing is based on the hop-count. A message is forwarded to the node that is closer to the gateway and which has a robust link. Once a minute, the reference nodes listen to messages for 250 ms in the broadcast channel for (1) updating their hop counts and neighborhood lists and (2) for performing RSS measurements to the fixed blind nodes. All these measurements are forwarded to the localization server.

The fixed blind nodes broadcast their ID and go immediately into a deep sleep mode to reduce energy consumption ([22]). We can further reduce the energy consumption by increasing the time between consecutive broadcasts (once every few seconds). This does not affect the localization performance, but only decreases the convergence rate in time. The fixed blind nodes do not measure RSS to each other and save energy by doing so.

5.4.3 Optimization Definition

Consider a wireless network that consists of R reference nodes (infrastructure and gateway nodes), F fixed blind nodes and one mobile blind node:

- We identify the positions of R reference nodes by: $x_1, y_1 \dots x_R, y_R$.
- We identify the positions of F fixed blind nodes by: $x_{R+1}, y_{R+1} \dots x_{R+F}, y_{R+F}$.
- One mobile blind node that does not know its location and changes its location every time instance. We identify the positions of the mobile blind node over T time instances by: $x_{M,1}, y_{M,1} \dots x_{M,T}, y_{M,T}$.

In each individual time instance t, the mobile node measures the RSS to the reference and fixed blind nodes:

- We identify RSS measurements to reference nodes by: $RSS_{t,1} \dots RSS_{t,R}$.
- We identify RSS measurements to fixed blind nodes by: $RSS_{t,R+1} \dots RSS_{t,R+F}$.

With these notations, the optimization problem is expressed by:

$$\min_{\theta} \sum_{t=1}^{T} \sum_{i=1}^{R} \left(\widehat{RSS}_{t,i} - RSS_{t,i} \right)^2 + \sum_{t=1}^{T} \sum_{j=R+1}^{R+F} \left(\widehat{RSS}_{t,j} - RSS_{t,j} \right)^2 \tag{5.16}$$

Here:

$$\widehat{RSS}_{t,i} = P_{d_0,i} - 10 \cdot n_i \cdot \log_{10} \sqrt{(\hat{x}_{M,t} - x_i)^2 + (\hat{y}_{M,t} - y_i)^2} \tag{5.17}$$

and:

$$\widehat{RSS}_{t,j} = P_{d_0,j} - 10 \cdot n_j \cdot \log_{10} \sqrt{(\hat{x}_{M,t} - \hat{x}_j)^2 + (\hat{y}_{M,t} - \hat{y}_i)^2} \tag{5.18}$$

Here $P_{d_0,i}$, n_i, $P_{d_0,j}$ and n_j represent the parameters of the Log-Normal Shadowing Model. We assume that these parameters are individually calibrated for each transmitter (reference nodes and fixed blind nodes). For simplicity, we assume that these parameters are calibrated before localization. However, we expect that these parameters can automatically be calibrated during the localization process as in [17] and [19]. θ represents the set of parameters that minimizes Equation 5.16. This set consists of mobile and blind node positions:

$$\theta = \{\hat{x}_{M,1}, \hat{y}_{M,1} \ldots \hat{x}_{M,T}, \hat{y}_{M,T}, \hat{x}_{R+1}, \hat{y}_{R+1} \ldots \hat{x}_{R+F}, \hat{y}_{R+F}\}$$

Note that Equation 5.16 can be generalized to incorporate more than one mobile node by adding mobile node positions and RSS measurements. Our localization algorithm uses Equation 5.16 to determine the unknown positions of all blind nodes, this includes positions of fixed and mobile blind nodes. We minimize Equation 5.16 with Matlab using the iterative non-linear large-scale optimizer. We use the measurements between the reference and the individual blind nodes to compute the start position of the individual blind nodes.

5.5 Performance Evaluation

In this section, we evaluate our space-based RSS localization system described in Section 5.4 in an LOS outdoor and NLOS indoor environment. We compare our localization system with existing TOF-, phase- and RSS-based systems.

Section 5.5.1 describes how we obtained the measurements with the localization systems and the algorithms used for evaluation. Section 5.5.2 presents the performance of the localization systems in an ideal LOS outdoor environment. The last section presents the performances in an NLOS indoor office environment.

5.5.1 Measurement Set-ups

In the following subsections, we describe the two-dimensional localization measurement systems used. During all measurement rounds, the raw measurements were sent to a computer and logged for post-processing.

Space-Based RSS System

In a space-based RSS set-up, we place and localize all fixed blind nodes at the same time while walking through the localization area with a mobile node. In the outdoor and indoor environment, we meandered through the localization area for roughly ten minutes. We use the localization system described in Section 5.4.

Existing RSS-Based Systems

We evaluate the performance of two existing RSS-based localization systems ([4] and [8]). These localization systems only process RSS measurements between reference and fixed blind nodes.

[4] describes the Maximum Likelihood Estimator given the Log-Normal Shadowing Model (see Section 5.2.3, Equation 5.12). Although [4] is a relatively old reference, the MLE of the Log-Normal Shadowing Model still provides competitive results ([14]) and is still used in the newest localization systems ([17]). We enhanced [4] by individually calibrating the transmitters (as in [17] and Section 5.4.3). This ensures that the MLE provides the best performance. Using a Least-Absolute-Deviations method instead of a Least-Squares method did not improve the performance, like in [17].

[8] uses a proximity-based localization algorithm. These localization algorithms only use the order of RSS measurements instead of converting RSS measurements to distances. The advantage of [8] is that it does not require calibration.

TOF-Based Localization System

We evaluate the performance of TOF using the TN100 platform ([23], 802.15.4a [12]). [23] transmits in the 2.4 GHz band and uses 80 MHz chirp signals. We only had two ranging devices at our disposal, one infrastructure node and one blind node. This means that we had to perform one measurement round per reference/blind node position pair. We expect that this approach increases the performance, because all TOF measurements have the same bias when using the same node pair ([10]). We computed the position with a Weighted Least Squares Method (WLSM):

$$\min_{\{\hat{x},\hat{y}\}} \sum_{i=1} W_i \left(\hat{d}_i - d_i)\right)^2 \tag{5.19}$$

Here, $\hat{d}_i$ is the distance between position estimate $(\hat{x}, \hat{y})$ and reference node i, d_i is the distance measurement to reference node i, and W_i is the weight associated with distance measurement d_i. In the outdoor environment, Equation 5.19 gave the best performance with $W_i = 1$. In the indoor environment, Equation 5.19 gave the best performance with $W_i = \frac{1}{d_i^2}$.

Phase-Based Localization System

We use the results of [18] for comparison, because the measurements in [18] were performed in the same set-up and in the same environment. [18] uses the CC2430 platform ([21]), which also transmits in the 2.4 GHz range.

5.5.2 Performance Outdoor Environment

The measurements with the RSS-, TOF- and phase-based localization systems were conducted in a 20×20 m^2 LOS outdoor environment. In all measurement set-ups, we placed one reference node at each of the four corners. We placed and localized the fixed blind nodes at 12 different locations in a 4x4 grid. We consider this environment as an ideal environment, so we assume that the localization systems provide the best possible performance. Table 5.2 summarizes the results obtained in this section. This table shows that:

- The existing RSS-based localization systems, using a classical network set-up, perform an order of magnitude less relative to other localization systems. This is in line with the theoretical and experimental results presented in Sections 5.2.3 and 5.3.1.

Table 5.2: Performance 20×20 m^2 Outdoor LOS Environment

Method	Mean error	Median error	Standard deviation
Proximity-based, [8]	3.8 m.	3 m.	1.2 m.
RSS- and Range-based, [4]	3 m.	2.9 m.	2 m.
Our space-based RSS	0.6 m.	0.4 m.	0.4 m.
TOF-based, [23]	0.3 m.	0.3 m.	0.2 m.
Phase-based, [18]	0.3 m.	0.2 m.	0.2 m.

Table 5.3: Performance 40×15 m^2 Indoor NLOS Environment

Method	Mean error	Median error	Standard deviation
Proximity-based, [8]	6.3 m.	5 m.	3.8 m.
RSS- and Range-based, [4]	2.6 m.	2.3 m.	1.2 m.
Our space-based RSS	1.1 m.	1 m.	0.6 m.
TOF-based, [23]	5 m.	4.9 m.	1.9 m.

- Our space-based RSS localization system performs less than the one-dimensional localization system presented in Section 5.3.1. This is probably because the mobile node did not sample the entire localization area with the required resolution as given in Section 5.4.1.

- Phase- and TOF-based localization systems provide comparable results as our space-based RSS. However, the phase- and TOF-based localization systems require specialized hardware or precise synchronization between nodes. Our localization system only requires 5 MHz in the 2.4 GHz band for localization, while the other localization systems use the entire 80 MHz in the 2.4 GHz band.

5.5.3 Performance Indoor Environment

RSS- and TOF-based localization was conducted in a 40×15 m^2 NLOS indoor office environment. We did not perform phase measurements in this environment, because our phase-based localization system became unreliable in a 15×15 m^2 LOS indoor environment ([18]).

Figure 5.6: Indoor NLOS environment

In all measurement set-ups, we placed six reference nodes in six different rooms over the total localization space that was divided into 20 separated compartments. We randomly placed 12 blind nodes over the area for localization. We consider this environment as a harsh environment, because most nodes are not in line-of-sight of each other. Moreover, most rooms have a large metal cabinet ($1.2 \times 0.5 \times 1.8$ m^3) and there are several walls of reinforced concrete. The measurements were conducted during working hours, so people were walking around and influenced the measurements. Figure 5.6 shows a map of the office space that we used for our indoor localization experiment. The green circles represent the reference nodes, the red squares represent the fixed blind nodes, the blue rectangles represent the large metal cabinets and the thick grey lines represent the reinforced concrete walls. Table 5.3 summarizes the results obtained in this section. This table shows that:

- [4] provides better results in the indoor environment than in the outdoor environment. We expect that this is because the indoor environment had two more reference nodes than the outdoor environment. In comparison with the outdoor environment, [8] performs significantly less than [4]. We expect that the individual calibration of the transmitters makes [4] more robust against environmental influences.

- TOF-based localization provides significantly less performance in indoor

environments than in outdoor environments. These results show that the resolving power of TOF in the time domain cannot cope with the environmental influences in indoor environments, like multipath effects and fading. Moreover, TOF radios estimate one distance estimate instead of using a stochastic approach as in [18]. We expect that a stochastic approach would improve the performance significantly in an indoor environment.

- Space-based RSS provides slightly less performance in this indoor environment than in the outdoor environment. These results show that space-based RSS is robust against the static and dynamic environmental influences of our office environment.

5.6 Related Work and Discussion

The theory in Section 5.2.4 shows that the resolving power of a space-based RSS localization system increases when the RSS measuring space increases. On the basis of this theory, we described two space-based RSS localization systems in Sections 5.3.1 and 5.4. However, there are many space-based RSS implementations possible, as long as the RSS measuring space provides information about one unknown range or position. For example, the system described in Section 5.3.1 relates RSS measurements over space to one unknown range by assuming that the distances between the measurements are known (see Equation 5.15).

Static networks also increase the RSS measuring space by increasing the number of measurements to fixed nodes. In that case, the localization performance depends on the number of nodes in the network (e.g. [4]). For example, [14] experimentally showed that a static network set-up requires 369 fixed nodes with known positions to provide a median error of 0.3-0.6 m in an 18×18 m^2 LOS environment. Roughly speaking, this means that a static RSS-based localization network requires one node per square meters to provide the same resolving power as our TOF- and phase-based localization measurements. We theoretically and experimentally showed that the same resolving power can be provided by measuring RSS over space with a mobile node, without increasing the number of fixed nodes. We also showed that the CRLB for radio waves cannot endlessly be decreased by adding nodes but is limited by diffraction of these waves by the finite dimensions of the measuring surface ([5]).

This is not the first paper that uses a mobile node in an RSS-based localization system (e.g. [6] and [17]). However, most work on RSS-based localization

with mobile nodes differ in network set-up, purpose and localization performance. For example, [6] uses a mobile reference node and [17] focuses on the ease of installation and the localization performance of the mobile node.

The resolving power of space-based RSS is limited by its under bound of roughly one wavelength divided by its ultimate upper bound of the speed of light times coherence time of the carrier waves. The resolving power of phase- and TOF-based localization systems are usually fixed by design, so that larger ranges lead to less localization performance. Due to the general wave character of our radio signals, Green's theorem over a two-dimensional surface reduces to a contour integration along the circumference of this surface. Our future research aims to simplify our space-based localization by taking the convex hull of our localization surface that is at least in the far field of any infrastructure node and measures RSS along this contour. Surface integration of radio signals then simplifies to contour integration, a technique widely applied in electromagnetic theory.

5.7 Conclusion

Our new space-based RSS localization system appears to work well in outdoor and indoor environments. In the one-dimensional case, the lower performance bound appears to be limited by the Rayleigh criterion and cannot be further decreased by just adding nodes or more measurements. In our two-dimensional outdoor experiments, we experimentally verified that our space-based RSS is designed to attain similar localization performances as the more complex localization systems based on phase measurements and TOF. Our two-dimensional indoor experiments in a harsh office environment with moving human beings, metal cabinets and armed concrete walls, our space-based RSS localization system appears to outperform existing localization systems known to us. Future research is aimed at further simplifying space-based RSS by not sampling RSS over localization space but along the circumference of that space.

Bibliography

[1] M.Sargent, E.Willis Lamb, R.L.Fork: Theory of a Zeeman Laser I. Physical Review, vol. 164, Issue 2, December 1967.

[2] Hashemi H.: The indoor radio propagation channel, Proc. IEEE, July 1993, pp. 943- 996.

[3] IEEE Standard 802.15.4-2003. http://standards.ieee.org/getieee802/download/802.15.4-2003.pdf, 2012.

[4] N.Patwari, A.O.H. III, M. Perkins, N. S. Correal, and R.J.O'Dea: Relative location estimation in wireless sensor networks. IEEE Transactions on Signal Processing, vol. 51, no. 8, August 2003.

[5] J.W.Goodman: Introduction to Fourier Optics. Roberts and Company Publishers, 3rd Edition edition, December 10, 2004.

[6] M.L.Sichitiu and V.Ramadurai: Localization of wireless sensor networks with a mobile beacon. MAHSS 2004.

[7] E.Elnahrawy, X.Li; R.P.Martin: The limits of localization using signal strength: a comparative study. SECON 2004.

[8] K.Yedavalli, B.Krishnamachari, S.Ravula, and B.Srinivasan: Ecolocation: A sequence based technique for RF-only localization in wireless sensor networks. IPSN 2005.

[9] M.Maróti, P.Völgyesi, S.Dóra, B.Kusý, A.Nádas, Á.Lédeczi, G.Balogh, K.Molnár: Radio interferometric geolocation. SENSYS 2005.

[10] J.Lampe: Nanotron Chirp Spread Spectrum Proposal. IEEE P802.15 Working Group for Wireless Personal Area Networks (WPANs), 2005.

[11] B.Kusý, Á.Lédeczi, M.Maróti, L.G.L.T.Meertens: Node density independent localization. In IPSN 2006.

[12] IEEE Standard. 802.15.4a-2007. http://standards.ieee.org/getieee802/download/802.15.4a-2007.pdf, 2012.

[13] E.Menegatti, A.Zanella, S.Zilli, F.Zorzi, E.Pagello: Range-only SLAM with a mobile robot and a Wireless Sensor Networks. In ICRA 2009.

[14] G.Chandrasekaran, M.A.Ergin, J.Yang, S.Liu, Y.Chen, M.Gruteser, R.P.Martin: Empirical Evaluation of the Limits on Localization Using Signal Strength. In SECON 2009.

[15] V.Honkavirta, T.Perala, S.Ali-Loytty, R.Piche: A Comparative Survey of WLAN Location Fingerprinting Methods. In WPNC 2009.

[16] Z.Xiuyuan, L.Hongbo, Y.Jie, C.Yingying, J.Francisco, R.P.Martin, L.Xiaoyan: Characterizing the impact of multi-frequency and multi-power on localization accuracy. In MASS 2010.

[17] K.Chintalapudi, A.Iyer, and V.Padmanabhan: Indoor localization without the pain. In MOBICOM 2010.

[18] B.J.Dil and P.J.M.Havinga: Stochastic Radio Interferometric Positioning in the 2.4 GHz Range. In SENSYS 2011.

[19] B.J.Dil and P.J.M.Havinga: RSS-based Self-Adaptive Localization in Dynamic Environments. In IOT 2012.

[20] http://www.etsi.org, 2012.

[21] http://focus.ti.com/lit/ds/symlink/cc2430.pdf, 2012.

[22] http://www.jennic.com, 2012.

[23] http://www.nanotron.com, 2012.

CHAPTER 6

CONCLUSION

This research explored location estimation in networks using radio communication in the far field. In the far field, the measured signals are a function of the wave parameters time, position, temporal frequency and spatial frequency. Localization systems estimate blind node positions by estimating these wave parameters from sampling radio signals over space, time, or phase domains. Mathematically, localization then reduces to fitting measured signals at unknown locations. This research theoretically and experimentally explored the performance and robustness of RSS-, TOF- and phase-based localization systems operating in the 2.4 GHz regime.

We showed that the effective number of measurements in time, temporal frequency band and space domain determine the resolving power of measured ranges or positions. The effective number of measurements is equal to the measuring range (upper bound) divided by the smallest measurable quantity (lower bound). This effective number of measurements is interchangeable in the three domains due to the general wave character of signals in their far fields. In other words, phase-, TOF- and RSS-based localization systems provide similar performance when the effective number of measurements is the same. We experimentally verified this theoretical insight in LOS outdoor environments.

We showed that the resolving power of RSS-based localization systems increases with the number of measurements over space until a certain bound is reached, the so-called Rayleigh criterion for incoherent electromagnetic signals. Rayleigh's diffraction limit bounds the localization performance and thus the measurement resolution to roughly one wavelength as stated in Hypothesis one. In traditional RSS-based localization setups, blind nodes measure signal intensities from an array of reference nodes. In such traditional setups, the effective number of measurements is equal to the number of reference nodes. In general, this number is significantly lower than with other localization systems.

In other words, TOF- and phase-based localization systems outperform RSS-based localization systems in traditional localization setups. In Chapter 2, we increased the resolving power by measuring connectivity between blind nodes. In that case, the resolving power depends on the blind node density, which is an unwanted property. In Chapter 5, we increased the resolving power by using a mobile node with unknown positions. We called this localization system space-based RSS. We experimentally verified that our space-based RSS localization system provides a similar performance as TOF- and phase-based localization systems in a 20x20m2 LOS outdoor environment with four reference nodes placed at the corners of the localization area. These experiments verified Hypothesis three.

The theoretically expected resolving power is obtained when the propagation model matches reality, like in an ideal LOS outdoor environment. In NLOS indoor environments, the performance of these localization systems depends on how well propagation models are able to capture static and dynamic environmental influences. Propagation models used by RSS-based localization systems are often empirical models that introduce parameters to capture these environmental influences. The optimal values of these parameters depend on the locally varying electromagnetic permittivity and permeability of the localization space. In other words, the propagation model needs to account for local and temporal differences in the localization environment. In Chapter 3, we determined the constraints under which such a propagation model can be optimally and automatically calibrated. Measurements showed that such approach can cope better with dynamic environmental influences like unknown antenna orientations, so that Hypothesis two is validated.

In Chapters 4 and 5, we performed localization measurements in an NLOS office environment to measure how well different localization systems can cope with NLOS environmental influences. These measurements showed that our space-based RSS localization system outperforms existing TOF- and phase-based localization systems in an NLOS indoor environment. The main difference between the approaches is that our space-based RSS localization system performs measurements in the space domain, while TOF- and phase-based localization systems perform measurements in the time domain. As one would theoretically expect, measurements in the space domain can cope better with the spatial dispersion in NLOS indoor environments than measurements in the time domain. The latter ones cannot cope with NLOS signals, whereas space-based measurements record useful signal information on the spatial dispersion of NLOS environments. Although these measurements over space did not completely validate our Hypothesis four, they established a new benchmark

as performance bound and confirmed the direction that our simple theory on bounds works.

As indicated in the "goals and challenges" section (Section 1.1), we strived to balance a combination of theoretical, experimental and practical aspects throughout our research. We implemented three different measurement systems on two different COTS radio platforms to perform the required measurements for experimental verification of the theoretical concepts we use. In Chapter 5, we implemented a space-based RSS localization system. This localization system automatically forms a multi-hop network to forward the necessary data to the gateway and server. The localization server uses the localization algorithm described in Chapter 3 to automatically calibrate the propagation model and position the mobile blind node. The algorithm described in Chapter 5 is used to position static blind nodes. The user only needs to set the positions of the infrastructure nodes. The localization system is "plug-and-play" and keeps the "deployment and maintenance costs" as low as possible. Moreover, the same network is used for forwarding sensor data. A website enables the user to observe localization as well as sensor data. We believe that this localization system serves as a step forward to further closing the gap between the ever growing set of practical requirements and our ever increasing scientific insight in the lost space in which we live.

Publications and Patents

Publications

- Dil, B.J. and Havinga, P.J.M. (2012) RSS-based Localization in Dynamic Environments. In: Proceedings of 3rd International Conference on the Internet of Things (IOT 2012), 24-26 Oct 2012, Wuxi, China. pp. 55-62. IEEE Computer Society. ISBN 978-1-4673-1347-6
- Dil, B.J. and Havinga, P.J.M. (2011) Stochastic Radio Interferometric Positioning in the 2.4 GHz Range. In: Proceedings of the 9th ACM Conference on Embedded Networked Sensor Systems (SENSYS 2011), 1 Nov - 4 Nov 2011, Seattle, USA. pp. 108-120. ACM. ISBN 978-1-4503-0718-5
- Dil, B.J. and Havinga, P.J.M. (2010) A Feasibility Study of RIP Using 2.4 GHz 802.15.4 Radios. In: Proceedings of Mobile Entity Localization and Tracking, MELT '09, 8-12 Nov 2010, San Francisco, USA. pp. 690-696. IEEE Computer Society. ISBN 978-1-4244-7488-2
- Dil, B.J. and Havinga, P.J.M. (2010) On the Calibration and Performance of RSS-based Localization Methods. In: Internet of Things, IOT 2010, 29 Nov - 1 Dec 2010 , Tokyo, Japan. pp. 1-8. IEEE Computer Society. ISBN 978-1-4244-7413-4
- Dil, B.J. and Havinga, P.J.M. (2010) RSS-based localization with different antenna orientations. In: Australasian Telecommunication Networks and Applications Conference, ATNAC 2010 , 13 Oct - 3 Nov 2010, Auckland, New Zealand. pp. 13-18. IEEE Computer Society. ISBN 978-1-4244-8171-2
- Dil, B.J. and Havinga, P.J.M. (2010) COM-LOC++: A distributed range-free localization algorithm in wireless networks. In: Sixth International Conference on Intelligent Sensors, Sensor Networks and Information Processing, ISSNIP 2010, 7-10 December, Brisbane, Australia. pp. 157-162. IEEE Computer Society. ISBN 978-1-4244-7174-4

- Dil, B.J. and Havinga, P.J.M. (2009) COM-LOC: A Distributed Range-Free Localization Algorithm in Wireless Networks. In: Proceedings of the 5th International Conference on Intelligent Sensors, Sensor Networks and Information Processing (ISSNIP), 7-12-2009, Mellbourne, Australia. pp. 457-462. IEEE. ISBN 978-1-4244-3518-0

- Dil, B.J. and Dulman, S.O. and Havinga, P.J.M. (2006) Range-Based Localization in Mobile Sensor Networks. In: Proceedings of Third European Workshop on Wireless Sensor Networks, 13-15 Feb 2006, Zurich, Switzerland. pp. 164-179. Lecture notes in computer science 3868. Springer Verlag. ISSN 0302-9743 ISBN 3-540-32158-6

Patents

- Dil, B.J. and Havinga, P.J.M. (2010) Method for determining the location of a mobile device, mobile device and for such method. Patent N2004070 (Application).

- Dil, B.J. and Havinga, P.J.M. (2010) Method and system for localization in a wireless network. Patent N2005603 (Application).